EXAMINING THIENO[3,4-B]PYRAZINE THROUGH A MULTIFACETED LENS: FROM EXTENDED RING FUNCTIONALIZATION TO AMBIPOLAR-ACCEPTOR COPOLYMERS

A Dissertation
Submitted to the Graduate Faculty
of the
North Dakota State University
of Agriculture and Applied Science

By

Evan Wayne Culver

In Partial Fulfillment of the Requirements
for the Degree of
DOCTOR OF PHILOSOPHY

Major Department:
Chemistry and Biochemistry

July 2022

Fargo, North Dakota

North Dakota State University
Graduate School

Title

Examining Thieno[3,4-*b*]pyrazine Through a Multifaceted Lens: From Extended Ring Functionalization to Ambipolar-Acceptor Copolymers

By

Evan Wayne Culver

The Supervisory Committee certifies that this ***disquisition*** complies with North Dakota State University's regulations and meets the accepted standards for the degree of

DOCTOR OF PHILOSOPHY

SUPERVISORY COMMITTEE:

Dr. Seth Rasmussen
Chair

Dr. Mukund Sibi

Dr. Pinjing Zhao

Dr. Andrew Croll

Approved:

August 10, 2022
Date

Gregory Cook
Department Chair

ABSTRACT

A class of materials known as conjugated polymers (CPs) has been shown to integrate the physical properties of organic plastics such as low-weight, flexibility, and synthetic modularity with electronic semiconducting properties typically found in inorganic materials. While a variety of parameters determine the resultant material's conductivity, a crucial factor is the bandgap (E_g). Specifically, thieno[3,4-*b*]pyrazine (TP) has found success in generating low E_g CPs (i.e. E_g < 1.5 eV), largely in part due to its ambipolar identity. Two strategies to achieve E_g values < 1 eV include extending the conjugation of TP through ring fusion and pairing TP with strong electron accepting moieties.

The investigation into extended ring TPs as low bandgap homopolymers was initially pursued with the synthesis of poly(acenaphtho[1,2-*b*]thieno[3,4-*e*]pyrazine), a record setting low E_g homopolymer. Upon this realization of driving E_g values down through ring fusion on the pyrazine portion of TP, additional analogues were considered with $2\lambda^4\delta^2$-dithieno[3,4-*b*:3',4'-*e*]pyrazine as one of the most promising candidates due to its predicted E_g of 0.14 eV. Efforts into this research have produced a variety of precursors and analogues, adding to the family of TPs for further study.

A second strategy for E_g reduction is through the pairing of electronically mismatched units known as donors and acceptors. While this does reduce E_g, the underlying principles of the cause is disputed. Thus, to further understand the interactions in these types of copolymer systems, a small molecule study was designed with a strong donor, a strong acceptor, and the ambipolar unit TP in which six possible dimer configurations were synthesized and analyzed to determine the extent of donor-acceptor interactions.

Lastly, an investigation into TP-acceptor alternating copolymers was carried out by pairing TP with two acceptors of varying accepting strength and contributions to polymer solubility. Because of the atypical design of these copolymers, a relatively new cross-coupling method known as direct arylation polymerization was used in their synthesis. The optimization of which produced a CP with an E_g of 0.93 eV. These results thus provide evidence for a new design motif for low bandgap CPs that further refines our understanding of donor-acceptor relationships.

ACKNOWLEDGMENTS

First and foremost, I would like to thank my advisor, Dr. Seth Rasmussen for his input on all aspects of my graduate career. The education I received at NDSU was above and beyond what I could have hoped for due to your expertise. I am coming away with a Ph.D. in chemistry, but also now have an education in historical research that I could not have gotten anywhere else. Additionally, I now have a palate for porters and stouts that could have only been refined by an Australian trip collaborating with our friends at the University of Newcastle.

I would also like to thank all my committee members, Dr. Mukund Sibi, Dr. Pinjing Zhao, and Dr. Andrew Croll. Your input at each step of the Ph.D. process was invaluable and provided me with the critical analysis needed to get a polished dissertation into print. This along with all other assistance in my graduate studies has made me a better scientist and it has been a pleasure working with all of you.

I would also like to thank all my collaborators. Dr. Ted Pappenfus, you directed me to direct arylation resources that advanced my research tremendously. Dr. Paul Dastoor, you hosted me at the University of Newcastle and expanded my understanding of the materials field. Dr. Angel Ugrinov, you helped me get crystal structures paramount to my research.

Lastly, I would like to thank all the Rasmussen group members past and present. Thanks to Dr. Eric Uzelac, Dr. Kristine Konkol, and Dr. Trent Anderson for their mentoring and training when I was just an undergraduate and into graduate school. Zane Hensel, thanks for making many precursors crucial in my research.

Special thanks to Wyatt Wilcox, and Spencer Gilman for enlightening conversations and feedback. As colleagues you are exceptional and will go on to do amazing things. We enjoyed beers at the Würst often and I look forward to having many more in the future.

DEDICATION

I would like to dedicate this disquisition to my amazing wife Marina who has supported me in both my military and academic career. I can truly say that none of this would have been possible without you. Your support in all the stressful times as well as your ability to critique my technical writing skills is something few people have access to, so I am truly lucky to call you my partner. This is milestone while monumental is just the beginning of what I know will be an amazing life together. You are a loving wife, and our son William has no one better to teach him to be a kind, accepting person.

I would also like to dedicate this to my mom and dad, Gae and Sidney Culver. You have always been supportive of me no matter what I was pursuing, and it allowed me to try new things and find out what I was passionate about. The discipline you instilled in me at an early age gave me the work ethic to accomplish this monumental task and I am forever grateful.

TABLE OF CONTENTS

LIST OF TABLES

LIST OF FIGURES

LIST OF ABBREVIATIONS

CPs .....conjugated polymers

OPVs .....organic photovoltaics

OLEDs .....organic light emitting diodes

OFETs .....organic field effect transistors

E_g.....band gap

HOMO .....highest occupied molecular orbital

LUMO.....lowest unoccupied molecular orbital

MO .....molecular orbital

CV .....cyclic voltammetry

E_{pc}.....cathodic peak potential

E_{pa}.....anodic peak potential

(Fc^+/Fc) .....ferrocenium/ferrocene

A.....absorbance

hν.....photon energy

BLA.....bond length alternation

NMR .....nuclear magnetic resonance spectroscopy

P3HT .....poly(3-hexylthiophene)

D-A .....donor-acceptor

TP.....thieno[3,4-*b*]pyrazine

CCM.....charge carrier mobility

HT .....head-to-tail

HH.....head-to-head

TT.....tail-to-tail

XRD .....X-ray diffraction

PCBM .....Phenyl-C61-butyric acid methyl ester

PLEDs.....polymer light-emitting diodes

NIR.....near-infrared

BHJ .....bulk heterojunction

DArP .....direct arylation polymerization

ERs.....extended fused-rings

TdzTP.....$2\lambda^4\delta^2$-[1,2,5]thiadiazolo[3,4-*b*]thieno[3,4-*e*]pyrazine

ATP .....acenaphtho[1,2-*b*]thieno[3,4-e]pyrazine

pTPs .....poly(2,3-dialkylthieno[3,4-*b*]pyrazines

pC_8TP.....poly(2,3-dioctylthieno[3,4-*b*]pyrazine

pATP .....poly(acenaphtho[1,2-*b*]thieno[3,4-]pyrazine)

ATPBr_2.....3,4-dibromoacenaphtho[1,2-*b*]thieno[3,4-*e*]pyrazine

ATPC_8H_{17} .....3-octylacenaphtho[1,2-*b*]thieno[3,4-*e*]pyrazine

DBTQ.....dibenzo[*f*,*h*]thieno[3,4-*b*]quinoxaline

TPP.....thieno[3',4':5,6]pyrazino[2,3-*f*][1,10]phenanthroline

FTP.....1,3-dihydrofuro[3,4-*e*]thieno[3,4-*b*]pyrazine

DHTTP.....1H,3H-dihydrodithieno[3,4-*b*:3'4'-*e*]pyrazine

MMPP .....monoperoxyphthalic acid magnesium salt

DHTTPS-oxide .....dihydrothieno[3,4-*b*]thieno[3,4-*e*]pyrazine-s-oxide

CMTP.....2,3-bis(cyanomethyl)thieno[3,4-*b*]pyrazine

EDOT.....3,4-ethylenedioxythiophene

BTD.....benzo[*c*][1,2,5]thiadiazole

DTP .....dithieno[3,2-*b*:2',3'-*d*]pyrrole

DFT .....density functional theory

BrBTD.....4-Bromo-2,1,3-benzothiadiazole

TMS .....trimethylsilyl groups

ICT .....intramolecular charge transfer

ε.....molar absorption coefficient

b.....path length

c.....concentration

f .....oscillator strength

$\lambda^{abs}{}_{max}$.....maximum absorption wavelengths

$TBAPF_6$.....tetrabutylammonium hexafluorophosphate

ITO.....indium tin oxide

$Pd(OAc)_2$.....palladium(II) acetate

P3ATs .....poly(3-alkylthiophene)s

PDOF-TFP .....poly[(9,9- dioctylfluorene-2,7-diyl)-*alt*-(2,3,5,6-tetrafluoro-1,4-phenylene)]

X.....halogen or pseudohalogen

CMD .....concerted metalation deprotonation

OA.....oxidative addition

RE .....reductive elimination

pC_6TP-BTD.....poly(2,3-dihexylthieno[3,4-b]pyrazine-alt-2,1,3-benzothiadiazole)

pEHTP-BTD .....poly(2,3-bis(2-ethylhexyl)thieno[3,4-b]pyrazine-alt-2,1,3-benzothiadiazole)

C_6TP.....2,3-dihexylthieno[3,4-b]pyrazine

EHTP.....2,3-bis(2-ethylhexylthieno[3,4-*b*]pyrazine

DMAc .....dimethylacetamide

TMPP .....tris(2-methoxyphenyl)phosphine

GPC.....gel permeation chromatography

TGA .....thermogravimetric analysis

Qx.....2,3-dihexylquinoxaline

pC_6TP-Qx.....poly(2,3-dihexylthieno[3,4-b]pyrazine-alt-2,3-dihexylquinoxaline)

Bz .....benzene

BTA.....2,1,3-hexylbenzotriazole

CPME.....cyclopentyl methyl ether

PCE .....power conversion efficiency

V_{OC}.....open circuit voltage

J_{SC}.....short circuit current

EQE.....external quantum efficiency

CHAPTER 1. INTRODUCTION

A class of materials known as conjugated polymers (CPs) are promising in that they incorporate the flexibility, low-weight, and processability of organic plastics, with the electronic semiconducting and conducting properties typically only observed in inorganic materials.[1] The conductive properties stem from the overlapping of p-orbitals along the polymer backbone which allows for the delocalization of electrons (Figure 1.1 (a)).[2] A multitude of repeat units have been investigated including the structurally simplistic -C_2H_2- in polyacetylene, as well as a variety of heterocycles (Figure 1.1 (b)) that merge these plastic and electronic properties.[1,2] These hybrid materials then allow for the fabrication of new devices such as organic photovoltaics (OPVs), organic light emitting diodes (OLEDs) and organic field effect transistors (OFETs) that can be applied in such areas as wearable electronics, cheap pop-up solar panels, and biomedical devices.[1-4]

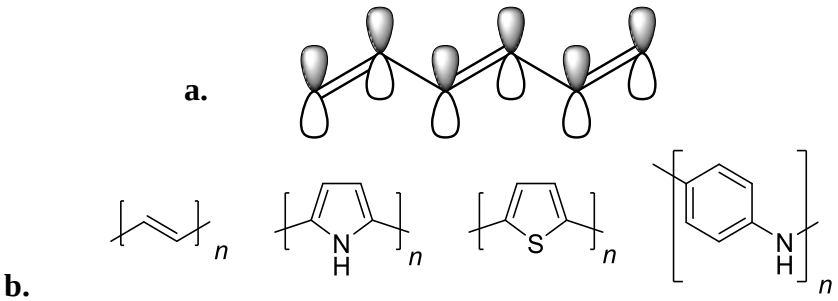

Figure 1.1. (**a**) p-Orbital orientation allowing for overlap along the polymer backbone and (**b**) common conjugated polymers: polyacetylene, polypyrrole, polythiophene, and polyaniline.

Conjugated Polymer History

CPs are materials often ascribed as having been discovered in the mid-20th century, largely in part to the 2000 Nobel prize award that was given to Alan J. Heeger, Alan G. MacDiarmid, and Hideki Shirakawa titled: “for the discovery and development of conductive

polymers".[5] While their contribution to the field is unquestionable in its scope and influence, it does seem to be an overstatement that they were the explicit discoverers of CPs as numerous reports predate their collaborative work in the 1970s.[6] The discovery of CPs can be considered to have occurred as early as 1834 with the experimentation by Friedlieb Ferdinand Runge on the oxidation of aniline salts to produce insoluble dark colored dyes.[7] While this early work in no way investigated the electronic properties and thus still may allow for credit of discovery of conducting polymers to go to the three Nobel laureates, it did provide evidence of the synthesis of a material that could be considered the first example of a conducting polymer significantly earlier than the 20th century.

However, even the property of conductivity in polymeric materials predates the late 1970s work of Heeger, MacDiarmid, and Shirakawa. A pioneering study in this respect was the research carried out by Donald Weiss in 1963 on polypyrrole as a method of water desalinization.[6] This study included conductivity measurements which showed that upon oxidation with iodine the overall conductivity increased to 0.005-0.9 S cm^{-1} for polypyrrole materials.[6] These were thus described as being "relatively good conductors of electricity" and determined to be electronic (as opposed to ionic) in origin. This information was not widely dispersed however, and the limited reception of these investigations and others has been thought to be due to the results being published in Australian journals and thus not permeating the greater materials literature at the time.[7]

Where the Nobel laureates unequivocally changed the field however was in the enhancement of the conductivity of their polyacetylene films from 0.5 to >500 S cm^{-1}.[8] Values if which were previously not observed in conjugated polymer systems and approached that of other highly conductive systems such as metals.[8] A feat that none of the previous materials had yet

achieved, and thus a pioneering milestone in the realization of the extent that CPs could play in electronic devices. This benchmark realization came after MacDairmid, Heeger, and Shirakawa began looking into the properties of polyacetylene films. Upon oxidation, in 1977 they reported changes in conductivity due to doping with various oxidants such as chlorine, bromine, and iodine.[9] Further investigations showed that the maximum improvements to conductivity via halogen doping were observed with iodine as an oxidant and gave conductivity measurements of up to 500 S cm^{-1} by 1978.[10]

Regardless of the previous research on these materials prior to the 1970s, the advances made by the Nobel laureates spurred significant interest in the field and brought real-world applications into view. It also brought forth an increase in understanding of the underlying principles and hence a point at which further work could progress at an expedited rate. Due to the organic nature of these materials, this progress would come largely in the form of tuning the material properties through synthetic design.[11] This ability to tune properties bringing with it an increasingly diverse class of materials to fit a variety of roles in electronic devices.

Conjugated Polymer Overview

A desire for low-cost materials with diverse properties for application in devices such as OLEDs, OPVs, OFETs has been a leading driving force for the synthesis and development of CPs[3,12,13] This, along with established printing technologies has provided the foundation for the fabrication of devices with plastic physical properties on a variety of substrates.[14] Therefore, the unification of optical/electronic properties with intrinsic plastic properties allows for CPs to be a promising choice for electronic devices that can be fabricated cheaply and function in a variety of roles.[15-20]

With their potential applications dependent on molecular design, CPs have been extensively researched in pursuit of their structure-property relationships.[21] This comprises of both increasingly complex homopolymers as well as copolymeric systems (Figure 1.2) that incorporate a variety of heteroatoms, side-chains, and repeat units. The molecular structures of CPs are critical to achieve the desired properties and requires engineering at each step of the synthetic process and beyond. This includes monomer design and synthesis, polymer design and synthesis, and solid-state film engineering. The critical properties that can be modified include the band gap, frontier orbital energy levels, ground-state structure (i.e aromatic vs. quinoidal contributions), charge carrier mobility, solubility, processability, and bulk solid-state packing.[1,11-13]

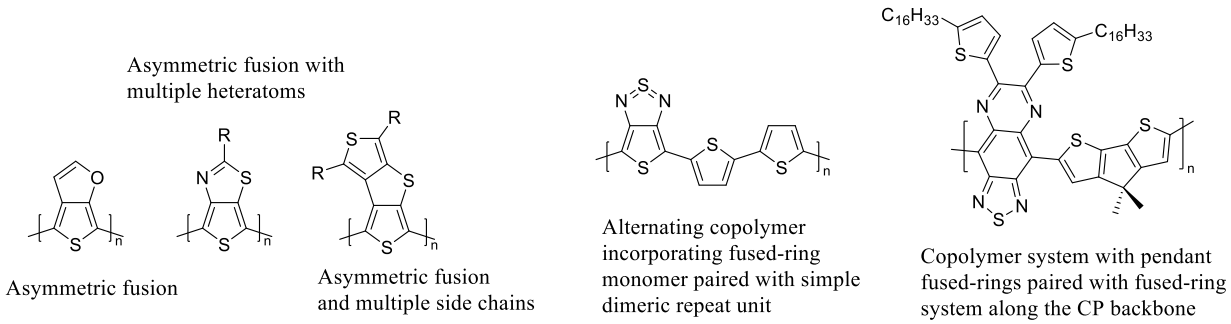

Figure 1.2. Examples of variety in synthetic design (top) homopolymers with added ring fusions; (bottom) copolymers showing diversity in complexity.

Band Gap & Band Structure

One of the most important parameters central to CP design is the band gap (E_g). This energy gap can be defined as the energetic difference between the valence and the conducting bands of the CP in the solid state.[1,12,13,22] The energy band structure is a direct translation of the frontier orbital energies in that the top of valence band is equivalent to the highest occupied molecular orbital (HOMO) and the bottom of the conduction band is equivalent to the lowest occupied molecular orbital (LUMO).[12,13] The E_g is dependent on several factors including bond length alternation[23], enhanced quinoidal character of the ground state[24], and the extent of

conjugation.[25,26] A material's E_g will largely dictate the electronic properties and classes of materials have been divided based on E_g ranges into three categories: conductors, semi-conductors, and insulators, with these defined by the E_g ranges for each being 0, 0-2, and >2 eV respectively[1] (Figure 1.3).

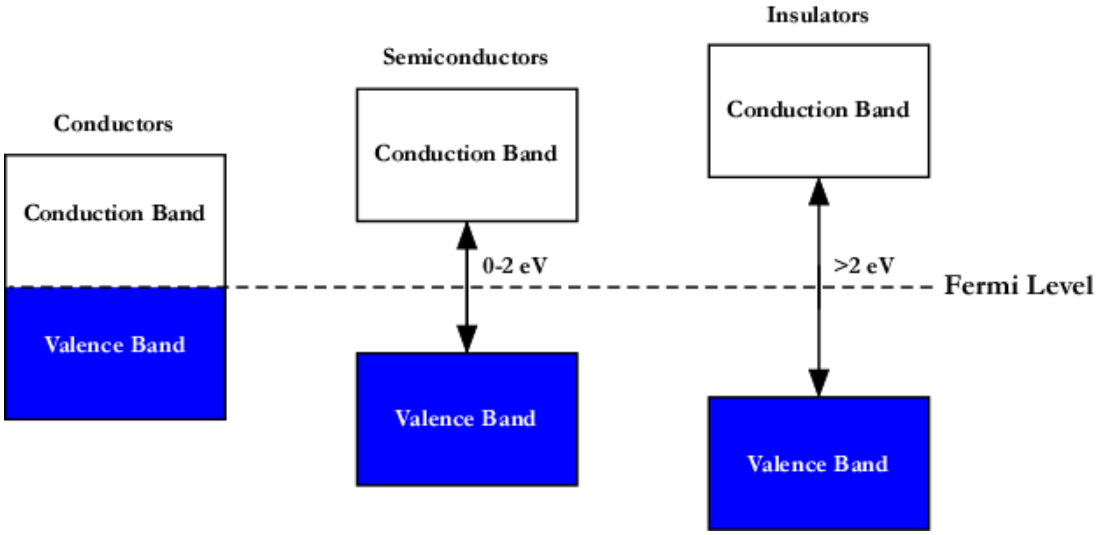

Figure. 1.3. Simplified band structure of materials.

As the bandgap is reduced, thermal population of the conduction band becomes increasingly favorable and increases the total number of intrinsic charge carriers, enhancing the overall conductivity of the material.[1,12] While this classification is used for convenience, it should be noted that other factors play a role in conductivity and for example a material with a bandgap greater than 2 eV may still have some concentration of free charge carriers.

Conjugation and Bandgap

CPs are considered periodic 1-dimensional systems, which allow for π-molecular orbital (MO) Hückel approximations to adequately describe frontier orbital behavior (HOMO/LUMO energies).[27] A simplified MO diagram can thus depict these orbitals and show the effects of increased conjugation on the HOMO/LUMO gap. This, as well as the transition from discrete

molecular orbitals in small molecules to the polymeric band structure in the solid-state is shown Figure 1.4.

In Figure 1.4, the simplest alkene with a π-system is ethylene and serves as a basic example for a starting point in π-MO approximations of larger conjugated systems. The frontier orbitals of ethylene consist of two MOs, in which one is a bonding orbital and the other an antibonding orbital due to in-phase and out-of-phase orbital interactions respectively. The two electrons from the contributing p-orbitals fill according to the Aufbau principle, where the in-phase MO contains both electrons (the HOMO) and the out-of-phase MO contains no electrons (the LUMO).

As the chain length is increased to a four-carbon system such as the conjugated system 1,3-butadiene, four hybrid MOs result from the mixing of a p-orbital from each carbon atom in an alternating double-single-double-bond configuration. The hybrid orbitals generated interact in four possible arrangements with increasing energy following an increasing number of out-of-phase (antibonding) interactions. Unlike the simplified ethylene case, 1,3-butadiene now requires two MOs for its four electrons and consequently the HOMO is destabilized by an antibonding interaction. Conversely, the LUMO now has bonding interaction which has a stabilizing effect.

Therefore, this splitting of MOs due to increased conjugation length causes a destabilization of the HOMO and a stabilization of the LUMO with an overall effect of reducing the energy gap between the two frontier orbital energy levels.[1,22] This trend continues as conjugation length is increased up to a limit known as the maximum effective conjugation length,[1] with further decreases coming from intermolecular interactions in the solid-state. These interchain interactions cause further delocalization by allowing for delocalization to now occur between adjacent chains and thus are largely dictated by π-π-interactions.[31]

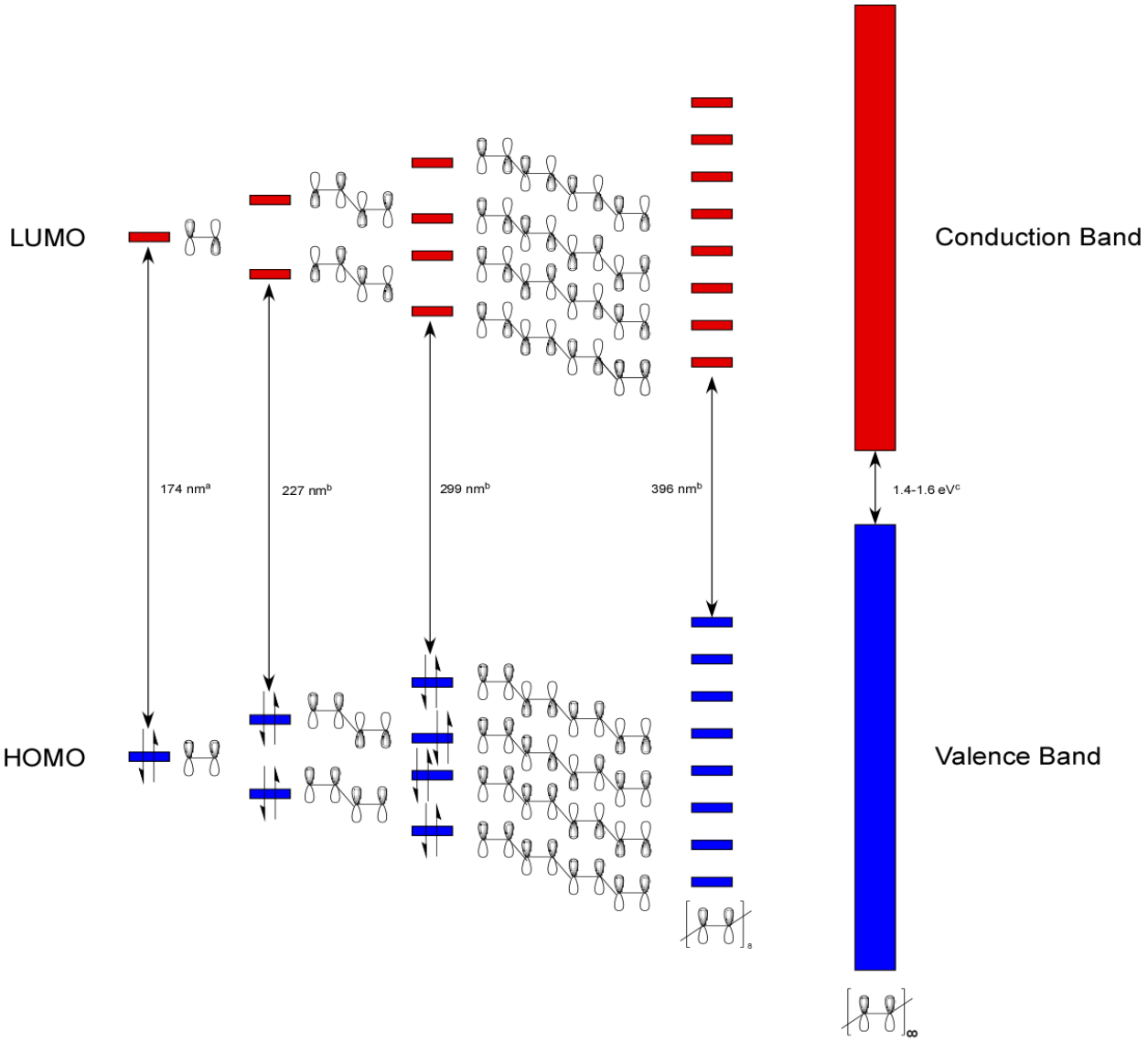

Figure 1.4. Molecular orbital diagram with representative p-orbitals showing an increase in conjugation length and a corresponding reduction in HOMO/LUMO gap. [a]Value from ref. 28. [b]Values from methyl capped polyenes in ref. 29. [c]Value from ref. 30.

π-Stacking

An isolated polymer will still have discrete molecular orbitals in solution and therefore the band structure only becomes appropriate in the bulk solid-state when delocalization of electrons can occur between adjacent polymers. The intermolecular interactions that cause this delocalization are typically referred to as π-stacking or π-π-interactions and are the result of the

quadrupolar shape of the electrostatic potential map present in unsaturated molecules.[32] The foundation of this understanding comes from an electrostatic argument in which an aromatic ring such as benzene should have partial negative charges above and below the faces of the ring with a partial positive charge around the perimeter of the ring that allows for attractive interactions between parallel off-centered rings or perpendicular edge-to-face rings (Figure 1.5).[33,34]

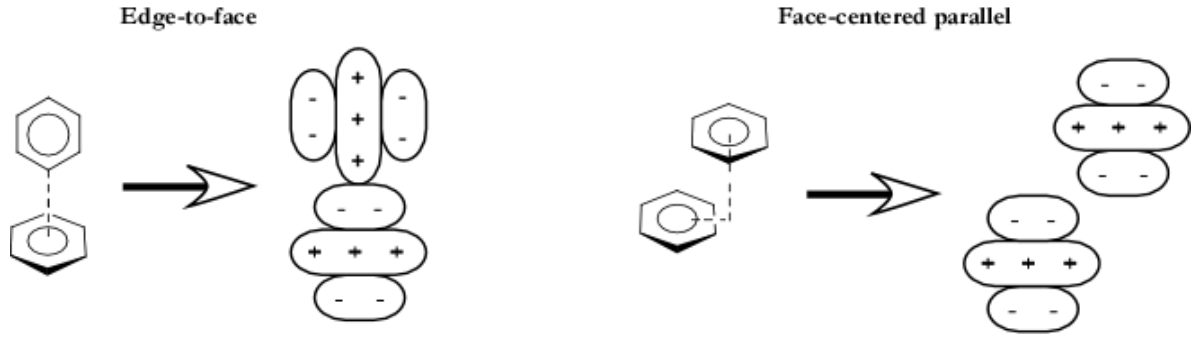

Figure 1.5. Possible π-stacking arrangements of benzene.

The highly rigid nature of CP backbones however means that all aromatic rings are oriented in the same direction and therefore the intermolecular interactions between polymer chains will be cumulative. As an example material, polythiophene will prefer an orientation in a face to face eclipsed slip-stack fashion.[35] The implications for these π-π-interactions for conjugated polymers is the further delocalization of electrons between polymer chains and a transition from closely spaced, discrete molecular energy levels to an overlapping band-type structure for both the bonding and antibonding orbitals as shown in Figure 1.4.[35]

Experimental Determination of Frontier Orbital Energies and Bandgap

To determine the HOMO-LUMO gap and E_g of a material, the two analytical techniques most often used are electrochemistry and absorption spectroscopy.[1] In the case of bandgap measurements these must be taken of solid-state films as this is a bulk solid-state property. Conversely, HOMO/LUMO energies as molecular property, can be determined in solution for

both small molecules and polymeric materials. For the electrochemical route of E_g determination this is typically performed via cyclic voltammetry (CV), while optical absorption method is done through UV-Vis-NIR absorption spectroscopy. Both techniques have their advantages and disadvantages, and often are used in conjunction with one another to complete the frontier MO/energy gap picture.

In an electrochemical CV method for E_g determination, the energy at which the first oxidation occurs in a polymer is measured by scanning through positive potentials up to a limit followed by a reverse scan back to the starting potential and measuring the change in current response.[36,37] In the electrochemical cell, the polymer under investigation is deposited on the surface of the working electrode where the potential cycling can allow for oxidation. This immobilized surface CV experiment differs from standard solution CV experiments in that ideal monodisperse electroactive analytes should have differences in cathodic (E_{pc}) (forward scan peak) and anodic (E_{pa}) (reverse scan peak) potentials that are minimized ($E_{pc} \approx E_{pa}$) due to the absence of diffusion which is observed for solvated analytes.[36,37] CPs however being polydisperse and multilayered on the surface of the electrode have a distribution of peak potentials due to the diffusion of electrolyte in and out of the bulk material and thus require the use of onset potentials to determine redox potentials. The HOMO/LUMO energies for a polymer can be determined by relating the respective E_{onset} to a standard redox couple such as the ferrocenium/ferrocene (Fc^+/Fc) redox couple, which as a known standard, has conversions to commonly used electrodes and the vacuum scale.[37] If a measurement is taken in the solid state, this first oxidation then corresponds to top of the polymer's valence band, which can be equated with the HOMO of the bulk, solid-state material and likewise for the first reduction peak and the LUMO.[1] The same evaluation of the LUMO/bottom of the conduction band can be achieved

through simply applying a negative potential to the working electrode, with the only caveat being that for these transition energies to be observable they need to fall within the "solvent window" of the specific solvent/electrolyte combination used in the experiment, meaning these transitions need to occur prior to the oxidation/reduction of the solvent and/or electrolyte to be observable.[36]

While CV analyzes the individual frontier MOs, absorption spectroscopy probes the gap between them. The absorption method does not have the solvent window problem inherent in the electrochemical method and thus is often a simpler method used for E_g determination. This technique uses light in the UV-Vis-NIR range to excite a species to a higher energy level through the absorption of photons and plots it as wavelength vs. intensity. The lowest energy transition corresponds to the HOMO-LUMO gap or optical E_g in the solid state and the onset of absorption is used to determine the energy of this transition.[1] To accurately represent the HOMO-LUMO gap or optical E_g, a Tauc plot can be used.[38] A Tauc plot uses the low-energy side of the absorption band, with the corresponding energies ($h\nu$) plotted versus $(A \times h\nu)^2$ (A = absorbance, $h\nu$ = photon energy). Alternatively, a rougher estimate of the E_g can also be done through a simple extrapolation of the absorption onset to the baseline.[1] The limitation with this technique when compared to CV is that while the HOMO-LUMO gap and E_g can be determined, specific frontier orbitals or band edges cannot, and thus the two techniques are often used in tandem which becomes important in specific cases where one or both frontier MOs fall outside the electrochemical solvent window.

Doping & Chemical Reactivity

Another way to further modify the band structure of conjugated polymers is through redox processes commonly referred to as doping. Sometimes distinguished as "chemical doping", the concept was adapted from the traditional inorganic view of doping in which atoms

of different electron valencies are introduced into a pure material to lower E_g and enhance conductivity of a neutral material. In the doping of inorganic materials, the new atoms are either more electron rich or more electron poor than the host atoms and create new lower energy state near the conduction band and higher energy state near the valence band respectively.

In the doping of CPs, the polymer is either oxidized (p-type doping) or reduced (n-type doping), both of which require an added ion (referred to as the "dopant"), which forms a complex with the doped form of the polymer. Oxidation or reduction of the polymer either adds electrons to the LUMO in the case of n-type doping or remove electrons from the HOMO as is the case for p-type doping.[39] The crucial result of this doping process of CPs is the introduction of charge carries (holes or electrons) that require electrostatically incorporated ions ("dopants") to achieve charge neutrality.[40] In the case of n-type doping this generates an anionic polymer by the addition of an electron which usually comes from a metal species such as Na or K and results in the dopant counterion being Na+ or K+. The p-type case, and more common of the two, can be done with a variety of oxidants (Br_2, I_2, AsF_5, $FeCl_3$, etc.)[41] and generates a cationic polymer with the corresponding counterion (Br^-, I_3^-,AsF_6^-,$FeCl_4^-$).[39] A simplified band structure view of both n- and p-type is shown in Figure 1.6 where p-doping removes electrons from the valence band creating a new lower energy conduction band into which electrons can be promoted. Similarly, in n-doping, additional electrons are introduced that are higher in energy and thus a new higher energy valence band is formed to reduce the E_g between this new band and the conduction band.

Structural Changes Upon Doping

Upon redox doping, significant structural changes can occur to a CP backbone as is the case in the oxidative p-type doping of polythiophene to generate a radical cation which is often

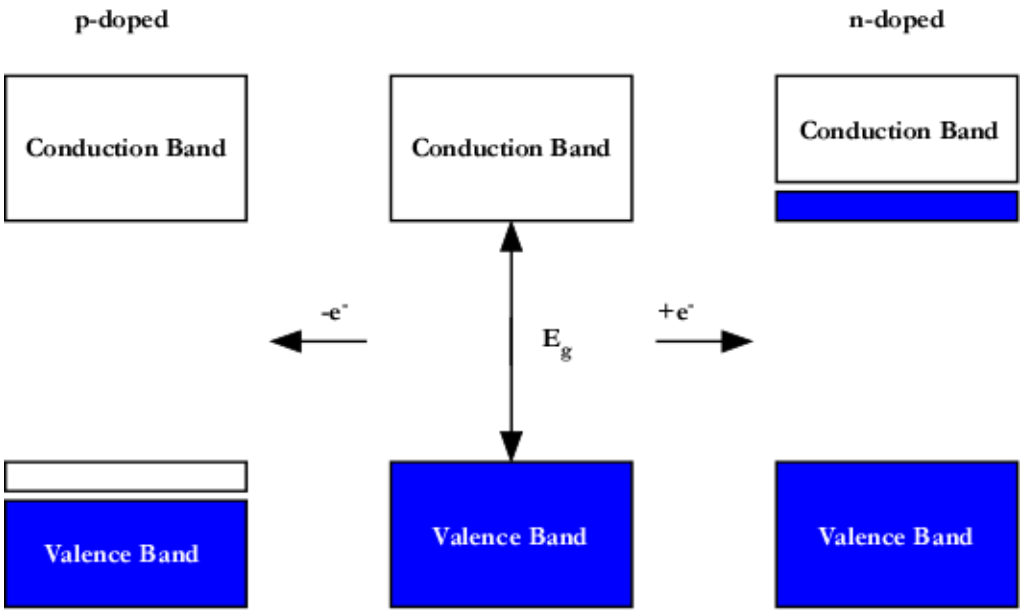

Figure 1.6. Modified band structure upon doping.

referred to as a polaron.[42-44] Further oxidation can then increase the charge carrier concentration along the polymer backbone with the addition of second polaron/radical cation which can be bound in a lower energy state known as a bipolaron.[42] These injected charges cause significant structural changes by increasing the quinoidal character of the CP backbone as shown in the example of polythiophene in Figure 1.7. Likewise, although less common is reductive n-type doping in which a radical anion is the generated excited species which can undergo a similar binding to form a negatively charged exciton pair.[45]

Doping and Polyaniline

In addition to oxidative and reductive doping, another method known as acid doping (or protonic doping) is also possible. In this method of doping, a two-step process occurs in which a protonation step, which does not change the total number of electrons, is associated with the oxidation of the polymer.[46,47] The archetypal polymer where this is observed is polyaniline due to its amine functionality which is susceptible to protonation.[42,46] The electronic properties of

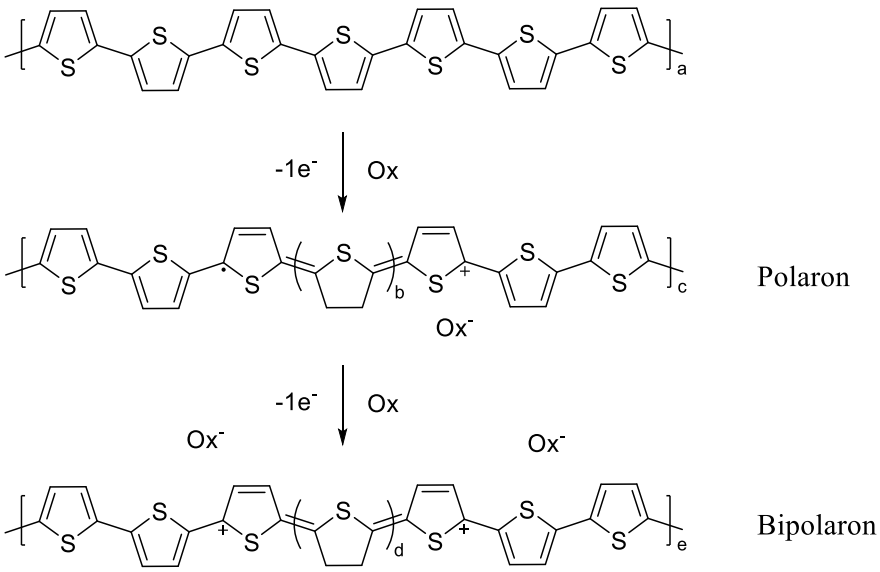

Figure 1.7. Structural changes to polythiophene upon oxidative doping.[42]

polyaniline were first investigated by Marcel Jozefowicz (b. 1934) while working under Rene Buvet (1930-1992) in the 1960s. In this work, aniline was polymerized oxidatively with persulfate in sulfuric acid.[1] Controlling the level of protonation then led eventually to the neutralization of the emeraldine sulfate to the emeraldine base. Through this pH control, conductivities ranged from 10^{-9} S cm^{-1} all the way up to 30 S cm^{-1} and were shown to increase linearly with decreasing pH.[1] Further investigations were carried out by MacDiarmid starting in the late 1980s which showed the importance of morphology, but conductivities of 10^{2} S cm^{-1} - were still the maximum values achieved, as had been previously reported by Jozefowicz in 1969.[40,46,47] MacDiarmid also proposed that the fully reduced leucoemeraldine could be oxidized to the emeraldine salt which is a conductive material that has an additional mesomeric structure with the polarons localized on alternating nitrogen atoms.[46-48] The emeraldine salt could then be deprotonated which generates the emeraldine base, a significantly less conductive polymer with conductivities of 1-4 S cm^{-1}.[46,47] In respect to the actual charge carriers, it should be noted that

spinless bipolarons, spin-carrying polarons, and polaron-bipolaron transformations have all been proposed.[49]

Bandgap Engineering

While doping modifies the polymer band structure, the reduction of the bandgap for neutral CPs is crucial for the realization of intrinsic conducting/semiconducting materials. This goal of bandgap reduction has led to the classification of materials into either reduced bandgap materials (1.5 eV < E_g < 2.0 eV)[50] or low bandgap materials as originally proposed by Pomerantz with E_g values <1.5 eV[12]. To achieve these reduced and low E_g ranges requires the delocalization of electrons and these reductions are largely determined by the extent of the conjugation.[1,13] The determining factors of which include bond length alternation, aromatic and quinoidal contributions to the ground state, electron confinement due to aromaticity, functional group electronics, steric induced torsional strain, and π-stacking (discussed in section 1.3).

Bond Length Alternation

A significant factor that has been stated for CPs to exist as low bandgap species is a minimization of bond length alternation (BLA), which is defined as the average difference between double and single bond lengths along the polymer backbone.[51] This, much like doping, has also been adapted from an inorganic viewpoint through the modeling of a 1-D metallic systems as proposed by the Peierls theorem and extrapolated to CP systems. This model predicts metallic conductivity for 1-D systems such as *trans*-polyacetylene if all bond lengths are equal (no BLA) along the conjugated backbone and semiconducting conductivity for species with significant BLA.[45,53-56] *trans*-Polyacetylene has a bandgap of 1.5 eV and is thus a semiconductor. Therefore, it should have some level of BLA that would prevent it from being an absolute conductor. This is indeed the case as has been shown experimentally by the specialized solid

state nuclear magnetic resonance spectroscopy (NMR) technique "nutation" NMR to be 1.36 and 1.44 Å for double and single bonds respectively with a BLA of 0.08 Å (Figure 1.8).[57,58] Thus the BLA of polyacetylene results in two different types of bonds in the conjugated backbone, where one type has more single bond character and conversely a second type has more double bond character.

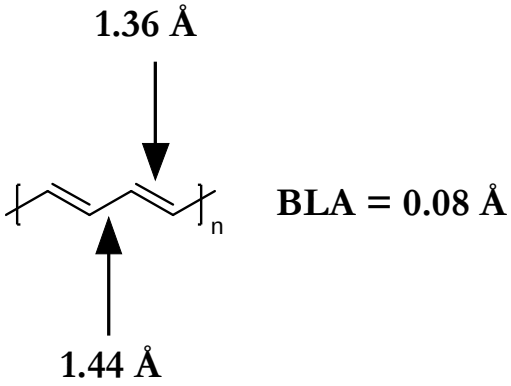

Figure 1.8. Bond length alternation of polyacetylene.

Aromatic and Quinoidal Contributions to the Ground State

While *trans*-polyacetylene showed impressive electronic properties in both the doped and undoped state, the need for more environmentally stable and processable CP systems shifted the emphasis to increasingly complicated systems. Thus, investigations of CPs have been largely pursued with heterocyclic species as the repeat unit along the CP backbone.[2] These heterocycles differ from the simplified polyenes in that the ground state structure has two nondegenerate resonance structures as contributors. Polythiophene is a classic example in this case with both an aromatic and quinoidal configuration contributing to the ground state structure (Figure 1.9).[13] The aromatic structure has C-C bonds adjoining adjacent rings with significant single bond character as shown with electron diffraction of gaseous bithiophene which gives a bond length of 1.480 Å.[59] The quinoidal structure moves the double bond character within the aromatic ring to

the C-C bonds connecting individual rings with calculations predicting a decrease in bond length between the carbons adjoining thiophene units of 0.118 Å for a new bond length of 1.362 Å.[59] The two configurations are not energetically equivalent however, and the aromatic form is the more stable of the two, contributing significantly more to the actual ground state structure.[22] Upon further investigation, it was shown that if the quinoidal contribution to the ground state was increased, a linearly correlated reduction in E_g was also observed.[12,13] The significant finding therefore was that for these systems with nondegenerate ground state resonance structures, a simplified BLA approach to E_g modeling would no longer suffice and the additional factor of how much the quinoidal structure contributes to the ground state configuration need also to be considered.[59,24]

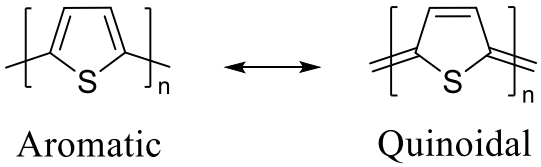

Figure 1.9. Aromatic and quinoidal forms of polythiophene.

Enhancing the Quinoidal Contribution to the Ground State

As stated previously, the quinoidal configuration in polythiophene is a minimal contributor and the ground state structure is dominated by the aromatic configuration. Therefore, to reduce bandgaps in these materials by increasing the quinoidal character, significant molecular modification needs to occur. An effective way to increase the quinoidal character, specifically in the case of five-membered rings such as thiophene is to incorporate an additional fused ring at the 3- and 4-positions. The first example of this was poly(isothianaphthene) which was synthesized in 1984[60] and was also the first example of a polymer with a lower E_g than polyacetylene and an experimentally determined value of 1.0 eV.[60] As shown in Figure 1.10. The

fusing of this six-membered ring allows for a quinoidal resonance form that has a higher contribution to the ground state because of the enhanced aromatic stability of the benzene ring over that of thiophene.[62]

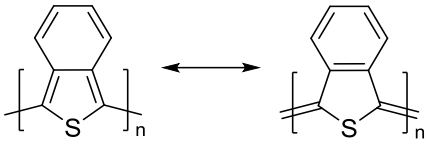

Figure 1.10. Aromatic and quinoidal forms of poly(isothianaphthene).

Electron Confinement and Aromaticity

While the quinoidal and aromatic contributions to the ground state can provide significant information regarding bandgap tuning, the confinement of electrons on the aromatic ring has also been considered as a factor that plays a sizeable role. This has largely been explained in terms of how aromatically stable the ring is, with changes to the repeat unit showing correlated changes in bandgap.[1,13] In conjunction with the observation that the ring fusion of a more aromatically stable species on the polymer backbone reduces the bandgap is the comparison of polarized heterocycles such as thiophene with a relatively nonpolar aromatic ring such as benzene. These two species have significant differences in their aromatic stability as well as a correlated change in E_g energy. with benzene having a 36 kcal/mol aromatic stability and a polyphenylene giving an E_g of 2.9 eV[63] and thiophene having an aromatic stability of 23 kcal/mol[64] and an E_g of 2.0 eV.[12] The rationalization of this coming through an electron confinement lens, in that benzene's aromatic stability prevents the delocalization of electrons along the polymer backbone while the polarization of thiophene due to the included sulfur heteroatom reduces electron affinity to allow for increased delocalization.[1]

Functional Group Electronics

From the above discussion the electronics of the aromatic ring used as the repeat unit show a direct influence on the bandgap of the resulting polymers. Therefore, changing the nature of the aromatic ring is one way to modify the bandgap. While this can be done through changing the identity of the ring, another route is through the addition of electronically altering side-chains. The side-chain tuning method has been shown to lower the oxidation potential of the polymer for polythiophene analogues through the addition of electron-donating substituents[13] as well as raise the oxidation potential through the addition of electron-withdrawing substituents.[65] Electron donating substituents are the more common of the two due to the ability to stabilize the polymers in the oxidized doped state and thus a variety of donating substituents have been investigated including alkoxy, mercapto, and amino groups as functionalized polythiophene analogues.[13]

Steric Induced Torsional Strain

Lastly, in addition to the electronics of substituents is the potential for steric clashing between substituents on adjacent rings. In the case of polythiophene, substituents are located on either the 3- or 4-positions with one of the most common analogues being poly(3-hexylthiophene) (P3HT).[1,13] Depending on the synthetic method, P3HT can exist in a regiorandom or regioregular arrangement along the polymer backbone (discussed in section 1.8). In a regiorandom arrangement, the possibility for steric clashing between substituents can then lead to torsional strain between thiophene units causing deviations from planarity along the CP backbone. A less planar backbone will then have reduced conjugation due to poor orbital overlap and a resultant increase in E_g.[1,12,13]

Donor-Acceptor Theory

Currently, one of the most common theories evoked when discussing low bandgap polymer synthesis is the donor-acceptor (D-A) theory. This approach originates from a 1992 paper by Havinga and coworkers on polysquaraines and polycroconaines, which was further investigated in 1993 and 1995.[66-68] The investigation showed that when an electron-rich donor species such as 1,2,3,5,6,7-hexahydro-3,3,7,7-tetramethyl-2,6-bis(methylene)benzo[1,2-*b*:4,5-*b*′]dipyrrole was paired with either of two different electron-deficient acceptor species, squaric acid or croconic acid, the resulting alternating copolymers had bandgaps as low as 0.5 eV.[66] This work was groundbreaking in that band gap reduction was previously pursued largely through the enhancement of the quinoidal contribution to the ground state of the polymer as in the case of poly(isothianaphthene) mentioned in the previous section, which has been reported as having an E_g of 1.0-1.2 eV.[60] This new insight into the pairing of energetically matched donors and acceptors has since been the cornerstone of most current research on low E_g CPs with a variety of explanations as to what is the cause of the observed E_g reduction.[69]

Explanations for E_g Reduction in D-A Systems

The rationalization for a reduction of the E_g in D-A systems has been explained in multiple ways, with one common explanation being a reduction in BLA due the formation of multiple resonance structures. These resonance structures can be expressed as single bond between the D-A moieties, as well as an additional resonance structure with a double bond between the donor and acceptor moiety and a now positively charged donor and negatively charged acceptor as shown in Figure 1.11 due to charge transfer from donor to acceptor. This implies that both donor and acceptor are of relatively high strength and that the averaging of the two resonance forms causes the BLA reduction.[70]

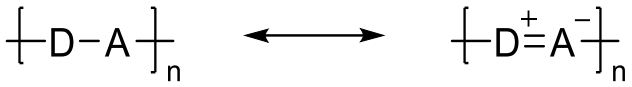

Figure 1.11. Possible resonance forms of donor-acceptor copolymers.

An additional explanation for the D-A approach and slightly more prevalent in the literature is the hybridization of frontier orbitals to reduce the E_g. In this interpretation, the donor which has a destabilized HOMO is paired with the acceptor which has a stabilized LUMO. The resulting polymer HOMO is then the hybridization of both the donor and the acceptor and only slightly destabilized whereas the LUMO only has significant contribution from the acceptor due to the energy mismatch making the donor species LUMO typically much higher in energy. This then results in a CP species that has an E_g lower than either donor or acceptor species could achieve in a homopolymer system of the respective components. This is represented in Figure 1.12 with A as a generic acceptor species and D as a generic donor species with both the energy levels of the homodimer and heterodimer species pictured.

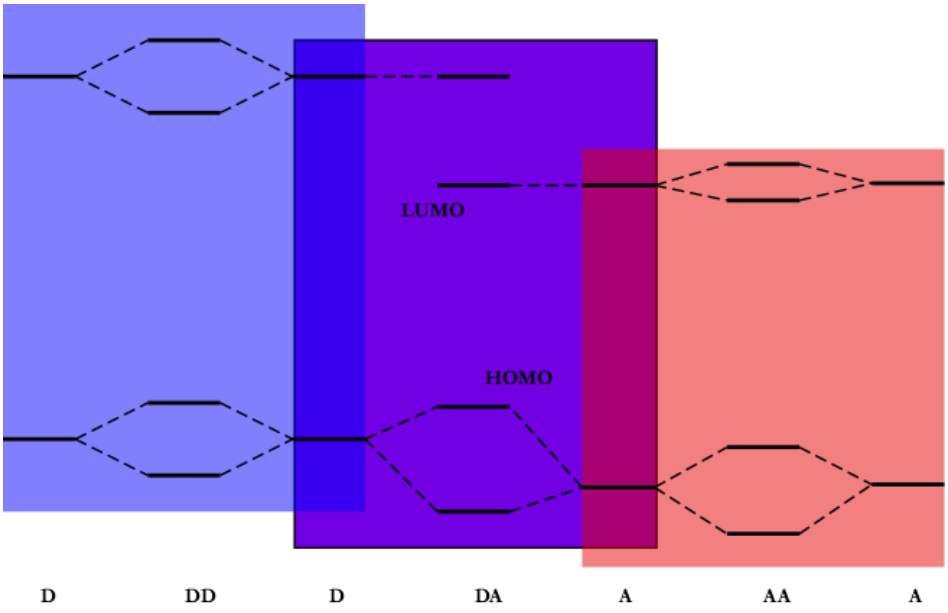

Figure 1.12. Frontier orbital energy level representation of donors and acceptors and the possible hetero- and homo-dimer combinations showing the extent of mixing.[69]

Limitations of D-A Theory

The D-A theory, while potentially useful in low E_g polymer synthesis, does have its limitations. For one, the validity of the theory has been questioned in that it may not be D or A moieties at all that result in lower E_g materials, but rather the alternation between aromatic and quinoidal units.[51] As mentioned in the previous section, it has been shown that increasing the quinoidal contribution to the ground state has a direct effect on reducing the bandgap. In Figure 1.13 some typical donor and acceptor moieties are shown. Interestingly all the common donor species depicted have a stabilized aromatic ground state while the acceptor species have a stabilized quinoidal ground state.[1] Whether or not this translates to increasing the quinoidal contribution to the ground state with a corresponding increase in double bond character of the resulting alternating copolymers when these donor and acceptors are paired has been disputed and is the subject of chapter 3 of this dissertation.

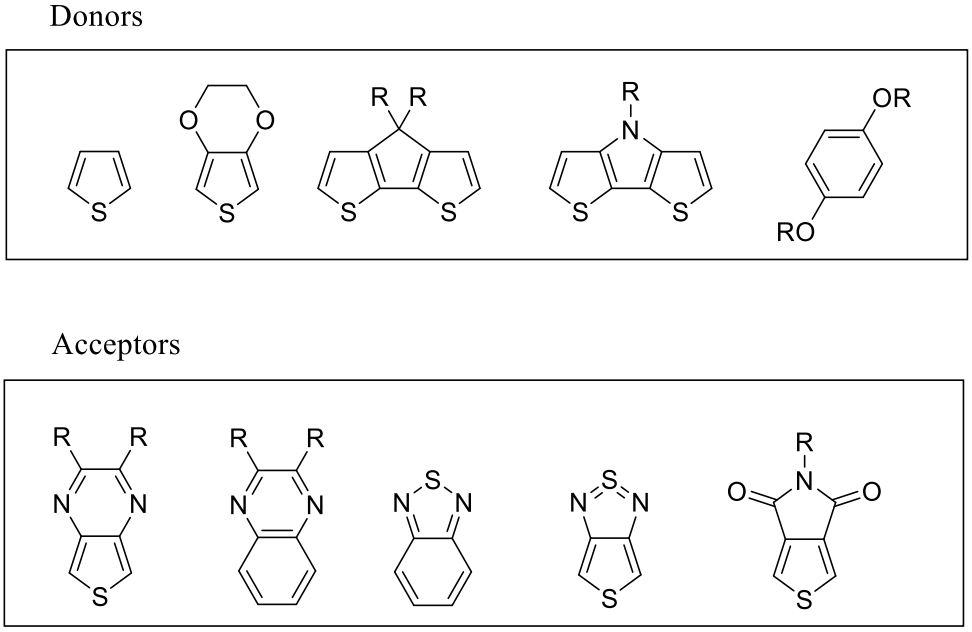

Figure 1.13. Common donors and acceptors used in conjugated polymer synthesis.

An additional issue arises when trying to categorize a species as either donor, acceptor, or spacer units. As mentioned previously the donor unit has a high-lying HOMO and is electron rich, the acceptor has a low-lying LUMO and is electron deficient. However, the spacer unit is often considered to have minimal contributions to the HOMO or LUMO and any reduction in E_g due to their incorporation in a CP is often explained by enhanced planarity of the CP backbone.[52] This understanding of spacers seems to be flawed in that any species participating in the conjugation path should be contributing to the polymer HOMO. This question of spacer unit contribution to frontier orbitals has since led to investigations into the addition and removal of spacer units and has shown their ability to alter the electronic properties of CPs beyond what a planarity argument alone could produce.[52]

While many species do fit conveniently into each role (donor or acceptor), examples such as thieno[3,4-*b*]pyrazine (TP), which has both strong donor and strong accepting qualities, transcends this definition. Initially TP was only investigated as an acceptor unit until evidence of its high-lying HOMO showed that it could also act as a strong donor comparable to one of the strongest donors, EDOT.[71] This discovery then spurred investigations into the pairing of TP with other acceptors which produced low E_g TP-A copolymers.[61,72] In these TP-A alternating copolymers significant bandgap reductions were observed, which according to the D-A theory should have only been possible with the pairing of an energy matched strong donor with an acceptor.[1,12] This has since led to the classification “ambipolar” for monomers which can act as both donor and acceptor to cover the often overlooked but important species in which this is the case.[21]

Charge Carrier Mobility

In conjunction with bandgap tuning is the ability of electrons and holes (sites with vacated electrons) to move freely throughout the CP backbone as well as between individual polymers in what is known as charge carrier mobility (CCM).[3,4,73] The conductivity of CPs is determined by the mobility of the dominant charge carrier which is typically hole mobility due to the enhanced mobility of positively charged polarons over negatively charged polarons.[3] The simplest and most convenient method for a CCM measurement is with thin-film OFETs due the simplicity of relating the charge transport to the applied electric field of the gate.[3,74] The CCM is crucial for device performance with hole mobilities needing to be at least 0.1 cm^2 V^{-1} s^{-1} and I_{on}/I_{off} ratios greater than 10^6.[3,74] The higher on/off ratios being a good representation of conductivity as it shows the current ratios in the on and off states without an applied voltage and thus how much current leakage is occurring. In addition, the I_{on}/I_{off} ratio shows environmental stability, as this value will decrease with the degradation of the material.[75]

The molecular design of CPs dictates how effective CCM will be along the polymer backbone. At the molecular level this is influenced directly by the charge delocalization and is on the timescale of <10 ps.[76] For the specific ladder-type polymers, poly(*p*-phenylene) analogues, it has been shown that intrachain hole mobilities of up to 600 cm^2/V s can be achieved. Both the intramolecular and intermolecular CCM play a role in the total CCM, but in the solid state intermolecular CCM dominates by an order of magnitude increase in energy transfer rate as has been shown in PEC-PIFTEH (Figure 1.14) materials.[77]

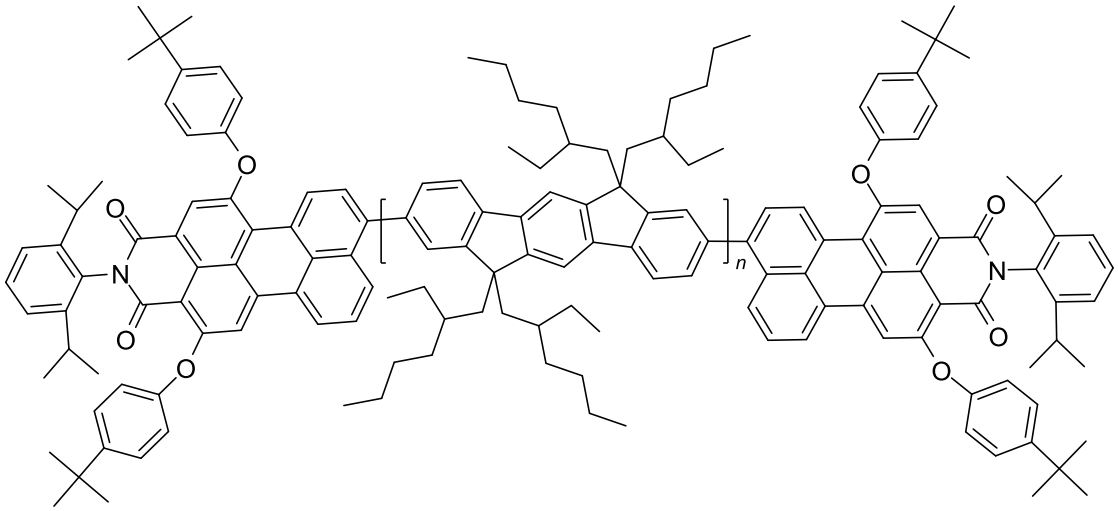

Figure 1.14. Structure PEC-PIFTEH.

As with most investigations on CP properties, polythiophene has been used as a model system to look at CCM in OFETs. A key finding in this area is the enhancement of mobilities of polythiophenes when sidechains are oriented consistently in a regioregular linkage. This will be discussed further in the next section, but as a note of importance, regiorandom polythiophenes have mobilities in the range of 10^{-4} to 10^{-5} cm^2 V^{-1} s^{-1} whereas regioregular polythiophenes have achieved mobilities up to 0.7 cm^2 V^{-1} s^{-1}.[74,78] Along with the regioregularity enhancement of mobilities, the larger molecular weight samples (M_n > 25 kDa) also provide high mobilities with the determining factor being good intermolecular mobility between crystalline domains.[79]

Side-Chain Tuning for Solubility and Processability

One of the often-stated benefits of CPs over their inorganic counterparts is their solubility and solution processability.[80] This feature of CPs allows for various processing techniques such as inkjet printing[81,82], spin coating[83], blade coating[84,85], and drop-casting with the potential application for large scale manufacturing of CP devices. While it is true that CPs can be solution processed, the specifics vary by the polymer system and each CP typically requires the tailoring of parameters to provide optimal device performance. Solubilizing side-chains is often the

answer for enhanced solution processability, but may introduce unwanted steric interactions and thus disrupt interchain charge mobility.[86] It then becomes crucial for sidechains to be oriented in a regioregular fashion to increase the crystallinity and coplanarity for ordered packing.[87] This in turn, can directly affect the electronic properties such as the bandgap, and hole mobility.[88] Additionally, the solubility of a given polymer will determine the polymer properties by impacting critical parameters such as molecular weight and polydispersity.

Poly(3-hexylthiophene) and Regioregularity

Investigations into poly(3-hexylthiophene) (P3HT) specifically have shown that the method of linking the monomers together can have a significant impact on the resultant polymer properties due to the presence of non-equivalent α-positions on 3-hexylthiophene allowing for variations in the final polymer product.[89,90] These are due to the three possible couplings, 2,5'-(head-to-tail, HT) 2,2′-(head-to-head, HH) and 5,5′-(tail-to-tail, TT) and are shown in Figure 1.15. The variable coupling sites can then result in four possible thiophene triads which have different proximities of adjacent side chains. If a polymer has a consistent linkage throughout the polymer it is said to be regioregular whereas if the linkage is inconsistent it is denoted as regiorandom.

In a regioregular sample of P3HT the improvement to the crystallinity has been shown by the presence of X-ray diffraction (XRD) patterns at 2Θ= 5.4˚, 10.8˚, and 16.3˚ which do not exist for regiorandom P3HT.[91] As far as the property changes, hole mobilities have been shown to increase from 10^{-5} cm^2 V^{-1} s^{-1} for regiorandom P3HT to 0.2 cm^2 V^{-1} s^{-1} for regioregular P3HT samples.[91] Shifts in absorption maximum are also observed in both solution and the solid state with increases to regioregularity. A 50% regioregular P3HT produced higher energy (blue-

shifted) peaks at 413 nm in solution and 420 nm in the solid-state when compared to an 80% regioregular sample produced 440 nm in solution and 518 nm absorption maximum in the solid-state.[92]

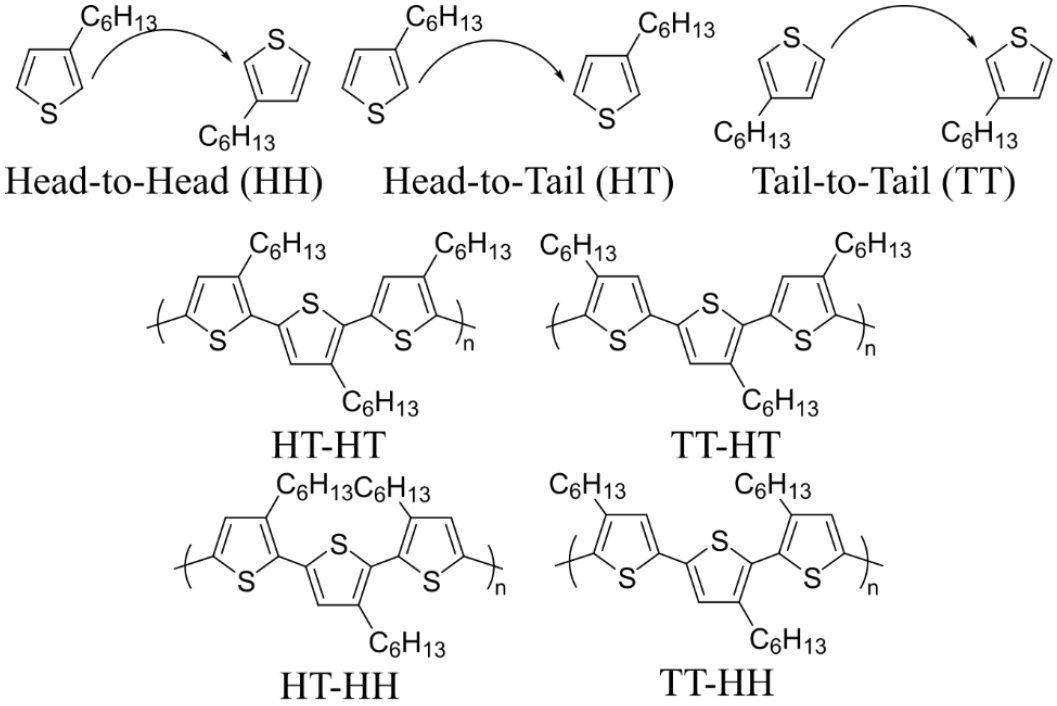

Figure 1.15. Allowable regiochemistry of P3HT with the three possible types of coupling between monomeric units.

Side Chain Tuning to Enhance Properties of CPs

Along with the regiochemistry, the type and length of sidechains also plays a significant role in the processability and resultant properties of the CP.[93-95] Without the presence of solubilizing sidechains CPs are typically insoluble in most common organic solvents.[96] In addition to simply being solution processible, the CPs must also blend sufficiently with other components in devices to reach optimal efficiency.[93] This tradeoff between optimal electronic properties of the CPs and the actual device performance has been investigated thoroughly and in the case of a set of polyphenylene polymers that showed very similar optical absorption and

electrochemical behavior, significant deviations in device performances were reported.[93] This was largely rationalized due to the variations in domain size that were observed with changes in sidechain length and quantity on the CPs. In the set of thiophene-quinoxaline-dialkoxybenzene copolymers (LBPP-2,5,6) investigated LBPP-6 when compared to LBPP-2 and LBPP-5 is absent two octyloxy and butoxy groups respectively on the pendant phenyl rings of the quinoxaline unit (Figure 1.16). This alteration was shown to produce drastic changes in morphology of the CP/Phenyl-C61-butyric acid methyl ester (PCBM) devices as made apparent by atomic force microscopy measurements.

The eventual findings for all CPs were that shorter alkyl lengths produced smaller domain sizes and better performing devices. Improvements in device efficiency by this sidechain adjustment were limited however in that for LBPP-6 where no alkyl substituents are present on the pendant phenyl rings of the quinoxaline unit, the solubility of the polymer was so low that the overall molecular weights of the polymers produced became a limiting factor and caused reductions in mobilities and in turn poorer performing devices.[93]

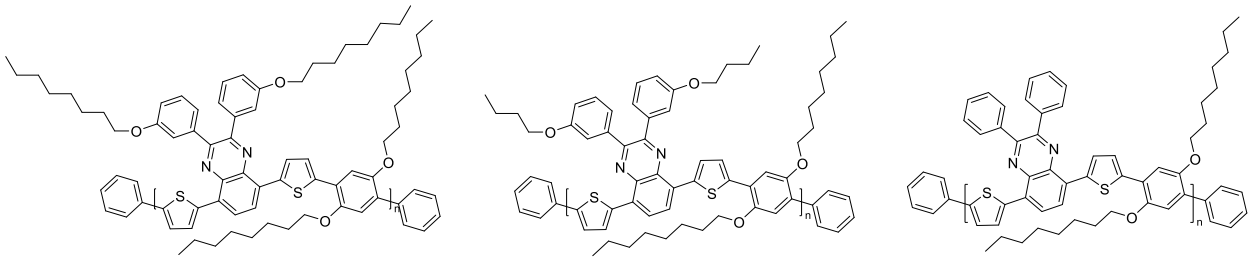

Figure 1.16. Thiophene-quinoxaline-dialkoxybenzene copolymers with side-chain tuning.[93]

Devices

The quest for further reductions/tuning of bandgaps, enhanced electron/hole mobilities, and improved processabilities is all pursued with the end goal of fabricating devices that either

compete with inorganic devices currently available or provide devices with new properties previously unavailable. Low-bandgap materials as active layers in OPVs are the most common device application[22] with others such as supercapacitors[22,50], polymer light-emitting diodes (PLEDs)[98], electrochromic materials[99], OFETs[100], coatings for corrosion control[101], and near-infrared (NIR) photodetectors[102] gaining increasing attention as the field advances. The three of which that will be discussed here due to their relevance to the present research are OPVs, NIR photodetectors, and OFETs.

OPV Design

An OPV works on the principle of the photovoltaic effect in which illumination on the photoactive layer of the device causes the generation of holes and electrons which migrate to opposite electrodes due to the potential difference between junctions within the cell (Figure 1.17).[103] In an inorganic PV device this charge generation is a free electron and free hole while in a typical OPV they are generated as a electrostatically bound electron/hole pair known as an exciton. The offset in energy between the HOMO of an electron donating layer and the LUMO of an electron accepting layer in the OPV then allows for a dissociation of these excitons into free charge carriers (i.e., unbound holes and electrons) which can flow to opposite electrodes and generate a current.[103,104] A hurdle in the design of OPVs however is that excitons have a limited lifetime (less than 1 ns) and a limited diffusion length (less than 20 nm) and thus a significant potential for geminate electron hole recombination prior to interaction with donor-acceptor interface.[104,105] This proves to be specifically challenging for single layer and bi-layer devices where the interfaces required for charge separation can be around 100 to 200 nm apart due to the thickness of each thin-film layer.[104] A solution to this problem is the fabrication of devices with a mixed photoactive electron donor species and electron acceptor species in what is known as a

bulk heterojunction (BHJ) solar cell. In a BHJ, the distance an exciton needs to travel for charge separation is dictated by the domain sizes of the donor and acceptor materials and thus can be tuned by molecular design and processing methods.

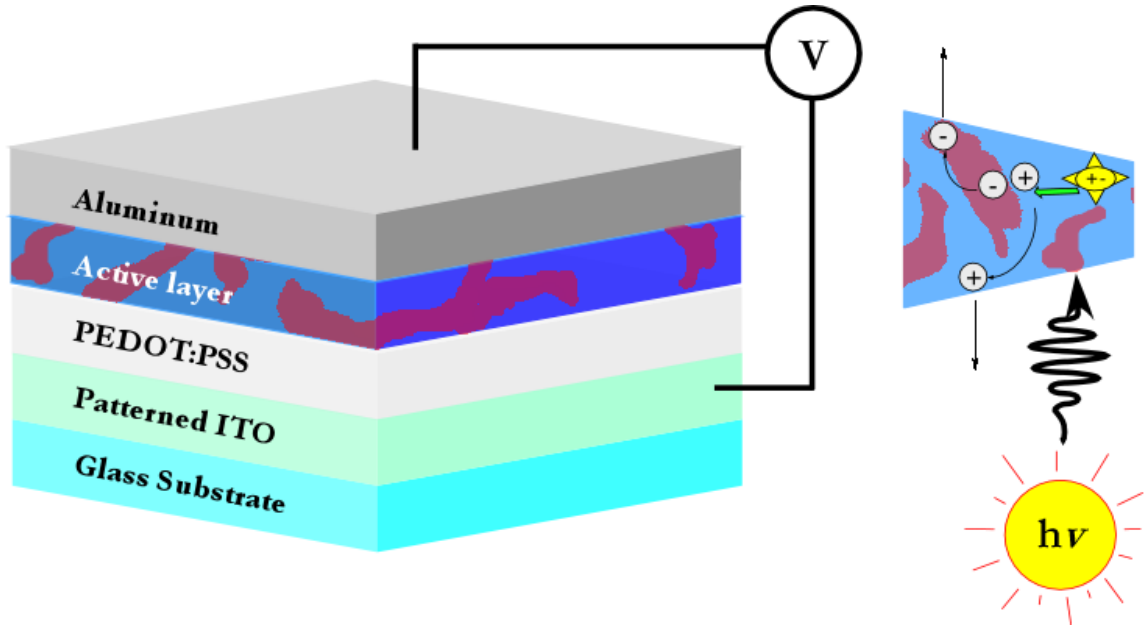

Figure 1.17. (left) Bulk heterojunction solar cell and (right) photoactive layer exciton generation followed by charge separation and migration.

NIR Photodetectors

In addition to the light harvesting application of OPVs is the light detection of organic photodetectors in a multitude of functions such as photoconductors[106,107], photodiodes[106-108], and phototransistors[106,108]. The principle and device structure in general are the same with the absorption of light generating charge that can be separated to generate a current. Where these types of devices differ however is that instead of simply looking at external quantum efficiency as the focus of device performance, other parameters become important such as specific detectivity which rates the ability of the device to detect weak intensity signals for roles such as optical communication, remote control, and chemical sensing.[102] These potential applications

have brought forth the need for materials which can probe further into the NIR which until recently was unachievable due to an E_g less than 1.5 eV being unavailable until only recently.[1,12]

OFET Design and Mobility Measurements

Another type of device that does not require the light harvesting properties of CPs but certainly depends on the semiconducting properties of CPs are OFETs. These devices are necessary components for the realization of fully organic integrated circuits and thus their development is paramount in the field of organic electronics.[109] In addition, OFETs are extremely valuable in our understanding of CP materials because they can provide information about CCM. In a specific case study of P3HT OFET devices it was found that different processing methods produced variations in how polymers stacked (parallel or normal to the substrate) and an over 100-fold increase in CCM (up to 0.1 $cm^2\ V^{-1}\ s^{-1}$).[35] The rationale for this increase in CCM being that in OFET devices the CCM is limited by π–π interchain rather than intrachain transport and thus when the orientation of polymer domains coincide with that of the OFET substrate, charge carriers have significantly improved π–π interchain interactions. This then increases the π–π interchain hopping and allows for more 2-D- charge transport as opposed 1-D transport along via intrachain transport.[35]

Research Goals

The promise of conjugated polymers in a variety of electronic devices is now a realized accomplishment and likely to grow in scope of application. For the field to continue to develop, our understanding of the structure-property relationships within CPs must also be advanced so that materials can be designed with an increasing ability to judiciously select appropriate materials for device application and performance. This includes reaching further into the bandgap energy well and designing materials that approach bandgaps closer to 0 eV through the

incorporation of new fused rings onto the already low bandgap poly(TP). It also includes the refinement of commonly evoked models for CP design such as the D-A theory which finds its limits tested with species such as TP that do not fit into this dichotomous grouping. This refinement requires model oligomeric systems to be developed that simplify the picture while also shedding light on the true nature of D-A interactions.

Additionally, for CPs to see increased applicability, the routes in which they are synthesized need to be increasingly green and economical. This requires new polymerization methods such as direct arylation polymerization (DArP) that reduce toxic byproducts as well as the total number of synthetic steps from monomer to polymer. Using DArP as an alternative to traditional cross-coupling methods requires a fine-tuning of reaction conditions for all CP systems investigated and therefore to optimize conditions requires an extensive survey of the reagents involved. Chapter four exhibits the synthetic results of TP-A copolymers coupled with device data to show how these polymers synthesized via DArP compare to their traditionally coupled counterparts. Lastly, in addition to the DArP optimization study, the effects of sidechains on the polymer properties have also been investigated and reported. This last avenue of the investigation looks at the variability in side-chain length and branching on the molecular weight and electronic properties of the polymers produced via DArP and under variable conditions.

References

1. Rasmussen, S. C. Low-Bandgap Polymers. *Encylopedia of Polymeric Nanomaterials;* Müllen, K. Ed.; Springer-Verlag: Berlin, **2015**; pp 1155-1166

2. Heeger, A. J. *Chem. Soc. Rev.* **2010**, *39* (7), 2354–2371.

3. Tiwari, S.; Greenham, N. C. *Opt. Quantum Electron.* **2009**, *41* (2), 69–89.

4. Coropceanu, V.; Cornil, J.; da Silva Filho, D. A.; Olivier, Y.; Silbey, R.; Brédas, J. L. *Chem. Rev.* **2007**, *107* (4), 926–952.

5. The Nobel Prize in Chemistry 2000. https://www.nobelprize.org/prizes/chemistry/2000/summary/, (accessed January 11, 2022)

6. Rasmussen, S.C. *Conductive Polymers: Electrical Interactions in Cell Biology and Medicine*; Zhang, Z., Rouabhia, M., Moulton, S., Eds.; CRC Press: Boca Raton, FL, USA, 2016.

7. Rasmussen, S. C. *Subst.* **2017**, *1* (12), 99–109.

8. Rasmussen, S. C. *Chempluschem* **2020**, *85* (7), 1412–1429.

9. Shirakawa, H.; Louis, E. J.; MacDiarmid, A. G.; Chiang, C. K.; Heeger, A. J. *J. Chem. Soc. Chem. Commun.* **1977**, No. 16, 578–580.

10. Chiang, C. K.; Park, Y. W.; Heeger, A. J.; Shirakawa, H.; Louis, E. J.; MacDiarmid, A. G. *J. Chem. Phys.* **1978**, *69* (11), 5098–5104.

11. Rasmussen, S. C. *AZoM* **2011**, 1–6. http://www.azom.com/article.aspx?ArticleID=5591

12. Rasmussen, S. C.; Pomerantz, M. In *Handbook of Conducting Polymers*, Skotheim T. A., Reynolds J. R., Eds.; Conjugated polymers: theory, synthesis, properties, and characterization. Handbook of conducting polymers, 3rd edn. CRC Press, Boca Raton, 2007, pp 12-1–12-42.

13. Rasmussen, S.C; Ogawa, K.; S. D. Rothstein, *Handbook of Organic Electronics and Photonics*, Nalwa, H. S. Ed.; American Scientific Publishers, Stevenson Ranch, CA, 2008, ch.1, vol. 1.

14. Logothetidis, S. *J. mater. Sci. eng.,B* **2008**, *152* (1), 96–104.

15. Sekitani, T.; Someya, T. *Adv. Mater.* **2010**, *22* (20), 2228–2246.

16. de Leeuw, D. M.; Cantatore, E. *Mater. Sci. Semicond. Process.* **2008**, *11* (5), 199–204.

17. Allen, K. J. *Proc. IEEE* **2005**, *93* (8), 1394–1399.

18. Forrest, S. R. *Nature* **2004**, *428* (6986), 911–918.

19. Matsui, H.; Takeda, Y.; Tokito, S. *Org. Electron.* **2019**, *75*, 105432.

20. Berggren, M.; Nilsson, D.; Robinson, N. D. *Nat. Mater.* **2007**, *6* (1), 3–5.

21. Wen, L.; Heth, C. L.; Rasmussen, S. C. *Phys. Chem. Chem. Phys.* **2014**, *16* (16), 7231–7240.

22. Roncali, J. *Chem. Rev.* **1997**, *97*, 173–205.

23. Brédas, J. L. *Electronic Properties of Polymers and Related Compounds*, H. Kuzmany, M. Mehring, and S. Roth, Eds., Springer Series in Solid-State Sciences, Springer-Verlang: Berlin, 1985, Vol 63, pp 166-172.

24. Brédas, J. L. *J. Chem. Phys.* **1985**, *82* (8), 3808–3811.

25. Brédas, J. L.; Silbey, R.; Boudreaux, D. S.; Chance, R. R. *J. Am. Chem. Soc.* **1983**, *105* (22), 6555–6559.

26. Ma, J.; Li, S.; Jiang, Y. *Macromolecules* **2002**, *35* (3), 1109–1115.

27. Tachibana, M.; Tanaka, S.; Yamashita, Y.; Yoshizawa, K. *J. Phys. Chem. B* **2002**, *106* (14), 3549–3556.

28. Price, W. C. *Phys. Rev.* **1935**, *47* (6), 444–452.

29. Bohlmann, F.; Mannhardt, H.-J. *Chem. Ber.* **1956**, *89* (5), 1307–1315.

30. Fincher, C. R.; Peebles, D. L.; Heeger, A. J.; Druy, M. A.; Matsumura, Y.; MacDiarmid, A. G.; Shirakawa, H.; Ikeda, S. *Solid State Commun.* **1978**, *27* (5), 489–494.

31. Cornil, J.; Beljonne, D.; Calbert, J.-P.; Brédas, J.-L. *Adv. Mater.* **2001**, *13* (14), 1053–1067.

32. Grimme, S. *Angew. Chem. Int. Ed.* **2008**, *47* (18), 3430–3434.

33. Cozzi, F.; Ponzini, F.; Annunziata, R.; Cinquini, M.; Siegel, J. S. *Angew. Chem. Int. Ed.* **1995**, *34* (9), 1019–1020.

34. Martinez, C. R.; Iverson, B. L. *Chem. Sci.* **2012**, *3* (7), 2191–2201.

35. Sirringhaus, H.; Brown, P. J.; Friend, R. H.; Nielsen, M. M.; Bechgaard, K.; Langeveld-Voss, B. M. W.; Spiering, A. J. H.; Janssen, R. A. J.; Meijer, E. W.; Herwig, P.; Deeleuw, D. M. *Nature* **1999**, *401*, 685–688.

36. Elgrishi, N.; Rountree, K. J.; McCarthy, B. D.; Rountree, E. S.; Eisenhart, T. T.; Dempsey, J. L. *J. Chem. Educ.* **2018**, *95* (2), 197–206.

37. Cardona, C. M.; Li, W.; Kaifer, A. E.; Stockdale, D.; Bazan, G. C. *Adv. Mater.* **2011**, *23* (20), 2367–2371.

38. Kinbara, E.; Kunugi, Y.; Harima, Y.; Yamashita, K. *Synth. Met.* **2000**, *114* (3), 295–303.

39. Kar, P. *Doping in Conjugated Polymers*; Scrivener Publishing: Beverly, MA, 2013: pp 20-30.

40. Rasmussen, S. C. *Chempluschem* **2020**, *85* (7), 1412–1429.

41. Simitzis, J.; Zoumpoulakis, L. *J. Mater. Sci.* **1996,** 31 (6), 1615–1620.

42. Van Mullekom, H. A. M.; Vekemans, J. A. J. M.; Havinga, E. E.; Meijer, E. W. *Mater. Sci. Eng.* **2001**, *32*, 1–40.

43. Bäuerle, P.; Segelbacher, U.; Maier, A.; Mehring, M. *J. Am. Chem. Soc.* **1993**, *115* (22), 10217–10223.

44. van Haare, J. A. E. H.; Groenendaal, L.; Peerlings, H. W. I.; Havinga, E. E.; Vekemans, J. A. J. M.; Janssen, R. A. J.; Meijer, E. W. *Chem. Mater.* **1995**, *7* (10), 1984–1989.

45. Heeger, A. J.; Kivelson, S.; Schrieffer, J. R.; Su, W. P. *Rev. Mod. Phys.* **1988**, *60* (3), 781–850.

46. MacDiarmid, A. G.; Epstein, A. J. *Faraday Discuss. Chem. Soc.* **1989**, *88*, 317–332.

47. MacDiarmid, A. G.; Epstein, A. J. *Synth. Met.* **1994**, *65* (2–3), 103–116.

48. Kim, Y. H.; Foster, C.; Chiang, J.; Heeger, A. J. *Synth. Met.* **1988**, *26* (1), 49–59.

49. Lux, F. *Polymer.* **1994**, *35* (14), 2915–2936.

50. Rasmussen, S. C.; Schwiderski, R. L.; Mulholland, M. E. *Chem. Commun*. **2011**, 47 (41), 11394.

51. Kertesz, M.; Yang, S.; Tian, Y *Handbook of thiophene-based materials: applications in organic electronics and photonics*, Perepichka, I.F., Perepichka, D.F. Eds., Wiley, West Sussex, vol. 1, pp 341–364.

52. Mulholland, M. E.; Konkol, K. L.; Anderson, T. E.; Schwiderski, R. L.; Rasmussen, S. C. *Aust. J. Chem.* **2015**, *68* (11), 1759–1766.

53. Yang, S.; Kertesz, M. *J. Phys. Chem. A* **2006**, *110* (31), 9771–9774.

54. Peierls, R. *Quantum Theory of Solids*; Oxford University Press: Oxford, 1955; p 108.

55. Hudson, B. S. *Materials.* **2018**, *11* (242).

56. Barborini, M.; Guidoni, L. *J. Chem. Theory Comput.* **2015**, *11* (9), 4109–4118.

57. Choi, C. H.; Kertesz, M.; Karpfen, A. *J. Chem. Phys.* **1997**, *107* (17), 6712–6721.

58. Yannoni, C. S.; Clarke, T. C. *Phys. Rev. Lett.* **1983**, *51* (13), 1191–1193.

59. Bredas, J. L.; Themans, B.; Fripiat, J. G.; Andre, J. M. *Phys. Rev. B - Condens. Matter Mater. Phys.* **1984**, *29* (12), 6761–6773.

60. Wudl, F.; Kobayashi, M.; Heeger, A. J. *J. Org. Chem.* **1984**, *49* (18), 3382–3384.

61. Anderson, T. E.; Culver, E. W.; Almyahi, F.; Dastoor, P. C.; Rasmussen, S. C. *Synlett* **2018**, *29* (19), 2542–2546.

62. Brédas, J. L.; Heeger, A. J.; Wudl, F. *J. Chem. Phys.* **1986**, *85* (8), 4673–4678.

63. Abdulkarim, A.; Hinkel, F.; Jänsch, D.; Freudenberg, J.; Golling, F. E.; Müllen, K. *J. Am. Chem. Soc.* **2016**, *138* (50), 16208–16211.

64. Vessally, E. *J Struct Chem*, **2008**, 49, 979–985.

65. Cutler, C. A.; Burrell, A. K.; Officer, D. L.; Too, C. O.; Wallace, G. G. *Synth. Met.* **2002**, *128* (1), 35–42.

66. Havinga, E. E.; ten Hoeve, W.; Wynberg, H. *Polym. Bull.* **1992,** 29, 119−126.

67. Havinga, E. E.; ten Hoeve, W.; Wynberg, H. *Synth. Met.* **1993**, *55* (1), 299–306.

68. Havinga, E. E.; Pomp, A.; ten Hoeve, W.; Wynberg, H. *Synth. Met.* **1995**, *69* (1–3), 581–582.

69. Anderson, T. E.; Culver, E. W.; Badı-Dominguez, I.; Wilcox, W. D.; Buysse, C. E.; Ruiz Delgado, M. C.; Rasmussen, S. C. *Phys. Chem. Chem. Phys.* **2021**.

70. Van Mullekom, H. A. M.; Vekemans, J. A. J. M.; Havinga, E. E.; Meijer, E. W. *Mater. Sci. Eng.* **2001**, *32*, 1–40.

71. Mulholland, M.; Schwiderski, R.; Evenson, S.; Rasmussen, S. *Polym. Eng.* **2012**, *107*, 36–37.

72. Culver, E. W.; Anderson, T. E.; López Navarrete, J. T.; Ruiz Delgado, M. C.; Rasmussen, S. C. *ACS Macro Lett.* **2018**, *7* (10), 1215–1219.

73. Zade, S. S.; Bendikov, M., *Handbook of thiophene-based materials: applications in organic electronics and photonics*, Perepichka, I. F., Perepichka, D. F. Eds., Wiley, West Sussex, 2009, pp 365-4177.

74. Ewbank, P. C.; Stefan, M.C.; Geneviéve, S.; McCullough, R. D. *Handbook of thiophene-based materials: applications in organic electronics and photonics*, Perepichka, I. F., Perepichka, D. F. Eds., Wiley, West Sussex, 2009, vol. 1, pp 157–217.

75. McCulloch, I.; Heeney, M.; Bailey, C.; Genevicius, K.; MacDonald, I.; Shkunov, M.; Sparrowe, D.; Tierney, S.; Wagner, R.; Zhang, W.; Chabinyc, M. L.; Kline, R. J.; McGehee, M. D.; Toney, M. F. *Nat. Mater.* **2006**, *5* (4), 328–333.

76. Fratini, S.; Nikolka, M.; Salleo, A.; Schweicher, G.; Sirringhaus, H. *Nat. Mater.* **2020**, *19* (5), 491–502.

77. Beljonne, D.; Pourtois, G.; Silva, C.; Hennebicq, E.; Herz, L. M.; Friend, R. H.; Scholes, G. D.; Setayesh, S.; Müllen, K.; Brédas, J. L. *Proc. Natl. Acad. Sci. U. S. A.* **2002**, *99* (17), 10982–10987.

78. Panzer, M. J.; Frisbie, C. D. *Adv. Funct. Mater.* **2006**, *16* (8), 1051–1056.

79. Chang, J. F.; Clark, J.; Zhao, N.; Sirringhaus, H.; Breiby, D. W.; Andreasen, J. W.; Nielsen, M. M.; Giles, M.; Heeney, M.; McCulloch, I. *Phys. Rev. B - Condens. Matter Mater. Phys.* **2006**, *74* (11), 1–12.

80. Yu, G.; Gao, J.; Hummelen, J. C.; Wudl, F.; Heeger, A. J. *Science (80).* **1995**, *270* (5243), 1789–1791.

81. Sekitani, T.; Noguchi, Y.; Zschieschang, U.; Klauk, H.; Someya, T. *Proc. Natl. Acad. Sci. U. S. A.* **2008**, *105* (13), 4976–4980.

82. Khim, D.; Lee, W. H.; Baeg, K. J.; Kim, D. Y.; Kang, I. N.; Noh, Y. Y. *J. Mater. Chem.* **2012**, *22* (25), 12774–12783.

83. Chang, C. C.; Pai, C. L.; Chen, W. C.; Jenekhe, S. A. *Thin Solid Films* **2005**, *479* (1–2), 254–260.

84. Giri, G.; Li, R.; Smilgies, D. M.; Li, E. Q.; Diao, Y.; Lenn, K. M.; Chiu, M.; Lin, D. W.; Allen, R.; Reinspach, J.; Mannsfeld, S. C. B.; Thoroddsen, S. T.; Clancy, P.; Bao, Z.; Amassian, A. *Nat. Commun.* **2014**, *5* (3573), 1–8.

85. Gu, X.; Yan, H.; Kurosawa, T.; Schroeder, B. C.; Gu, K. L.; Zhou, Y.; To, J. W. F.; Oosterhout, S. D.; Savikhin, V.; Molina-Lopez, F.; Tassone, C. J.; Mannsfeld, S. C. B.; Wang, C.; Toney, M. F.; Bao, Z. *Adv. Energy Mater.* **2016**, *6* (22).

86. Meyer, D. L.; Schmidt-Meinzer, N.; Matt, C.; Rein, S.; Lombeck, F.; Sommer, M.; Biskup, T. *J. Phys. Chem. C* **2019**, *123* (33), 20071–20083.

87. Kiriy, N.; Jähne, E.; Adler, H. J.; Schneider, M.; Kiriy, A.; Gorodyska, G.; Minko, S.; Jehnichen, D.; Simon, P.; Fokin, A. A.; Stamm, M. *Nano Lett.* **2003**, *3* (6), 707–712.

88. Zhang, Z. G.; Li, Y. *Sci. China Chem.* **2015**, *58* (2), 192–209.

89. Pappenfus, T. M.; Almyahi, F.; Cooling, N. A.; Culver, E. W.; Rasmussen, S. C.; Dastoor, P. C. *Macromol. Chem. Phys.* **2018**, *219* (21), 1–8.

90. Pouliot, J.-R.; Wakioka, M.; Ozawa, F.; Li, Y.; Leclerc, M. *Macromol. Chem. Phys.* **2016**, *217* (13), 1493–1500.

91. McCullough, R. D.; Tristram-Nagle, S.; Shawn P, W.; Lowe, R. D.; Jayaraman, M. *J. Am. Chem. Soc.* **1993**, *115* (11), 4910–4911.

92. Xu, B.; Holdcroft, S. *Macromolecules* **1993**, *26* (17), 4457–4460.

93. Lindgren, L. J.; Zhang, F.; Andersson, M.; Barrau, S.; Hellström, S.; Mammon, W.; Perzpn, E.; Inganäs, O.; Andersson, M. R. *Chem. Mater.* **2009**, *21* (15), 3491–3502.

94. Nguyen, L. H.; Hoppe, H.; Erb, T.; Günes, S.; Gobsch, G.; Sariciftci, N. S. *Adv. Funct. Mater.* **2007**, *17* (7), 1071–1078.

95. Inganäs, O.; Svensson, M.; Zhang, F.; Gadisa, A.; Persson, N. K.; Wang, X.; Andersson, M. R. *Appl. Phys. A Mater. Sci. Process.* **2004**, *79* (1), 31–35.

96. Li, W.; Qin, R.; Zhou, Y.; Andersson, M.; Li, F.; Zhang, C.; Li, B.; Liu, Z.; Bo, Z.; Zhang, F. *Polymer (Guildf).* **2010**, *51* (14), 3031–3038.

97. Uke, S. J.; Mardikar, S. P.; Kumar, A.; Kumar, Y.; Gupta, M.; Kumar, Y. *R. Soc. Open Sci.* **2021**, *8* (10).

98. Bhuvana, K. P.; Joseph Bensingh, R.; Abdul Kader, M.; Nayak, S. K. *Polym. - Plast. Technol. Eng.* **2018**, *57* (17), 1784–1800.

99. Beaujuge, P. M.; Reynolds, J. R. *Chem. Rev.* **2010**, *110* (1), 268–320.

100. Pandey, M.; Kumari, N.; Nagamatsu, S.; Pandey, S. S. *J. Mater. Chem. C.* **2019**, *7* (43), 13323–13351.

101. Yan, M.; He, J.; Tallman, D. E.; Rasmussen, S.; Bierwagen, G. *ECS Trans.* **2009**, *16* (52), 183–194.

102. Rasmussen, S. C.; Gilman, S. J.; Culver, E. W.; Wilcox, W. D. *Gen. Chem.* **2021**, *7*, 200019(1–6).

103. Liang, Z.; Wang, Q. Conjugated Polymer Based Solar Cells in *Handbook of Organic Electronics and Photonics*, ed. H. S. Nalwa, American Scientific Publishers, Stevenson Ranch, CA, 2008, pp 177- 223.

104. Tamai, Y.; Ohkita, H.; Benten, H.; Ito, S. *J. Phys. Chem. Lett.* **2015**, *6* (17), 3417–3428.

105. Wojcik, M.; Michalak, P.; Tachiya, M. *Appl. Phys. Lett.* **2010**, *96* (16).

106. Li, Q.; Guo, Y.; Liu, Y. *Chem. Mater*. **2019**, 31, 6359–6379.

107. Chow, P. C. Y.; Someya, T. *Adv. Mater*. **2020,** 32, 1902045.

108. Li, N.; Lan, Z.; Cai, L.; Zhu, F. *J. Mater. Chem*. C **2019**, 7, 3711– 3729.

109. Cui, T., Liu, Y. *Handbook of Organic Electronics and Photonics*, ed. H. S. Nalwa, American Scientific Publishers, Stevenson Ranch, CA, 2008, pp 263- 303.

CHAPTER 2. EXTENDED RING THIENO[3,4-*b*]PYRAZINES

Introduction

A method that allows for further tuning of the electronic properties of thieno[3,4-*b*]pyrazine (TP) building blocks and their respective materials is through the incorporation of additional fused rings onto the pyrazine portion of TP.[1–4] This strategy is of interest due to the possibility of bandgap (E_g) reduction through stabilization of the LUMO for which the pyrazine portion of TP is largely responsible while having less of an effect on the destabilization of the HOMO for which thiophene is the main contributor.[1,3–5] Furthermore, the quinoidal contribution from the pyrazine portion of TP can also be modified through the addition of extended fused-rings (ERs) and thus the modification with respect to all these parameters is of particular importance for production of low E_g conjugated materials.[4]

Extended Ring Thieno[3,4-b]pyrazines With Conjugation Extension

Upon the incorporation of ERs, the destabilization of the HOMO and stabilization of the LUMO due to extended conjugation can produce TP analogues with overall smaller HOMO-LUMO gaps and resultant polymers with more quinoidal character in the ground state.[1–4,6] These HOMO-LUMO reductions have been shown in a variety of examples (Figure 2.1) experimentally by their characteristic lower energy reductions and oxidations.[3] The drawback of this additional conjugation is that in many cases, the polymers of these extended analogues are sparingly soluble or completely insoluble, limiting both their applicability to devices as well as the ability to fully characterize them.[3,4] This solubility deficiency is thought to be largely due to the enhanced rigidity in addition to the lack of solubilizing side-chains for many examples.[3] So, while extended ring TPs (ERTPs) are a route to ever decreasing low E_g systems, further tailoring is required to make these materials processable for future device applications.

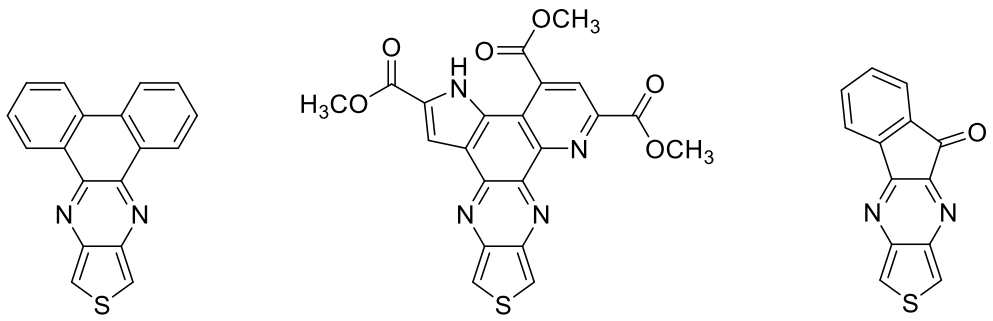

Figure 2.1. Examples of extended ring thieno[3,4-*b*]pyrazines with extended conjugation.[6–8]

Modifying the Thieno[3,4-b]pyrazine Frontier Orbitals Through Nonconjugated Ring Fusion

While an approach based on increasing the conjugation does seem to be the most significant in terms of HOMO-LUMO gap reductions, the ability to modify the LUMO of TP at the pyrazine *b*-face with the fusion of nonconjugated ERs also allows for further fine-tuning of MOs. This is significant for TP materials because the already elevated HOMO can result in oxidative instability, limiting their usage in devices.[9] These types of ERTPs (Figure 2.2) are a separate class in that conjugation is not extended through the EFR and all MO modifications occur through electron donating and withdrawing effects.

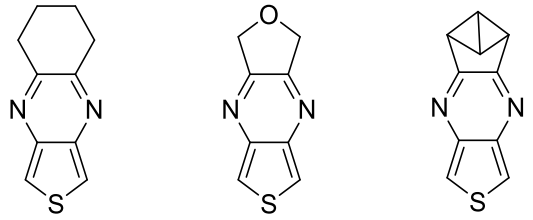

Figure 2.2. Examples of extended ring thieno[3,4-*b*]pyrazines without extended conjugation.[10–12]

Initial Work on Extended Ring Thieno[3,4-b]pyrazines

Synthesis of an isolable ERTP monomer was first reported by Tanaka and Yomashita in 1997 with the synthesis of $2\lambda^4\delta^2$-[1,2,5]thiadiazolo[3,4-*b*]thieno[3,4-*e*]pyrazine (TdzTP) and its analogues (Figure 2.3).[13] The intention of this work was to produce new monomers with

narrowed HOMO-LUMO gaps due to increased delocalization and the enhancement of the quinoidal ground state in alternating copolymer systems.[13,14]

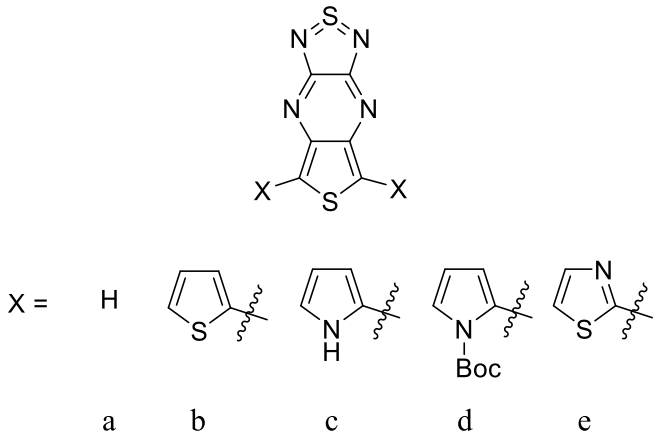

Figure 2.3. $2\lambda^4\delta^2$-[1,2,5]thiadiazolo[3,4-*b*]thieno[3,4-*e*]pyrazine and its analogues.[13]

While the parent ERTP was found to be unstable for this system, the trimers were chemically stable enough to undergo electrochemical characterization.[13,14] This electrochemical analysis indeed showed that the fused ring trimer systems significantly narrowed the HOMO/LUMO gap when compared to the parent unfunctionalized TP with the gap shrinking from 2.19 to 1.06 eV for the TP-terthienyl and the TdzTP-terthienyl respectively.[14] Likewise the TdzTP-terthienyl polymer was determined electrochemically to have the lowest E_g of all species investigated with a value of 0.3 eV and later followed up with an optical E_g measurement of 0.5 eV.[13,14] This seminal work showed that the design motif of ERTPs could be a powerful tool for E_g reduction, but were still restricted to copolymer systems. The synthesis of ERTP homopolymers would not occur until the early 2000s largely in part due to the Rasmussen group advancing and optimizing TP monomer synthesis.[11,15]

Previous Rasmussen Work on Extended TPs

The ability to tune the electronic properties of TP by the addition of fused rings was initially attempted by the Rasmussen group with acenaphtho[1,2-*b*]thieno[3,4-*e*]pyrazine (ATP).[16] The ATP homopolymer was shown to have the unique ability of reducing the bandgap when compared to poly(2,3-dialkylthieno[3,4-*b*]pyrazines) (pTP) while also being a much more stable to overoxidation.[16,17] The added ring only had a substantial effect on the stabilization of the LUMO (bottom of theconduction band of the polymer) and therefore the reduction in bandgap was not at the cost of polymer stability.[16,17]

The synthesis of ATP was carried out similarly to previous TP analogues[15], by reacting 3,4-diaminothiophene with acenaphthenequinone as the appropriate dione to undergo a double condensation and form the pyrazine ring (Figure 2.4).[16,17] With the monomer in hand, polymerizations were carried out electrochemically via oxidative polymerization (Figure 2.4) allowing for oxidation/reduction potentials to be determined in the process.[16,17] The observed thin film potential at which oxidation occurs fell between the two poly(2,3-dioctylthieno[3,4-*b*]pyrazine) (pC_8TP) oxidation peaks of -250 mV and 130 mV at -25 mV (vs. Ag/Ag^+).[16] Of the two oxidation peaks for pC_8TP the -250 mV peak is the larger of the two and therefore the oxidation at -25 mV of poly(acenaphtho[1,2-*b*]thieno[3,4-]pyrazine) (pATP) indicates a slightly more easily oxidized polymer overall. The reduction potential was not only much lower (-970 mV vs. Ag/Ag^+) than previous TP analogues[18] but was also shown to be significantly more reversible indicating an expected stability that the additional fused ring on pyrazine provides without the undesirable HOMO destabilization.[16–18] The electrochemical bandgap was then calculated by the oxidation and reduction onsets of pATP films and found to be ~0.45 eV.[16]

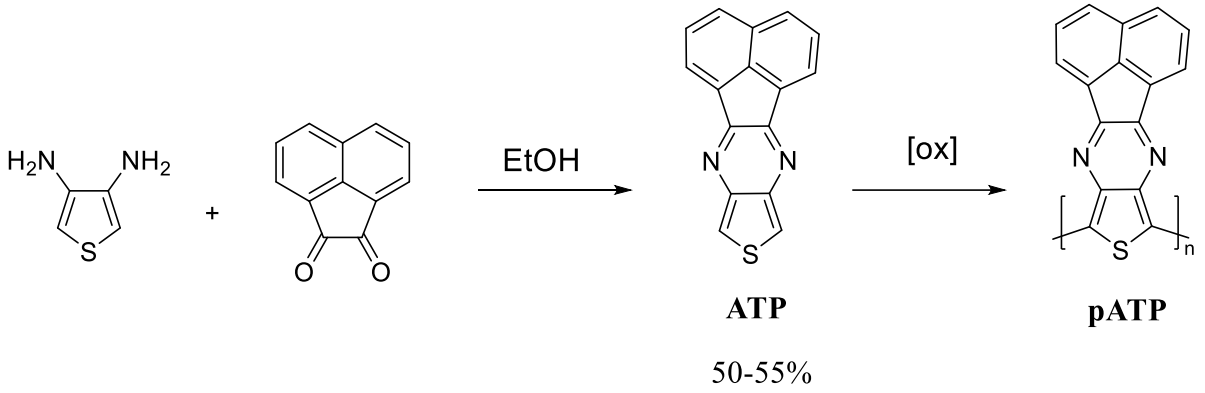

Figure. 2.4. Synthesis of acenaphtho[1,2-*b*]thieno[3,4-*e*]pyrazine via condensation of 2,3-diamminothiophene with acenaphthenequinone followed by electrochemical oxidative polymerization.[16,17]

To further probe the impacts of extended conjugation on the TP unit, the Rasmussen group looked at four additional species: 3,4-dibromoacenaphtho[1,2-*b*]thieno[3,4-*e*]pyrazine ($ATPBr_2$), 3-octylacenaphtho[1,2-*b*]thieno[3,4-*e*]pyrazine ($ATPC_8H_{17}$), dibenzo[*f*,*h*]thieno[3,4-*b*]quinoxaline (DBTQ), and thieno[3',4':5,6]pyrazino[2,3-*f*][1,10]phenanthroline (TPP) (Figure 2.5).[2]

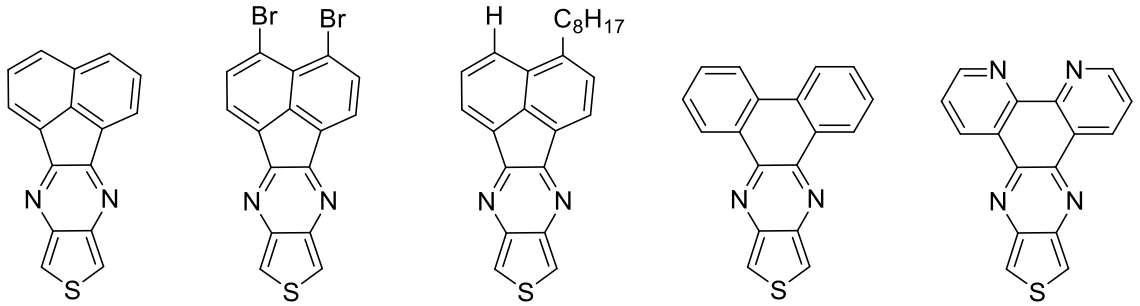

Figure 2.5. Extended ring thieno[3,4-*b*]pyrazine analogues included in comparative analysis.

These four ERTPs were compared to 2,3-dimethylTP and 2,3-diphenylTP with the objective to better understand the structure-function relationships as ERTP monomers were modified while paying specific attention to changes in the frontier MOs.[2] (2,3-dimethyl)TP

without additional conjugation should then have the largest HOMO/LUMO gap, while (2,3-diphenyl)TP should be somewhat reduced due to the phenyl rings that while not completely planar due to torsional twisting does extend the π-system.[2,5,11,15]

In this study all TP moieties were analyzed via electrochemistry and UV-vis absorption spectroscopy to determine and compare frontier orbital energy levels (Tables 2.1 and 2.2). A significant finding in the electrochemical analysis was the limited changes in HOMO energies (~0.5 eV) with a greater variance in LUMO energies (~0.8 eV) between all analogues compared (Figure 2.6).

Table 2.1. Electrochemical data for extended ring thieno[3,4-*b*]-pyrazine analogues.[2]

Compound	E_p[a] (V)	$E_{1/2}$ (V)	ΔE (mV)	HOMO[b] (eV)	LUMO[b] (eV)
(2,3-dimethyl)TP	1.33	-2.04	90	6.38	3.01
(2,3-diphenyl)TP	1.26	-1.78	75	6.33	3.34
ATP	1.18	-1.67	60	6.23	3.38
$ATPBr_2$	1.47	-1.25	150	6.52	3.80
$ATPC_8H_{17}$	1.15	-1.75	90	6.20	3.30
DBTQ	0.98	-1.51	90	6.03	3.54
TPP	1.45	-1.27	110	6.50	3.78

[a]Potentials measured vs Ag/Ag+ using 0.1 M $TBAPF_6$ in CH_3CN.
[b]Determined vs ferrocene (5.1 eV vs vacuum).

As expected, all ERTPs show a reduction in the HOMO/LUMO gap when compared to 2,3-dimethylTP and 2,3-diphenylTP with optical measurements showing the lowest HOMO/LUMO gaps coming from DBTQ and TPP. This is as expected due to the additional two π-electrons in comparison to the ATP analogues and thus additional conjugation when going from the five to six membered fused-ring.

Table 2.2. UV-vis data for extended thieno[3,4-*b*]pyrazine analogues.[2]

Compound	λ^{abs}_{max} (nm)
2,3-dimethylTP	350
2,3-diphenylTP	340
ATP	375
ATP(C_8H_{17})$_2$	376
DBTQ	426
TPP	418

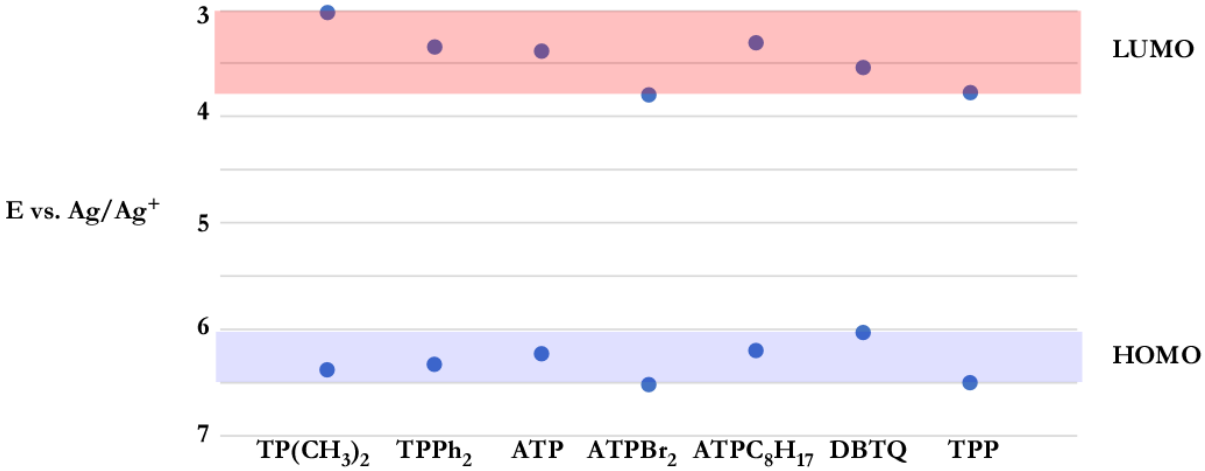

Figure 2.6. Variations in HOMO and LUMO energies for extended ring thieno[3,4-*b*]pyrazines.[2]

The results of this investigation into the frontier MOs of ERTPs showed that the greatest level of tuning via this method is of the LUMO energies. For the ERTPs the LUMOs are significantly reduced (0.3-0.7 eV) compared to their alkyl analogues with LUMO levels tuned through heteroatoms, pendant substituents, and annulated ring size. The method thus provides a route to CP precursors with reduced HOMO/LUMO gaps while keeping HOMO levels stabilized to oxidation.

Nonconjugated Extended Ring TPs and Lumo Modification

Investigations by the Rasmussen group into other 2,3-disubstituted TPs produced another extended ring TP, 1,3-dihydrofuro[3,4-*e*]thieno[3,4-*b*]pyrazine (FTP) (**2.1**).[11] This fused ring

differs from ATP in that conjugation does not extend through the new fused ring due to the presence of sp^3 carbons on the furan ring disrupting further conjugation. This then limits electronic effects to the electron donating nature of the furan ring which destabilizes the LUMO and results in a larger HOMO-LUMO energy. The HOMO-LUMO gap was determined via absorption spectroscopy and found to be 3.49 eV.[11]

The furan-TP analogue **2.1** was an unexpected result from the substitution of bromine in 2,3-bis(bromomethyl)thieno[3,4-*b*]pyrazine **2.2** with potassium hydroxide in attempts to make the corresponding diol-TP (Figure 2.7).[11] While it has not been investigated beyond the initial study it did provide a potential route for ERTPs that could start with compound **2.2**.

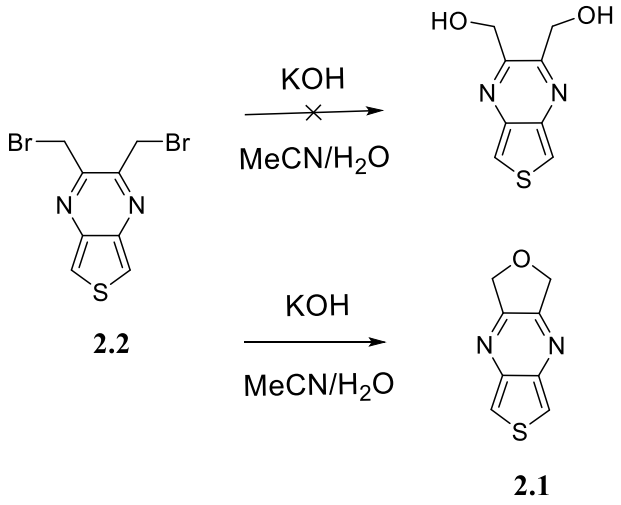

Figure 2.7. Synthesis of **2.1** via ring substitution on bromine on **2.2** followed by ring closure.

Compound **2.1** was limited in its applicability to ERTP materials largely in part to the presence and location of oxygen on the newly fused five-membered ring. If the oxygen heteroatom were changed to a species beyond row two of the periodic table, the potential for octet expansion would become available and allow for further conjugation and delocalization.

This then became the starting point of an investigation into dithieno[3,4-*b*:3',4'-*e*]-pyrazine (**2.3**) (Figure 2.8) where the ER now has a sulfur heteroatom with virtual d-orbitals low

enough in energy to allow for octet expansion[19] and thus a dehydrated heterocycle that can extend the conjugation on TP. The final goal being a new low bandgap ERTP with the potential for a record setting low E_g homopolymer. To date the research conducted on both the monomer and any potential polymers outside of the Rasmussen group has been computational only[20–22] and thus any synthesis and experimental analysis would be the first for the ERTP **2.3**.

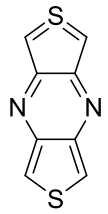

2.3

Figure 2.8. Structure of 2λ^{4}δ^2-dithieno[3,4-*b*:3',4'-*e*]pyrazine (**2.3**).

Extended Ring TP Computational Investigations

Initial computational investigations into **2.3** were carried out in 2002 by Yoshizawa and coworkers in attempts to understand the relationship between bond length alternation and bandgap through the addition of fused rings and enhancement of the quinoidal character. What was found was that when paired with thiophene and pyrrole in alternating copolymer systems, as the amount of **2.3** increased the bandgap decreased. In addition, a homopolymer of **2.3** had a bandgap that was calculated to be 0.14 eV.[22]

Additional computational work was then performed in 2006 by Wang on the nature of nonclassical thiophene derivatives and their electronic structure, aromaticity, singlet/triplet splitting energies, and vertical ionization energy.[21] An important conclusion from this study was that the adiabatic splitting energies were determined to be low enough to allow for the existence of a diradical species as a possible contributor to the ground state structure (Figure 2.9).

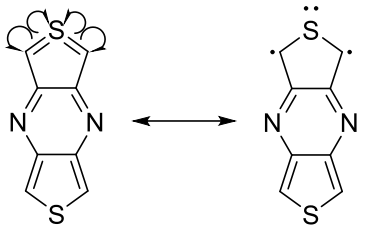

Figure 2.9. Aromatic and diradical contributions to the ground state structure of **2.3**.

So, while **2.3** has been determined to be a potential candidate for low E_g polymers, it also has a resonance contributor that may result in unwanted diradical reactivity. With these properties in mind, synthesis was carried out on both the parent unfunctionalized **2.3** as well as additional protected analogues with the end goal of low E_g homopolymers.

Development Of 2$\lambda^4\delta^2$-Dithieno[3,4-*B*:3',4'-*E*]pyrazine Monomers

Based upon these previous results I was tasked with the synthesis of a new monomer which required a multi-step synthesis. The following sections in this chapter are the experimental design and results of that investigation.

Nitration of 2,5-Dibromothiophene Optimization

In addition to the incorporation of extended ring functionality on TP was an investigation into the optimization of a key step in TP synthesis, the nitration of 2,5-dibromothiophene (**2.4**). The method used to make this TP precursor had been optimized previously by the Rasmussen group with yields of up to 94% obtained for the synthesis of 2,5-dibromo-3,4-dinitrothiophene (**2.5**).[23] Under these conditions the Rasmussen group was able to modify the initial conditions by removing the need for fuming nitric acid which had previously only given yields of **2.5** of 30-47%.[15,24] The conditions of this reaction were optimized such that **2.4** was added dropwise to a 50/50 *v*/*v* solution of H_2SO_4(conc.)/ H_2SO_4(fuming) while maintaining the temperature below 20 ˚C (Figure 2.10). This was then followed by the slow addition of concentrated nitric acid with the

temperature kept under 30 ˚C. It was then determined that both the order and the rate at which the acids were added played a significant role in the increase in product yields of **2.5** by reducing the unfavorable nitrosation caused by decomposition of nitric acid to NO_2.[23]

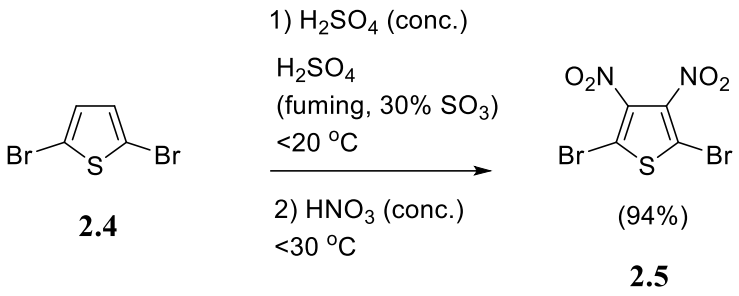

Figure 2.10. Synthesis of 2,5-dibromo-3,4-dinitrothiophene **2.5**.[23]

Due to changes in the availability of fuming sulfuric acid precursors, the general procedure has since been modified to carry out the reaction with 20% fuming sulfuric acid. The modifications were made such that the ratio of concentrated sulfuric acid to fuming sulfuric acid would produce an equivalent concentration of free SO_3 to that of the optimized conditions (30%). Under these conditions attempts were made to synthesize **2.5** and after repeated trials, yields of 58-72% were obtained (Table 3).

Further investigations were then pursued in altering the ratio of concentrated H_2SO_4/20% fuming H_2SO_4 as shown in Table 1. While these conditions did not show any improvements beyond the previous conditions with 20% fuming sulfuric acid, the trend observed was that as the concentrated H_2SO_4/20% fuming H_2SO_4 ratio increased, as did the product yield. With the maximum yields coming from the initial modifications to account for the fuming H_2SO_4 source and peaking at 72% (entry 7 Table 3). Other minor modifications included changes to the concentration of nitric acid, with an increase from 35 mL to 50 mL (Entry 6 Table 3) showing no discernable increase in product yields.

Table 2.3. Reaction conditions in the optimization study of **2.5**.

	Volume Concentrated (18 M) sulfuric acid (mL)	Volume of fuming sulfuric acid (20%) (mL)	Volume of nitric acid (mL)	2,5-dibromothiophene (mL)	Yield (%)
1	50	150	39	28	58
2	50	150	35	25	58
3	50	150	35	25	65
4	0	200	35	26	28
5	25	175	35	26	44
6	50	150	50	25	66
7	50	152	35	24	72

Parent Extended Ring Thieno[3,4-b]pyrazine Synthesis

As stated previously, the interest in a potential record setting low bandgap polymer then led our investigation into the synthesis of the monomer and eventual polymers of **2.3**. The synthesis was a direct development of previous work on **2.2** which was used to synthesize **2.1**.[11] The initial synthesis of **2.3** would follow a similar route in which **2.2** would be reacted with sodium sulfide in the S_N2 double substitution ring closing reaction to form 1H,3H-dihydrodithieno[3,4-*b*:3'4'-*e*]pyrazine (DHTTP) (**2.6**). This method however proved to have limited success with only an 8-14% yield (Figure 2.11).

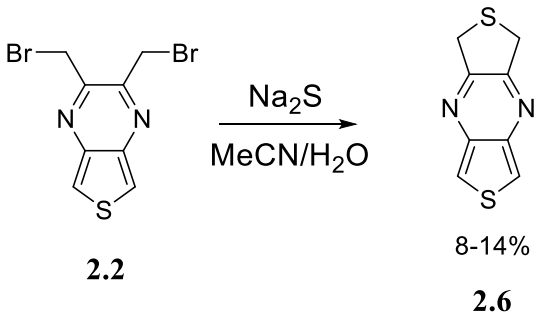

2.2 **2.6**

Figure 2.11. Initial conditions for the synthesis of **2.6**.

A second method was then attempted in which the incorporation of the sulfur on the newly formed ring would occur through sodium hydrosulfide. This method being attempted due to the enhanced solubility of sodium hydrosulfide over sodium sulfide in both aqueous and polar organic solutions. The new method did indeed show improvement over the previous strategy in that yields of up to 63% were obtained (Figure 2.12) for **2.6**.

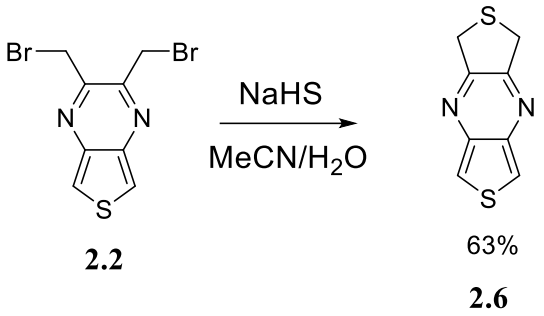

2.2 **2.6**

Figure 2.12. Optimized conditions for the synthesis of **2.6** from **2.2**.

When compared to **2.1**, **2.6** shows a significant upfield chemical shift of ~1 ppm of the protons on the α-carbons next to the newly incorporated sulfur (oxygen in **2.1**). This is as expected due to the significant reduction in electronegativity from oxygen to sulfur causing increased shielding of these protons in **2.6**. This same enhanced shielding effect is apparent in the ^{13}CNMR on the α-carbons themselves with a ~35 ppm chemical shift observed in **2.6**. The electronic implications of the substitution of oxygen for the less electronegative and slightly more electron rich sulfur on the new ring is a destabilization of LUMO as shown by the 100 mV shift from -1.87 to -1.77 in Table 2.4. This then corresponds to a decrease in the potential for oxidation with an increase in the potential for reduction.

As proposed by Cava et. al. the next step along the pathway of a fully aromatic ring was the oxidation of sulfur to form the sulfoxide.[25] This was carried out by Cava successfully in the

oxidation of l,3-dihydrothieno[3,4-*b*]quinoxaline with monoperoxyphthalic acid magnesium salt (MMPP) to form 1,3-dihydrothieno[3,4-*b*]quinoxaline 2-oxide (Figure 2.13).[25]

Table 2.4. Electrochemical Data for alkoxy- and nonconjugated-ERTPs.

Compound	oxidation	reduction		HOMO/LUMO Gap (eV)
	E_p^a (V)	$E_{1/2}$ (V)	ΔE (mV)	
furan (**2.1**)[11]	1.45	-1.87	100	3.32
DHTTP (**2.6**)	1.45	-1.77	100	3.22
DHTTP-s-oxide (**2.7**)	1.70	-1.85[b]	-	3.55
$(C_5H_{11}OCH_2\text{-})_2TP$[11]	1.49	-1.85	100	3.34

[a]All potentials vs Ag/Ag^+. [b]Irreversible, value corresponds to E_p^c

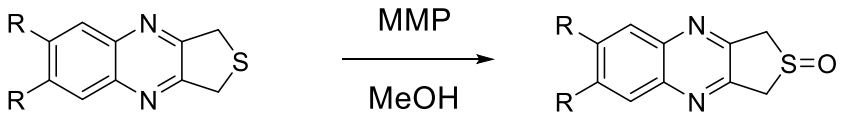

Figure 2.13. Formation of sulfoxide on l,3-dihydrothieno[3,4-*b*]quinoxaline.[25]

This was the same strategy employed for the oxidation of **2.6** to form dihydrothieno[3,4-*b*]thieno[3,4-*e*]pyrazine-s-oxide (DHTTPS-oxide) (**2.7**) using MMPP as an oxidant with the results being modest yields of 6-25 %. Additional oxidants were used to attempt to improve yields and included hydrogen peroxide and sodium periodate with no improvement and overall worse product yields.

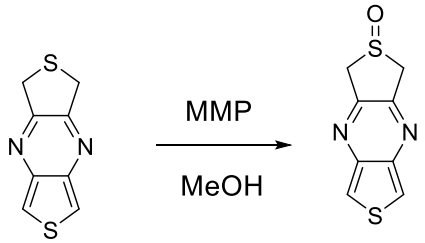

2.6 **2.7**

Figure 2.14. Oxidation of **2.6** to form **2.7** with MMP via Cava method to oxidize quinoxalines.

Analysis of DHTTP-s-oxide was performed via electrochemistry (Table 2.4) and compared to **2.6** as well as the previously synthesized 2,3-Bis(pentoxymethyl)thieno[3,4-*b*]pyrazine (2,3-pentoxyTP**)** and 2,3-dimethylthieno[3,4-*b*]pyrazine dimethyl-TP (Figure 2.15). As expected, **2.7** has a lower energy reduction when compared to **2.6** and and dimethyl-TP. Interestingly however is the nearly identical reduction when compared to 2,3-pentoxyTP which implies that the electronic effects of the sulfoxide are enough to shift the reduction potential in an equivalent capacity to that of two pentoxymethyl groups. Where **2.7** differs significantly is in the oxidation potential, where an irreversible oxidation is observed just within the solvent window and 0.2 mV higher in energy than 2,3-pentoxyTP. This can be rationalized through the locked in configuration of the fused ring provding an enhanced dipole to further remove electron density from thiophen on the TP unit as opposed to the allowable rotation in the pentoxymethyl groups that have the potential to cancel out a portion of the dipole moment to reduce its effect.

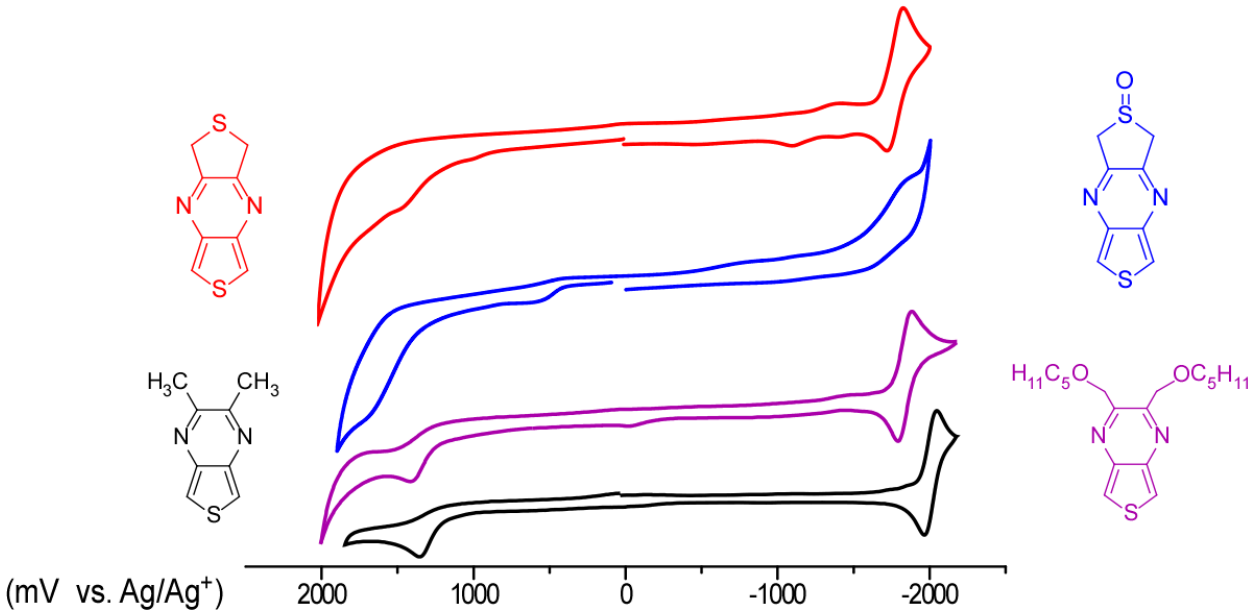

Figure 2.15. Cyclic voltammogram of **2.6** (red), **2.7** (blue), 2,3-pentoxyTP (violet), and 2,3-dimethyl-TP (black).

With the DHTTPS-oxide **2.7** in hand and following the Cava strategy to make thieno[3,4-*b*]quinoxaline the reduction of the s-oxide to the fully aromatic ring was then carried out initially with potassium hydroxide in toluene using sonication to avoid unwanted reactivity due to heating in what is known as a Pummerer dehydration.[26] All attempts, however, in this regard were unsuccessful in generating **2.3** (and ^{1}HNMR showed the reformation of **2.6** (Figure 2.16)).

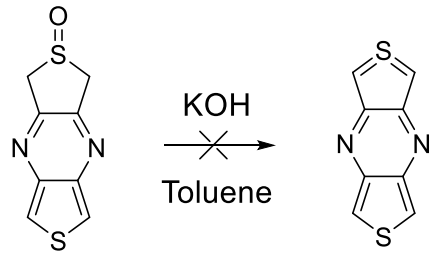

2.7 **2.3**

Figure 2.16. Synthetic scheme for unsuccessful Pummerer dehydration of **2.7** to form **2.3**.

This lack of successful results was likely due to the potential diradical contribution to the ground-state structure mentioned previously and proposed for other species such as thieno[3,4-*c*]thiophene.[27,28] If indeed this is the case the insoluble black material that is formed during the reaction is likely a polymerization product, but more analysis is needed to confirm this qualitative observation.

Routes to Reduce Monomer Reactivity

Attempts to stabilize the monomer were then pursued with the initial species investigated being a cyano analogue. This method was first discovered by Cava et. al. this time on thieno[3,4-*c*]thiophenes.[29] Lakshmikantham and Cava et. al. had previously concluded that this species existed as the 1,3-diradical species and wanted to create substituted stable analogs. The attempts on TP were carried out by the substitution of bromine on **2.2** with a nitrile group using either sodium or potassium cyanide to make 2,3-bis(cyanomethyl)thieno[3,4-*b*]pyrazine (CMTP) (**2.8**)

(Figure 2.17). Not only would a nitrile group block the alpha positions on the newly formed ER, but the electron withdrawing effects of the nitrile group would also favor the tetravalent sulfur on the ER portion of TP and reduce the diradical contribution on the original thiophene ring, allowing it to potentially remain unprotected for future polymerization.

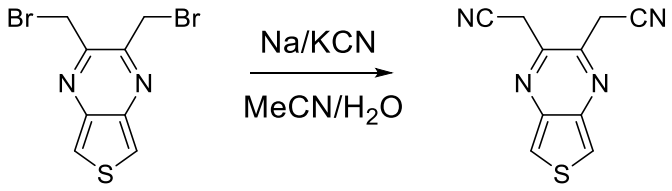

2.2 **2.8**

Figure 2.17. Synthesis of **2.8** by cyano-substitution of **2.2**.

Another strategy to block the positions alpha to the sulfur on the extended ring was to incorporate methyl substituents. This was approached by a modification of the dione used to make **2.2** by brominating 3,4-hexanedione with Br_2 to make 2,5-dibromo-3,4-hexanedione (**2.9**) (Figure 2.18). With this method, the ER protected with methyl substituents would still have resonance structures in which the diradical could move to the unprotected thiophene and thus protection of the original thiophene would be necessary at a later step prior to the Pummerer dehydration step.

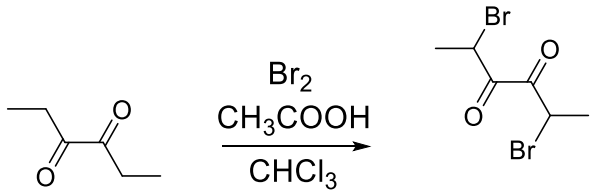

2.9

50%

Figure 2.18. Dibromination of 3,4-hexanedione.

Even with the modest yields of **2.9**, the corresponding TP (2,3-bis(1-bromoethyl) thieno[3,4-*b*]pyrazine) (**2.10**) was then synthesized under the typical conditions used for previous

TPs[15] (Figure 2.19). This method was found to be successful with yields of 80% obtained. With **2.10** in hand the ring closure was performed as before with **2.6** to make (**2.11**) and moderately successful with yields of 57% obtained (Figure 2.20).

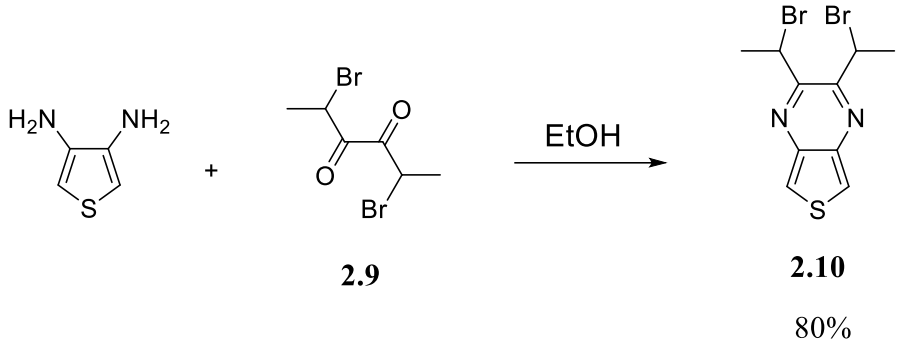

Figure 2.19. Synthesis of **10** under typical TP condensation conditions.[15]

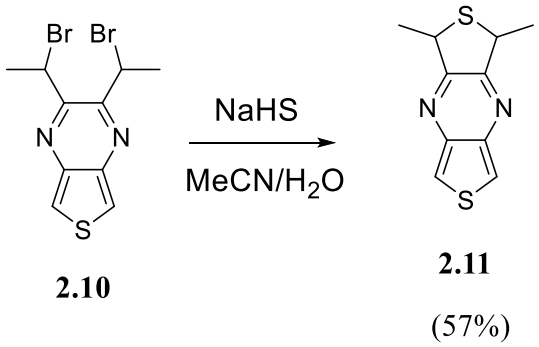

Figure 2.20. Synthesis of **2.11** from **2.10** via optimized conditions for **2.6**.

The synthesis of 1,3-dimethyldithieno[3,4-*b*]thieno[3,4-*e*]pyrazine-*S*-oxide **(2.12)** was then attempted with the same conditions as **2.7** with no resultant product formed. Further optimization is this required to pursue this protection route. As mentioned previously, once **2.12** has been synthesized, the incorporation of additional protecting groups may be necessary to prevent unwanted reactivity at the thiophene within TP. A possible solution here would be to brominate these two positions by the previously reported methods[30] with *N*-bromosuccinimide.

Polymerization could then be carried out by Grignard metathesis to synthesize the desired homopolymer.

Conclusions

In these investigations into ERTPs, the synthesis of **2.3** as of this point seems to be out of reach due to the reactivity of the monomer to uncontrollably self-polymerize. This has since led to further investigations into the protection of **2.3** via alkyl and cyano substitution which require further development and optimization to become potential candidates for low E_g homopolymers. While **2.3** itself is unstable, its precursors are not, and their synthesis has added new analogues to the family of TP units for the potential use in low E_g polymers. If an analogue of **2.3** can be successfully synthesized, it may also be of interest to compare the optical and electronic properties to that of the original series[2] of extended TP analogues.

Experimental

Materials

2,5-Dibromothiophene[15], 3,4-diamino-2,5-dibromothiophene[23], BMTP[11] and FTP[11] were prepared as previously reported. Unless specified, all other reagents were purchased and used without further purification. Reactions were carried out under a nitrogen environment with a Schlenk line setup in which all vessels were evacuated and backfilled three times to ensure an air free atmosphere.

Synthesis

1*H*,3*H*-Dihydrodithieno[3,4-*b*:3'4'-*e*]pyrazine (DHTTP) (2.6). Formation of the extended ring TP with the sulfur containing heterocycle was carried out by adding NaHS (0.71 g, 9.6 mmol) to **(2.2)** (0.40 g, 1.2 mmol) in 40 mL of 50:50 acetonitrile/water solution while stirring at room temperature. Solution was stirred for 3 ½ hours and 20 mL of H_2O was added and

stirring stopped. The product was then extracted with dichloromethane and dried with sodium sulfate. Once dry, solvent was removed under reduced pressure and the crude product was purified by a 20/80% EtOAc/hexanes, silica gel, column which yielded 0.12 g (50%) of pure product. mp 119.1-119.3 ˚C. ^{1}HNMR ($CDCl_3$, 400 MHz) δ 7.91 (s, 2H), 4.22 (s, 4H); ^{13}C NMR ($CDCl_3$, 400 MHz) δ 155.6, 141.1, 116.9, 34.1

1*H*,3*H*-Dihydrothieno[3,4-*b*]thieno[3,4-*e*]pyrazine-*S*-oxide (2.7). Oxidation of the ER sulfur on DHTTP was carried out by adding **(2.6)** (0.23 g, 1.1 mmol) to 60 mL of MeOH and heated until all solids dissolved. Once dissolved, a 1% magnesium monoperoxyphthalate (0.60 g, 1.2 mmol) solution (in 60 mL of H_2O) was added in 5 mL aliquots. The mixture was then stirred until TLC (30/70% EtoAc/Hexanes on silica) showed starting material was no longer visible under longwave UV-light. Product was then extracted with dichloromethane, washed with Na_2CO_3, and dried with Na_2SO_4. Once dry, product was purified by a 50/50% EtOAc/hexanes, silica gel, column which yielded 0.010 g (5.9%) of pure product. ^{1}HNMR ($CDCl_3$, 400 MHz) δ 8.00 (s, 2H), 4.33 (dd, 4H, J = 12 Hz)

2,3-Bis(cyanomethyl)thieno[3,4-*b*]pyrazine (2.8). Cyano substitution of bromine on **(2.2)** was carried out by adding **(2)** (0.68 g, 2.1 mmol) and potassium cyanide (0.72 g, 11 mmol) to 50 mL of formamide. The red/brown solution was analyzed with TLC (30/70% EtOAc/hexanes on silica) after 1 hour under UV-light and starting material was no longer visible. The solution then stirred for 2.5 more hours, and product was extracted with dichloromethane, dried with Na_2SO_4, and solvent removed under reduced pressure. Crude product was then purified by column chromatography using silica gel and 40/60% EtOAc/hexanes to give a trace amount of pure product. ^{1}HNMR ($CDCl_3$, 400 MHz) δ 8.15 (s, 2H), 4.16 (s, 4H)

2,5-Dibromo-3,4-hexanedione (2.9). The bromination of 3,4-hexanedione was carried out by adding acetic acid (250 mL), chloroform (250 mL), and 3,4-hexanedione (5.78 g, 50 mmol) together and cooled to 0 ˚C while stirring. Molecular bromine (16.0 g, 100 mmol) was then added dropwise, and the mixture was heated to reflux. Mixture was heated under reflux for 3 hours and upon completion was quenched with saturated sodium bicarbonate solution. Product was then extracted with chloroform, dried with magnesium sulfate, and solvent removed under reduced pressure. Crude product was then purified by column chromatography using silica gel and hexanes to yield 6.84 g (50.1 %). ^{1}HNMR ($CDCl_3$, 400 MHz) δ 5.30 (q, 2H, *J* = 6.7 Hz), 1.84 (d, 6H, *J* = 6.7 Hz).

2,3-Bis(1-bromoethyl)thieno[3,4-*b*]pyrazine (2.10). 2,5-Dibromo-3,4-hexanedione (5.46 g, 20.0 mmol) was dissolved in 20 mL of absolute ethanol and cooled to 0 ˚C. In a separate flask 3,4-diaminothiophene (2.48 g, 21.7 mmol) was dissolved in 60 mL of absolute ethanol and cooled to 0 ˚C. diamine solution was then added to dione solution via cannula and the solution was stirred for 3 hours. The crude product was purified by column chromatography (10/90% EtOAc/Hexanes on silica) to give 5.63 g (80.4%) of pure product. ^{1}HNMR ($CDCl_3$, 400 MHz) δ 8.06 (s, 2H), 5.75 (q, 2H, *J* = 6.6 Hz), 2.25 (d, 2H, *J* = 6.6 Hz)

1,3-Dimethyldithieno[3,4-*b*:3’4’-*e*]pyrazine. (2.11) Formation of the methyl protected extended ring TP with the sulfur containing heterocycle was carried out by adding NaHS (2.47 g, 24.4 mmol) to **(2.10)** (1.75 g, 5.00 mmol) in 200 mL of 90/10% acetonitrile/water solution while stirring at room temperature. Solution was stirred for 3 ½ hours and 20 mL of H_2O was added and stirring stopped. The product was then extracted with dichloromethane and dried with sodium sulfate. Once dry, solvent was removed under reduced pressure and the crude product was purified by a 20/80% EtOAc/hexanes, silica gel, column which yielded 0.63 g (57%) of pure

product. ^{1}HNMR ($CDCl_3$, 400 MHz) δ 8.06 (s, 2H), 5.75 (q, 2H, *J* = 6.6 Hz), 2.25 (d, 6H, *J* = 6.6 Hz).

References

1. Konkol, K.; Schwiderski, R.; Rasmussen, S. *Materials* **2016**, *9* (404), 1–16.
2. Nietfeld, J. P.; Schwiderski, R. L.; Gonnella, T. P.; Rasmussen, S. C. S *J. Org. Chem.* **2011**, *76* (15), 6383–6388.
3. Rasmussen, S. C.; Schwiderski, R. L.; Mulholland, M. E. *Chem. Commun.* **2011**, *47* (41), 11394–11410.
4. Rasmussen, S. C.; Mulholland, M. E.; Schwiderski, R. L.; Larsen, C. A. *J. Heterocycl. Chem.* **2012**, *49* (3), 479–493.
5. Rasmussen, S. C.; Sattler, D. J.; Mitchell, K. A.; Maxwell, J. *J. Lumin.* **2004**, *109* (2), 111–119.
6. Mondal, R.; Miyaki, N.; Becerril, H. A.; Norton, J. E.; Parmer, J.; Mayer, A. C.; Tang, M. L.; Brédas, J.-L.; McGehee, M. D.; Bao, Z. *Chem. Mater.* **2009**, *21* (15), 3618–3628.
7. Paz, M. A.; Martin, P.; Flückiger, R.; Mah, J.; Gallop, P. M. *Anal. Biochem.* **1996**, *238* (2), 145–149.
8. Wu, X.; Li, X.; Li, Z.; Yu, Y.; You, Q.; Zhang, X. *J. Med. Chem.* **2018**, *61* (24), 11280–11297.
9. Wen, L.; Heth, C. L.; Rasmussen, S. C. *Phys. Chem. Chem. Phys.* **2014**, *16* (16), 7231–7240.
10. Outurquin, F.; Paulmier, C. *Bull. Soc. Chim. Fr.* **1983**, No. 5–6, 159–163.
11. Wen, L.; Nietfeld, J. P.; Amb, C. M.; Rasmussen, S. C. *J. Org. Chem.* **2008**, *73* (21), 8529–8536.

12. Christl, M.; Krimm, S.; Kraft, A. *Angew. Chem.* **1990**, *102* (6), 704–706.

13. Tanaka, S.; Yamashita, Y. *Synth. Met.* **1997**, *84* (1–3), 229–230.

14. Tanaka, S.; Yamashita, Y. *Synth. Met.* **1995**, *69* (1–3), 599–600.

15. Kenning, D. D.; Mitchell, K. a; Calhoun, T. R.; Funfar, M. R.; Sattler, D. J.; Rasmussen, S. C. *J. Org. Chem.* **2002**, *67* (25), 9073–9076.

16. Nietfeld, J. P.; Heth, C. L.; Rasmussen, S. C. *Chem. Commun. Camb. Engl.* **2008**, No. 8, 981–983.

17. Wen, L.; Nietfeld, J. P.; Amb, C. M.; Rasmussen, S. C. *Synth. Met.* **2009**, *159* (21–22), 2299–2301.

18. Kenning, D. D.; Rasmussen, S. C. *Macromolecules* **2003**, *36*, 6298–6299.

19. Reed, A. E.; Weinhold, Frank. O. *J. Am. Chem. Soc.* **1986**, *108* (13), 3586–3593.

20. Tseng, C. Y.; Taufany, F.; Nachimuthu, S.; Jiang, J. C.; Liaw, D. J. *Org. Electron.* **2014**, *15* (6), 1205–1214.

21. Shen, W.; Li, M.; Huang, H.; Li, Y.; Wang, S. *Mol. Simul.* **2006**, *32* (6), 457–464.

22. Tachibana, M.; Tanaka, S.; Yamashita, Y.; Yoshizawa, K. *J. Phys. Chem. B* **2002**, *106* (14), 3549–3556.

23. Wen, L.; Rasmussen, S. C. *J. Chem. Crystallogr.* **2007**, *37* (6), 387–398.

24. Mozingo, R.; Harris, S. A.; Wolf, D. E.; Hoffhine, C. E.; Easton, N. R.; Folkers, K. *J. Am. Chem. Soc.* **1945**, *67* (12), 2092–2095.

25. Pohmer, J.; Lakshmikantham, M. V.; Cava, M. P. *J. Org. Chem.* **1995**, *60* (25), 8283–8288.

26. Nakayama, J.; Ishii, A.; Kobayashi, Y.; Hoshino, M. *J. Chem. Soc. Chem. Commun.* **1988**, No. 14, 959.

27. Muller, C.; Schweig, A.; Cava, M. P.; Lakshmikantham, M. V. T. *J. Am. Chem. Soc.* **1976**, *22*, 7187–7189.

28. Amaresh, R. R.; Lakshmikantham, M. V.; Baldwin, J. W.; Cava, M. P.; Metzger, R. M.; Rogers, R. D. *J. Org. Chem.* **2002**, *67* (8), 2453–2458.

29. Beye, N.; Cava, M. P. *J Org Chem* **1994**, *59* (8), 2223–2226.

30. Wen, L.; Duck, B. C.; Dastoor, P. C.; Rasmussen, S. C. *Macromolecules* **2008**, *41* (13), 4576–4578.

CHAPTER 3. MODEL DIMER SYSTEMS

Introduction

As the field of conjugated polymer (CP) synthesis advanced so did the focus as to what parameters would make a material useful in an electronic device. These parameters include processability, stability, high conjugation length, a suitable E_g, and sufficient charge mobility.[1,2] While all are necessary for the implementation of CPs in devices, the E_g has been given special attention due to its correlation to potential emission and onset of absorption.[1–6] Additionally, the E_g has a direct relationship with the frontier orbital energies and therefore the tuning of the E_g can also be responsible for environmental stability as well as the energetic matching with other components within a device.[5]

The tuning of the E_g in CPs has been understood primarily by two structure-function models. One being the enhancement of the quinoidal nature of the polymer backbone and the second being an alternating donor-acceptor (D-A) framework.[2–13] The latter of which has been the most frequently evoked in the literature when considering low E_g CP design.

Donor-Acceptor Model

The initial research on D-A frameworks was carried out on strong alternating donor-acceptor polysquaraines/polycroconaines by Havinga and coworkers with E_g values as low as 0.5 eV.[14,15] Later publications would investigate the cause of the reduction in E_g with the explanation elucidated in terms of the reduction of bond length alternation via the addition of a new resonance structure (Figure 3.1).[2,9–12] This new resonance structure required each unit to be relatively strong in their respective role (i.e. strong donor and strong acceptor), with the averaging of the two structures producing an overall lower alternation in bond length along with a corresponding decrease in E_g.[2,9–12]

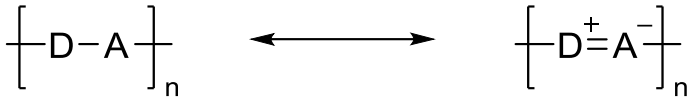

Figure 3.1. D-A interactions forming an additional resonance structure.

However, the most common rationalization in the literature for the E_g reduction by D-A frameworks is the mixing and hybridization of frontier orbitals. This being the donor as the main contributor to the HOMO and the acceptor as the main contributor to the LUMO which upon mixing produce a material with an overall lower HOMO/LUMO gap (Figure 3.2). [2,9–12]

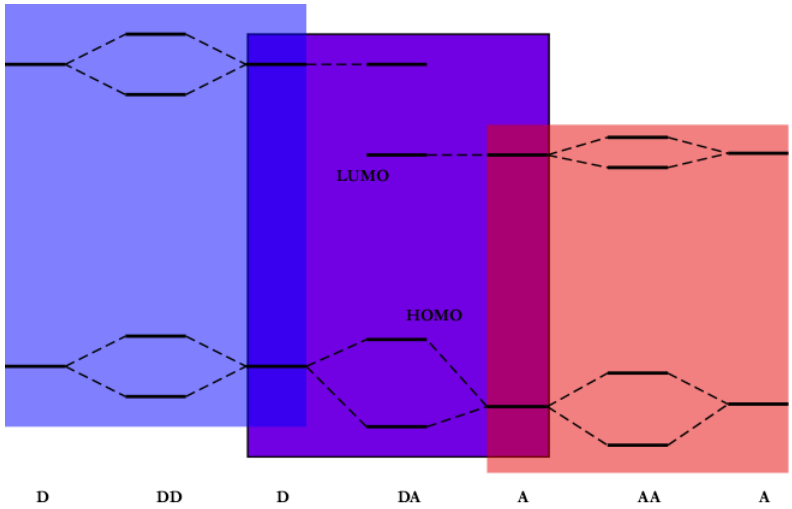

Figure 3.2. D-A hybridization diagram showing reduction in HOMO/LUMO gap.

Limitations in the D-A Model and the Aromatic-Quinoidal Approach

Even with these competing fundamental understandings, the validity of the D-A approach as a complete picture for copolymeric systems has been called into question in recent years due to the narrow scope of compounds in the initial investigation with limited modifications thereafter for other D-A systems.[8,15,16] This has since brought a new emphasis on the quinoidal model and multiple computational studies have proposed that in most cases, acceptor units provide quinoidal character while donors bring more aromatic character, resulting in a ground

state structure hybrid of the two structures that reduces the overall BLA with a corresponding reduction in E_g.[17–20]

Further complications to the D-A approach were also realized when certain monomers failed to fall into a single category of either donor, acceptor, or neutral spacer unit.[21] This has been observed specifically in the case of thieno[3,4-*b*]pyrazine (TP), because of TP's high lying HOMO which allows it to act as a strong donor while also having a low lying LUMO to act as a strong acceptor.[22] TP while not unique in these characteristics is one of the more commonly used monomers to exhibit these traits due to additional desirable properties such as relative ease of synthesis and tunability at the 3- and 4-positions. Therefore, the discovery of the nature of TP has led to the need for a new definition for this class of monomers, which have since been denoted as ambipolar units.[22] As a result of this phenomenon, TP has since been paired with both strong donors[4] and strong acceptors[6,7] as alternating copolymers to produce low band gap polymers.

Modeling D-A Interactions Through Dimeric Systems

To understand the monomeric species commonly found in CPs in a more thorough capacity it then becomes important to quantify the changes that the combining of a strong donor with a strong acceptor creates. In addition, the ambipolar subclass of monomers has been rarely studied and thus how these species interact with both donors and acceptors is of paramount importance if these units are to be developed and incorporated into organic semiconducting devices. One method to accomplish this is through the synthesis and analysis of model D-A dimeric systems. This simplified dimeric picture with a limited and consistent conjugation length allows for D-A interactions to be investigated and compared between a variety of donor, acceptors, and ambipolar units. A well-designed series can then show how these D-A

interactions correlate to frontier orbital energies, structural changes of the monomers, as well as HOMO-LUMO gap narrowing.

Dimer Design

In the dimer investigation presented here, three different monomers were selected to represent the three electronically significant units encountered in conjugated polymer systems (Figure 3.3). The three selected were 3,4-ethylenedioxythiophene (EDOT) as the donor[11,23] benzo[*c*][1,2,5]thiadiazole (BTD) as the acceptor[24,25] and 2,3-dihexylthieno[3,4-*b*]pyrazine (TP) as the ambipolar species. Both homo- and hetero-dimer species were synthesized from all three monomers to make the six possible configurations (Figure 3.3). These six different dimer combinations would then provide case studies for D-D species, A-A species, and ambipolar-ambipolar dimeric species in addition to a D-A, ambipolar-D, and ambipolar-A species.

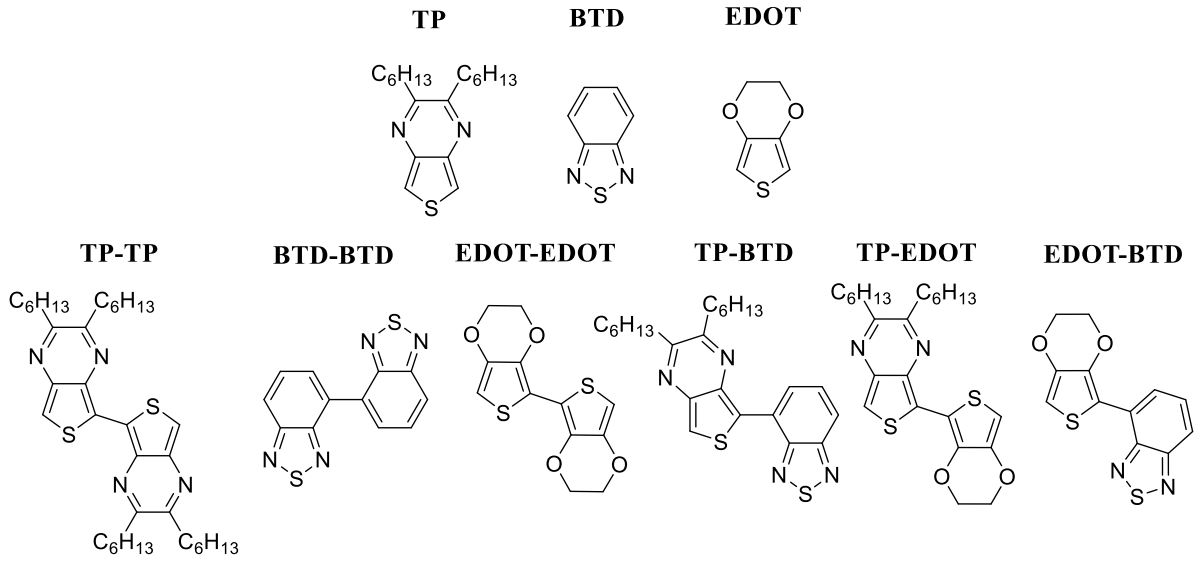

Figure 3.3. TP (ambipolar species), BTD (acceptor), and EDOT (donor) and the six possible dimer configurations.

The selection of these three monomers also served the purpose of maintaining a consistent conjugation length with only a single aromatic ring per monomer contributing to the

conjugation length from each monomer. A consistent conjugation length ensures that any contribution to optical and electronic properties in these configurations is comparable and that any D-A effects would arise from differing configurations (i.e identity and connectivity of atoms).[2] Issues in these types of comparisons have been shown for example in the case of donor strength between TP and dithieno[3,2-*b*:2',3'-*d*]pyrrole (DTP) (Figure 3.4).

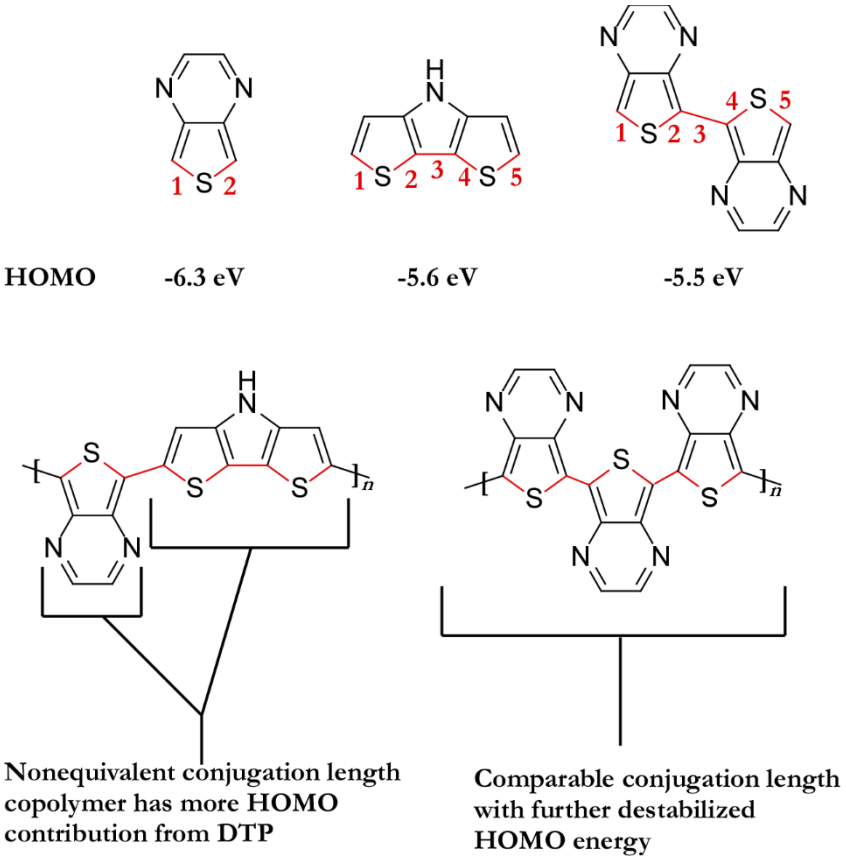

Figure 3.4. (top) HOMO energies of TP, DTP, and TP-TP. (bottom) potential polymeric systems showing HOMO destabilization is maximized with TP-homopolymer.

In this specific example TP has a much deeper HOMO of -6.3 eV than that of DTP which has a HOMO energy of -5.6 eV. At first impression this implies that DTP is a significantly better donor than TP, but if the two are to be accurately compared an adjustment needs to be made to accommodate for an equivalent conjugation path length that would exist along the

polymer backbone and thus contribute to the HOMO of the polymer. To make an accurate comparison of these two species would require a TP dimer which as expected has a HOMO of -5.5 eV and is very similar to a DTP monomer (Figure 3.4).[8] Thus, if a polymeric system were to be designed with the goal of driving up the HOMO a TP-homopolymer would be have a more destabilized HOMO than a 1:1 TP:DTP and be the lower E_g material.

This chapter will thus be focused on the comprehensive study carried out by the Rasmussen group on these six dimeric species.[16] This study includes synthetic details for monomers and dimers, characterization of each species, density functional theory (DFT) analysis, and finally a discussion of the implications that the results of this study imply.

Results and Discussion

Due to the electronic differences between monomers, the coupling reactions differed significantly for each species and required specific reaction sequences to be pursued for each dimer generated. This included incorporating different handles at the coupling sites as well as the incorporation of protecting groups and solubilizing sidechains. To synthesize the symmetric dimers, various homocoupling methods were used and are shown in Figure 3.5[26,27] while Stille coupling was employed for the asymmetric dimers and carried out by Trent Anderson.[28] In addition, redox stability of unfunctionalized TP has been shown to be an issue previously and thus the functionalized 2,3-dihexyl analogue was used which also provided the added benefit of increased solubility and limited impacts on the electronic properties.[4,29,30]

EDOT required separate handles for all three dimers synthesized. For the symmetric dimer a lithiation step preceded the oxidative homocoupling with Cu(II) as previously reported.[27] The TP-EDOT species utilized a bromide handle on EDOT and coupling via Stille coupling with an organostannane TP. Lastly the EDOT-BTD dimer was also synthesized via Stille coupling,

however with a reverse role for EDOT as the organostannane reagent and 4-Bromo-2,1,3-benzothiadiazole (BrBTD) as the halogenated species.

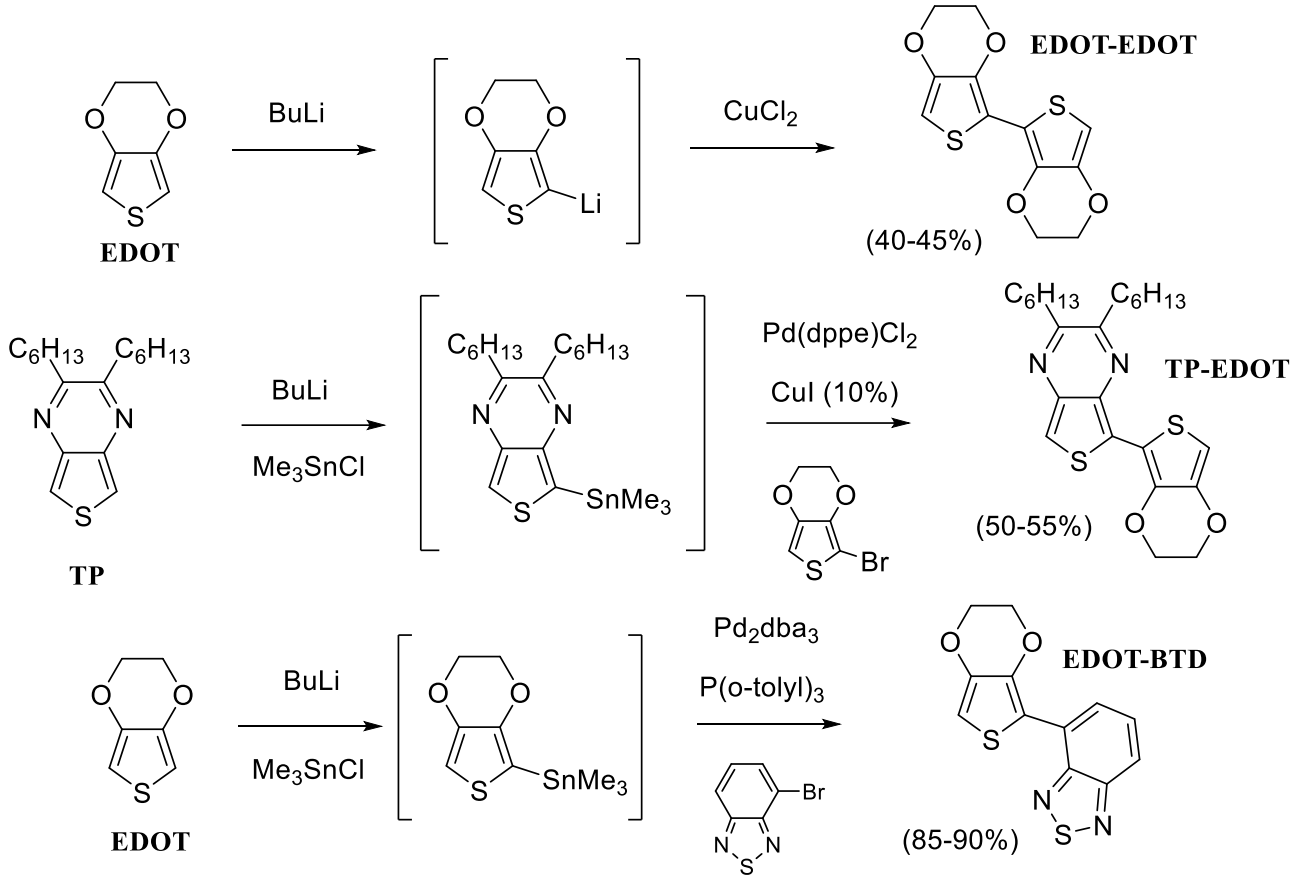

Figure 3.5. Three possible EDOT dimers and the cross-coupling methods required for synthesis.

For the remaining two BTD species, both utilized a bromide handle in BrBTD as the site for coupling to occur (Figure 3.6). In the homocoupling reaction the symmetric dimer was synthesized via a nickel catalyzed pathway in the presence of stoichiometric amounts of zinc.[26] The BTD-TP dimer was synthesized via Stille coupling as previously stated with the TP as the organostannane species and BrBTD as the halogenated species.

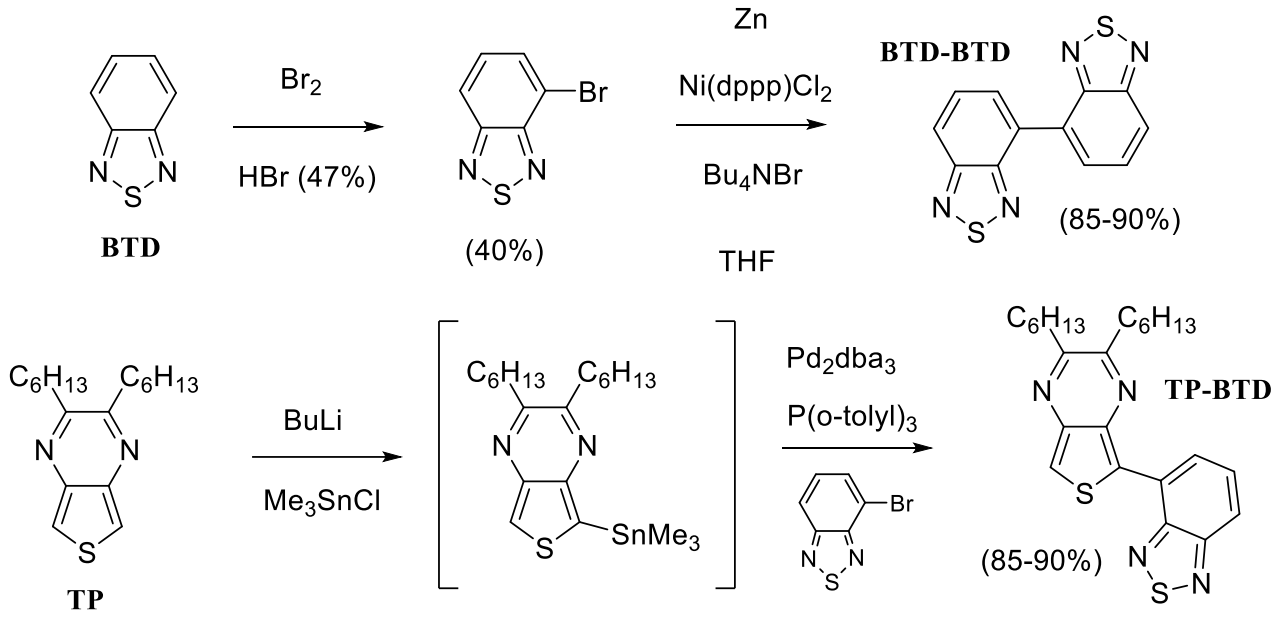

Figure 3.6. Remaining BTD dimers and the cross-coupling methods required for synthesis.

Lastly, the remaining TP homodimer (TP-TP) being slightly environmentally unstable to oxidation required further modification of trimethylsilyl groups (TMS) on the exterior alpha positions to block unwanted reactivity at these sites (Figure 3.7). These were added with the knowledge that these groups would contribute little to the electronic properties allowing for a consistent comparison to be made across all investigated oligomers.[22] Once the TMS group was added to Br_2TP. The TP-TP homodimer was then synthesized as previously reported via Stille coupling by Li Wen.[22]

Dimer Characterization

Characterization of all dimer species was necessary to show evidence of their synthesis as well as potential D-A effects. This characterization included ^{1}HNMR, ^{13}CNMR, X-Ray crystallography (when possible), electrochemistry, and UV-vis absorption spectroscopy.

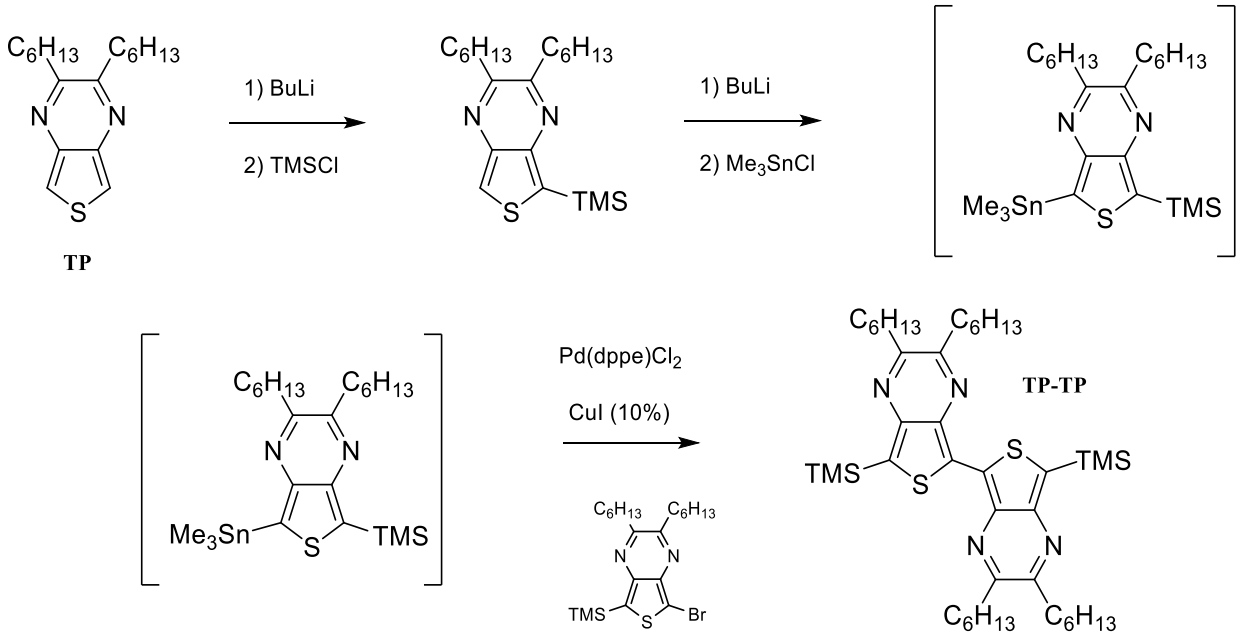

Figure 3.7. TP-TP synthesis with TMS protecting groups.

Molar Absorption Coefficients, Oscillator Strengths, and Maximum Absorptions

The optical transitions of the six dimers were analyzed by UV-vis absorption spectroscopy and comparisons were made between dimers to see what changes occurred to characteristic intramolecular charge transfer (ICT) band as well as the π-π^* transition. In addition to the energy at which a species absorbs light, the molar absorption coefficient (ε) is also an important parameter to determine the probability of absorption for a given transition. This parameter appears in the Beer-Lambert law with its most simplified form shown in Eq.1. In this Equation the variables are absorbance (A), which is unitless, the path length (b) in cm, and the concentration (c) in M which then gives units of M^{-1} cm^{-1} for ε. Solving Eq. 1 for ε then requires a known concentration of analyte and if concentrations are below 10^{-3} M can be assumed to follow ideal behavior and Beer's law.[31] The ε parameter therefore gives information regarding each maxima in a UV-vis spectra, but not electronic transitions as a whole, and thus an integrated

parameter combining the various vibrational variations in a transition is needed to provide a more complete picture of absorption probability.

$$A = \varepsilon bc \quad \text{(Eq. 1)}$$

The integrated form of absorption probability is known as the oscillator strength (*f*). This parameter can be determined from Eq. 2 with the experimental ε value plotted against the energy in wave numbers of the absorption.[32]

$$f \equiv 4.3 \times 10^{-9} \int \varepsilon d\bar{\nu} \quad \text{(Eq. 2)}$$

The maximum absorption wavelengths ($\lambda^{abs}{}_{max}$), ε, and *f* values for all dimers investigated are shown in Table 3.1. As can be seen from the table each $\lambda^{abs}{}_{max}$ has an associated ε value while the calculated f values are a combination of vibrational modes of the same transition. EDOT-EDOT having no pendant accepting groups has just a single *f* value as all three $\lambda^{abs}{}_{max}$ peaks correspond to the π-π* transition of an all-donor species. As pendant accepting groups are incorporated, the previously mentioned ICT transition appears along with two additional higher energy π-π* transitions that are within the spectral window (BTD-BTD falls just outside the window).

UV-vis Absorption Spectroscopy and Donor-Acceptor Interactions

The ICT was paramount in this investigation due to being the lowest energy transition for D-A systems and providing an avenue to accurately estimate the HOMO-LUMO gap and thus part of the picture of the D-A interactions that may exist between the two units.[11] The higher energy π-π* transition is a result of the optical transition of the delocalized all-donor backbone

Table 3.1. Photophysical data for dimer series.[a]

Compound	$\lambda^{abs}{}_{max}$ (nm)	ε (M^{-1} cm^{-1})	*f*
EDOT-EDOT	296	9000	0.50
	307	10 900	
	320	15 400	
	335	13 200	
BTD-BTD	308	21 600	0.31
	316	28 600	
	363	9100	0.16
EDOT-BTD	287	17 400	0.35
	306	15 300	0.48
	319	15 400	
	409	6600	0.11
EDOT-TP	260	13 300	0.36
	306	17 800	0.33
	456	5000	0.11
TP-BTD	274	12 300	0.20
	284	12 700	
	316	16 200	0.17
	435	6000	0.13
TP-TP	257	21 800	0.57
	304	17 000	0.32
	503	7300	0.15

[a]Measured from dilute $CHCl_3$ solutions in 1 cm quartz cuvettes. Data collected from Ref. 16

and becomes the only observable band in CPs without D-A interactions and likewise represents the HOMO-LUMO gap for an all-donor CP system.[11,16]

Looking at the analogues that do not contain ambipolar TP (EDOT-EDOT, BTD-BTD, and EDOT-BTD) and represent an all-donor species, all acceptor species, and D-A species respectively, some expected trends are present (Figure 3.8). The all-donor EDOT dimer is unique in that the ICT is noticeably absent due to a lack of D-A interactions. Additionally, the π-π^*

transition has a bathochromic (red) shift relative to the other analogues due to enhanced HOMO destabilization from a greater donor concentration along the CP backbone. Conversely, the BTD dimer having pendant electron deficient rings on the CP backbone does show both characteristic transitions (ICT and π-π^*) albeit with the π-π^* hypsochromically (blue) shifted compared to the EDOT dimer due to the acceptor contribution stabilizing the HOMO. Lastly, the archetypical D-A example EDOT-BTD dimer has both transitions. The ICT of EDOT-BTD has a significant red shift compared to the BTD dimer due to the acceptor contribution to the LUMO (stabilization) and the donor contribution to the HOMO (destabilization) for an overall lower HOMO-LUMO gap.

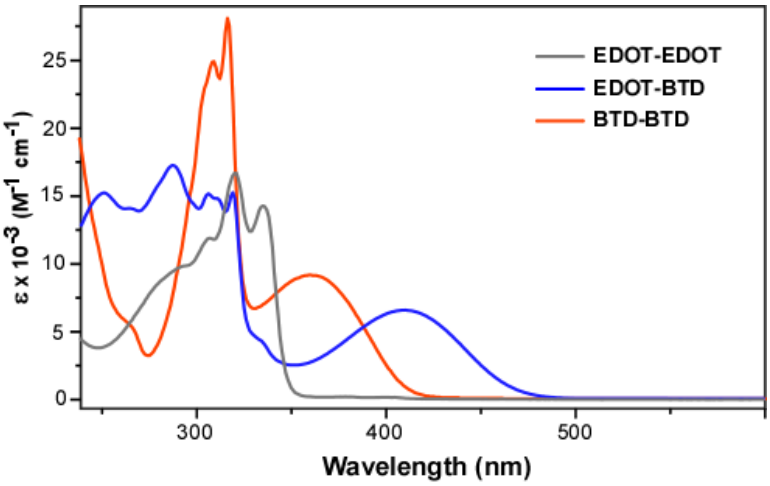

Figure 3.8. UV-vis spectra for D-D, D-A, and A-A species.[16]

The ambipolar TP unit requires special attention here because if it were to be treated as a typical electron acceptor species the trends in the UV-vis at first may seem inconsistent with the current knowledge of D-A interactions, but upon further investigation fit well with the current understanding. As shown in Figure 3.9 A, when TP is paired with a strong donor species such as EDOT both the ICT and π-π^* transitions are present. This is as expected, but where the D-A theory seems to breakdown is in the relation to TP-TP, which shows a red shifted ICT compared

to TP-EDOT. Looking at this from a D-A approach, the paring switch from an EDOT donor to a TP "acceptor" should result in a blue shifted ICT assuming the traditional electron acceptor role for TP and thus an assumed A-A type species. However, because TP is ambipolar, the HOMO is stabilized to a nearly equivalent degree to that of EDOT-TP while also incorporating additional LUMO stabilization. The LUMO stabilization is being enhanced through a hybridization of two pyrazine rings as opposed to a singular electron deficient pyrazine ring in TP-EDOT.

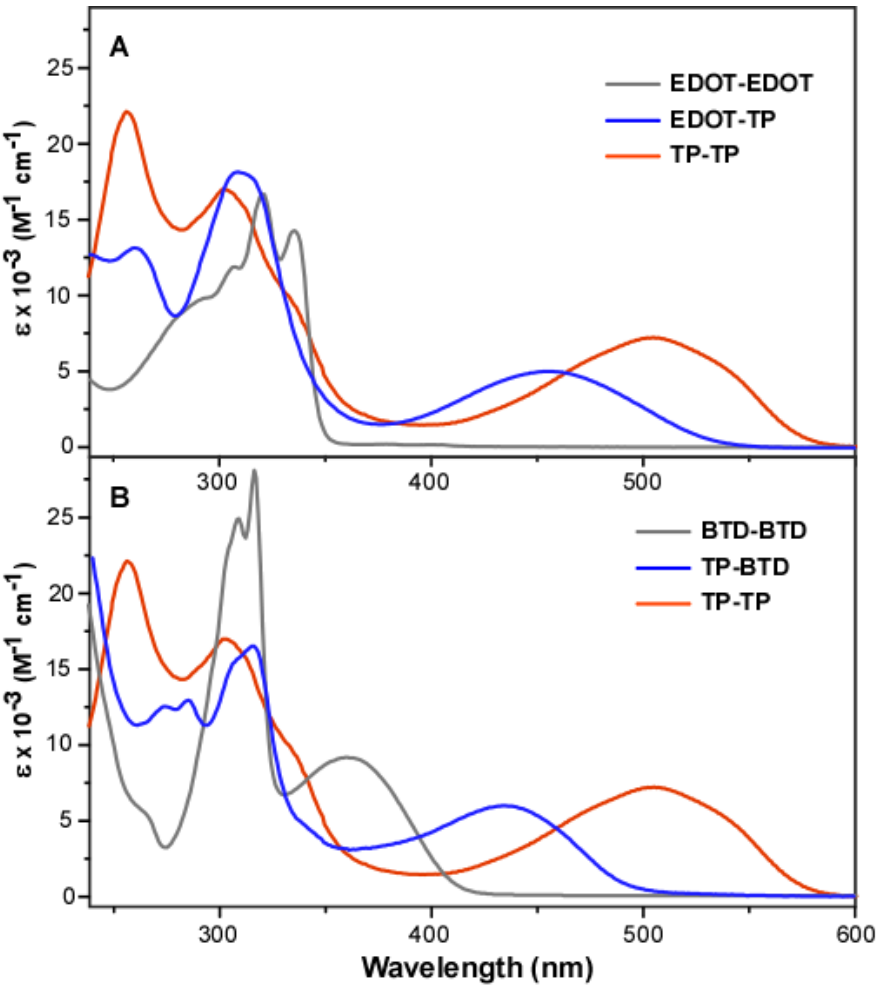

Figure 3.9. UV-vis spectra for (A) D-D, D-TP, TP-TP and (B) A-A, TP-A, and TP-TP.[16]

In conjunction, Figure 3.9 B shows the comparison between the various TP and BTD species to depict the ambipolar-A interactions. As with the D-TP system, the TP-A dimer

produces an ICT transition that is inconsistent with the treatment of TP as a traditional acceptor. The ICT transition here is blue shifted in comparison to TP-TP and due to a BTD contribution to the HOMO. This once again illustrates the ambipolar nature of TP in that when a traditional acceptor such as BTD interacts with another strong acceptor as in BTD-BTD the ICT is significantly blue shifted. The strong donor characteristics of TP however red shift the ICT when paired with BTD and the ICT is red shifted even further in TP-TP.

Fluorescence Spectroscopy and Solvatochromism

Further attempts to quantify charge transfer effects in the symmetrical BTD-BTD analogue were pursued through fluorescence spectroscopy. The BTD-BTD analogue being investigated specifically because BTD monomer shows no ICT transition in its absorption spectrum.[33] If the higher energy absorption in BTD-BTD is indeed an ICT transition then the influence of the solvent on the energy of the excited state should show a solvatochromic shift with varying solvent polarity.[34]

In Figure 3.10, four solvents were investigated with the relative polarities of chloroform < acetone < acetonitrile < methanol. While chloroform, acetone, and acetonitrile are relatively close in emission energy, they do show a red shift that follows an increase polarity trend. The most significant shift came from the most polar solvent methanol and implied that the excited species is indeed stabilized by a polar solvent. A characteristic that a CT species with an increase in dipole moment would show from a solvent that could stabilize the excited state through dipole interactions.[34] The difference between the monomer and dimer therefore is likely increased delocalization between phenyl rings which destabilizes the HOMO and thus makes the biphenyl a better donor for CT to occur.

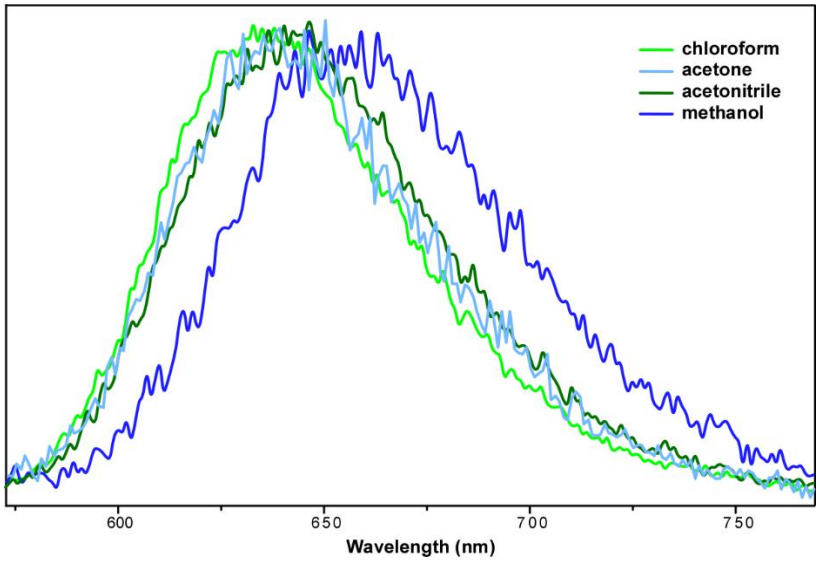

Figure 3.10. Fluorescence spectroscopy showing the solvatochromism of BTD-BTD.[16]

Electrochemistry

The electrochemical analysis of the six dimer species was carried out through cyclic voltammetry (CV) and the frontier orbital MOs estimated by first oxidation/reduction onsets with reference to the ferrocenium/ferrocene (Fc^+/Fc) couple which has a formal potential of -5.1 eV in

Table 3.2. Electrochemical data for dimer series containing EDOT, TP, and BTD units.[16]

Compound	E_{pa}[a](V)	$E_{1/2}$[a](V)	ΔE (mV)	HOMO (eV)[b]	LUMO (eV)[c]
EDOT-EDOT	0.49			-5.44	
BTD-BTD	1.58	-1.68, -1.94[d]	60,60[d]	-6.56	-3.50
EDOT-BTD	0.91	-1.76	80	-5.80	-3.45
EDOT-TP	0.49	-1.88	70	-5.43	-3.30
TP-BTD	0.93	-1.70	220	-5.85	-3.55
TP-TP	0.50	-1.83	110	-5.45	-3.40

[a]*vs.* Ag/Ag^+. [b]E_{HOMO} =-($E_{[onset, ox vs. Fc^{\bullet}/Fc]}$+5.1)(eV). [c]$E_{LUMO}$ = -($E_{[onset,red vs. Fc^{\bullet}/Fc]}$ + 5.1) (eV).
[d]Unpublished data

relationship to the vacuum scale.[35] All species (Table 3.2.) show an irreversible oxidation as expected in thiophene containing small molecules due to the oxidized species ability to couple via a thiophene based radical cation.[36] This rationalization extends to a phenyl-based radical cation for BTD-BTD which contains no thiophene and similarly undergoes oxidative coupling. Other significant structural differences in voltammograms of the dimeric species are the reversibility of the reductions. For a process to be considered reversible the $\Delta E = |E_{pc} - E_{pa}|$ must be ≤ 57 mV/n (@ 25 ˚C) and indicates that oxidized and reduced species are at equilibrium on the electrode surface.[37]

All dimeric species investigated showed a quasi-reversible ($\Delta E > 57$ mV/n) reduction except for EDOT-EDOT which has no reduction within the solvent window (Figure 3.11). This reduction occurring by electron injection on the electron deficient portion of a monomer which is pyrazine in TP, and thiadiazole in BTD and thus not present in EDOT-EDOT which has a

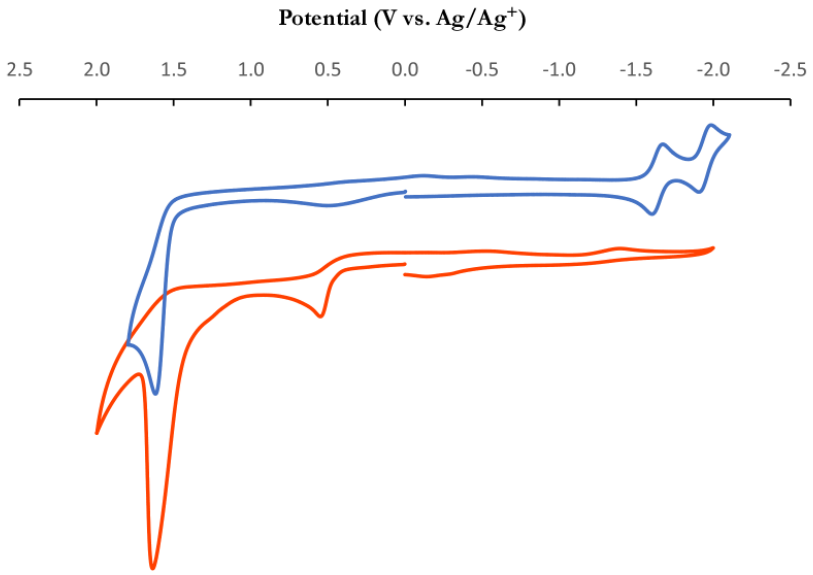

Figure 3.11. Cyclic voltammograms of BTD-BTD (blue) and EDOT-EDOT (orange).

pendant ring that is electron rich. Additionally, BTD-BTD has an additional higher energy quasi-reversible reduction that has also been observed in TP-trimers[22]. This likely being from each electron deficient pendant ring being capable of reduction and in the case of BTD-BTD, low enough in energy to be within the solvent window (Figure 3.11).

Electrochemistry of Dimers: Comparison and Analysis

An initial comparison can be made between the symmetric species to better characterize donors, acceptors, and ambipolar units in general. The all-donor EDOT-EDOT has as expected a significantly destabilized HOMO while its LUMO so high in energy as to be outside the solvent window requiring comparisons to be made with its calculated value of -1.01 eV (B3LYP)[16] and thus also the highest in energy of any dimer in the series. Conversely, the all-acceptor BTD-BTD has the most stabilized HOMO as well as a significantly stabilized LUMO. The TP-TP species has a HOMO comparable to EDOT-EDOT and LUMO slightly more destabilized than BTD-BTD which as expected makes it both a strong donor and strong acceptor and as a result the lowest HOMO/LUMO gap of all the dimers in the series. Therefore, as a tool for HOMO/LUMO reduction in polymeric materials, a unit that can both destabilize the HOMO and stabilize the LUMO may be more crucial than simply incorporating the strongest donors or acceptors in the polymer backbone.

A look at the asymmetric dimer species likewise shows how significant the presence of the ambipolar TP unit is in HOMO/LUMO reduction. If the series is looked at from the simplistic view of traditional D-A theory of pairing the strongest donor with the strongest acceptor, then the EDOT-BTD should produce the dimer with the smallest HOMO/LUMO gap. As mentioned previously, this is not the case, and TP-TP claims this title. In fact, the significant trend is that all dimers containing TP show the lowest HOMO/LUMO gaps in the series. As a

specific counter example to the confined D-A class system, TP often regarded as an acceptor in D-A theory, when paired with BTD in TP-BTD has a lower HOMO/LUMO gap than EDOT-BTD indicating that TP is a better donor than EDOT if the standard "strongest donor with strongest acceptor generates lower bandgaps" logic applies. While the HOMOs of EDOT-EDOT and TP-TP are within 0.01 eV, the crucial component that reduces the HOMO/LUMO of TP-BTD is the additional LUMO stabilization due to hybridization from each unit in the dimer. Lastly, EDOT-TP according to D-A theory has a strong donor paired with a strong acceptor and as expected produces a dimer with a significantly reduced HOMO/LUMO gap. However, once again when compared to TP-TP, the destabilization of the HOMO due to both units being strong donors is still less significant than an all ambipolar system that has hybridization occurring at both the HOMO and the LUMO.

X-ray Crystallography

Attempts to grow single crystals of all dimer species was carried out by the Rasmussen group with the limited success of EDOT-BTD (Figure 3.12) (grown by Trent Anderson), EDOT-EDOT (Figure 3.13) (previously reported by Jean Roncali), and BTD-BTD (Figure 3.14) (giving crystals suitable for analysis.[16] This limited success however did give useful information and comparisons to the known structures of thiophene and BTD[38] and allowed for significant conclusions about frontier orbital energies to be drawn.

The EDOT-BTD dimer crystallizes in the monoclinic space group $P2_1/c$, with four molecules per unit cell. The dimer exists in the anti-configuration with a completely planar BTD unit and an EDOT unit with an 18˚ rotation about the interannular bond twisting it slightly out of the plane. When compared to thiophene, the EDOT unit shows little structural differences on the thiophene portion with bond lengths that are nearly identical on the thiophene portion of EDOT.

The comparison of BTD in the dimer does however show significant structural changes when compared to BTD in that the dimer BTD has a six membered ring that has bond lengths closer to benzene.

The significant bond regarding the contribution of the additional resonance structure as predicted by the D-A model is the C-C bond between EDOT and BTD. This bond was found to be 1.469 Å which indicates significantly more single bond character than double bond character when compared to the typical C-C length of 1.52 Å and a typical C=C length of 1.35 Å.[39] This in conjunction with the presence of a 18˚ interannular twist thus indicates that structurally the EDOT-BTD dimer has little to no double bond character at the C-C bond linking the two units together and thus limits the contribution if any of the potential additional resonance structure outlined in Figure 3.1.

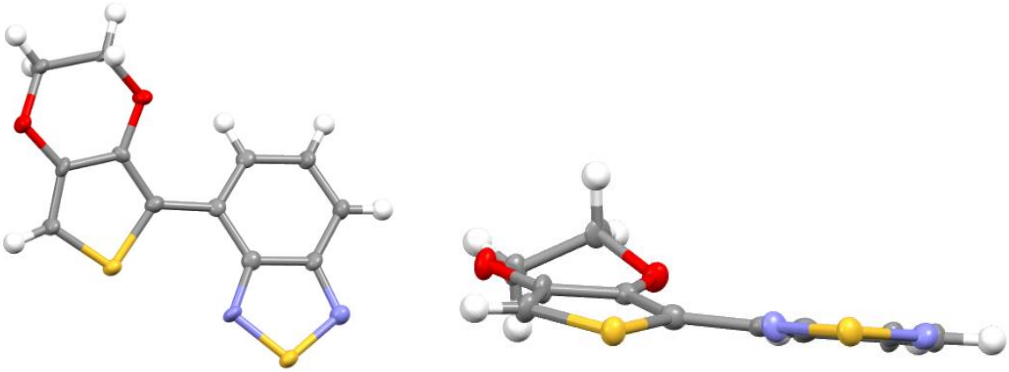

Figure 3.12. (left) Face and (right) edge ellipsoid plots of EDOT-BTD at the 50% probability level.[16]

The X-ray quality crystals of EDOT-EDOT agreed precisely with that of the previously reported data.[23,40] EDOT-EDOT is unique among the dimer models investigated in that the potential for two non-bonding S-O interactions are possible. These interactions have been shown to be well within the sum of the van der Waals radii of sulfur and oxygen (3.25 Å) with a distance of 2.92 Å, indicating a strong interaction between the two atoms. Consequently, this

interaction results in a system with a high level of planarity (0˚ interannular twist) along the conjugated portion with significant rigidity (Figure 3.12).[40] As a comparison, EDOT-BTD shows significant twisting out of the plane between EDOT and BTD with the previously mentioned 18˚ interannular twist. While there is the potential for S-N interactions, there is also a hydrogen bonding opportunity between the interior O on EDOT with the interior H on BTD that further twists the dimer out of planarity.

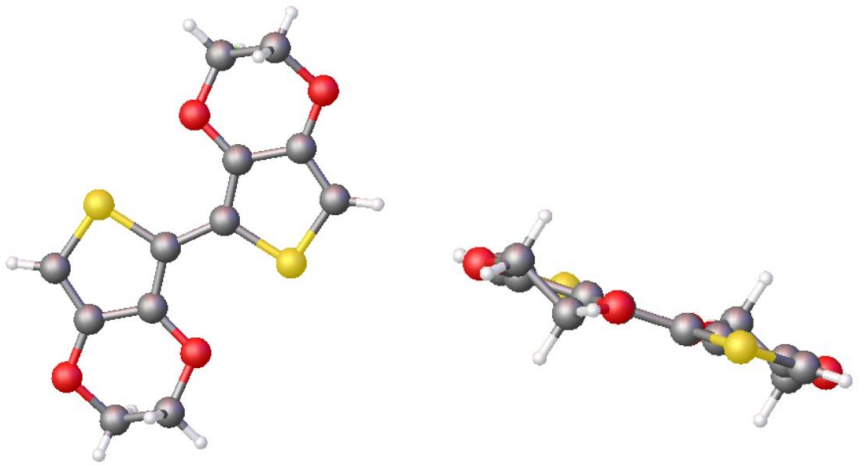

Figure 3.13. (left) Face and (right) edge ball and stick plots of EDOT-EDOT from single crystal X-ray analysis.[40]

Lastly, the previously unreported BTD-BTD X-ray quality crystals were grown via slow evaporation from toluene at room temperature followed by cooling to 0 ℃. The most significant structural change between BTD-BTD and the previously discussed structures (EDOT-BTD and EDOT-EDOT) is the large twisting out of planarity of 43˚ between the two BTD units (Figure 3.14). This large twisting indicates hydrogen bonding is minimized between N002 and the hydrogen attached to C004 and results in a repulsive interaction.

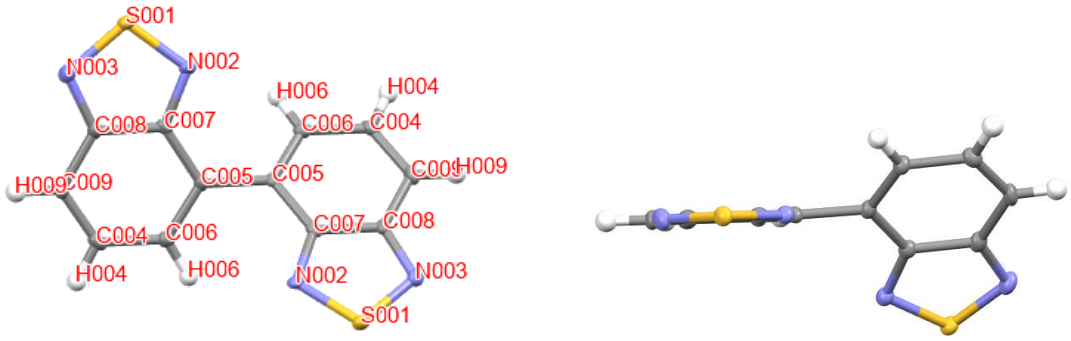

Figure 3.14. Face and edge ellipsoid plots of BTD-BTD at the 50% probability level.

Limited hydrogen bonding is also indicated by the distance between N002 and the attached hydrogen to C004 with a calculated value of 2.663 Å (Figure 3.15). This distance is significantly longer than the H···O distance in EDOT-BTD which was calculated to be 2.267 Å as well as the. H···N distance in TP-BTD which was calculated to be 2.230 Å.[16] While the hydrogen bonding distance is increased in BTD-BTD, it is still within what is considered a significant interaction distance of 2.7-3.5 Å[41] and thus this interaction while apparently weaker may still have some favorable interaction.

In addition to the increase in the H···N distance is the decrease C-H···N angle of BTD-BTD which was calculated to be 107.6˚. In comparison EDOT-BTD's C-H···O angle was calculated to be 124.8˚ while TP-BTD's C-H···N was calculated to be 127.5˚. Therefore, comparatively BTD-BTD has an enhanced deviation from linearity and thus minimizes hydrogen bonding interactions.[41] Thus if both the distances and angles of these interactions are to be taken into account EDOT-BTD TP-BTD, and BTD-BTD all have hydrogen bonding distances that fall within what are deemed significant interactions (2.7-3.5 Å) while BTD-BTD's ~20˚ increased angle out of linearity reduces the possibility of overlap and indicates the distance is purely due to purely coincidental structural factors.

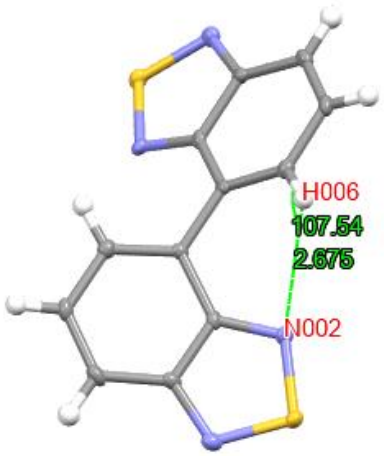

Figure 3.15. Estimated distance between H006 and N002 for potential hydrogen bonding.

Additionally, the crystal packing indicates the presence of significant π-π interactions with the packing showing a face on slip-stacked orientation (Figure 3.16). This interaction has a face-to-face distance of 3.712 Å which falls within the upper end of window (3.3-3.8 Å) of what is considered significant π-π interactions.[42] Outside of π-π intermolecular interactions is the potential of other interactions such as hydrogen bonding and heteroatom lone-pair interactions such as S···N interactions (Figure 3.17). While these two interactions may be present here, they appear to be relatively weak. Specifically, in the case of the S···N interaction that which although oriented in a favorable position with two potential interactions has a distance (3.674 Å) larger than that of the van der Waals radii of sulfur and nitrogen (3.35 Å)[39].

Two potential hydrogen bonding cases with sulfur and nitrogen are also possible (Figure 3.16). The S···H interaction is favorably oriented and somewhat elongated (3.314 Å) indicating a weak interaction. While the N···H interaction is favorably oriented and significantly shorter (2.702 Å) than the S···H interaction implying that the N···H has the more significant hydrogen bonding character and thus should be the greater contributor to the crystal packing structure.

Comparison of the different interannular bonds of the respective dimer units analyzed via X-ray spectroscopy (Table 3.3) have interesting implications when considered through a D-A rationalization. First and foremost, of the three the shortest C-C distance between units is EDOT-EDOT which indicates the most double bond character. The BTD-BTD conversely has the longest interannular C-C distance of the three indicating the least double bond character. Lastly, EDOT-BTD has a C-C distance which is almost exactly the average of the other two.

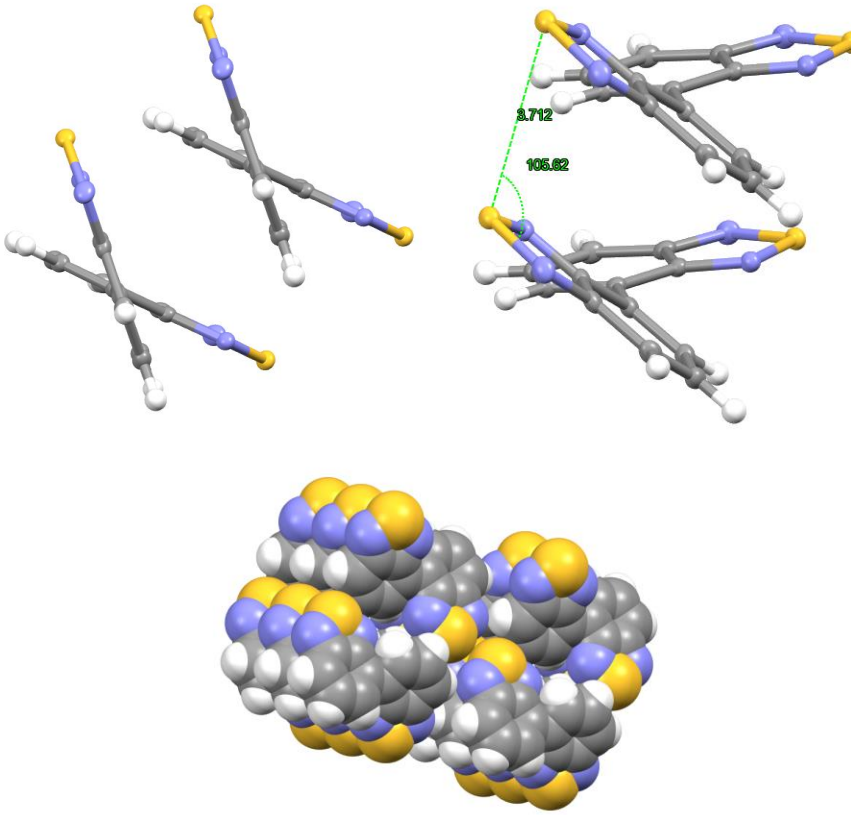

Figure 3.16. Evidence of π-π interactions in the crystal structure of BTD-BTD.

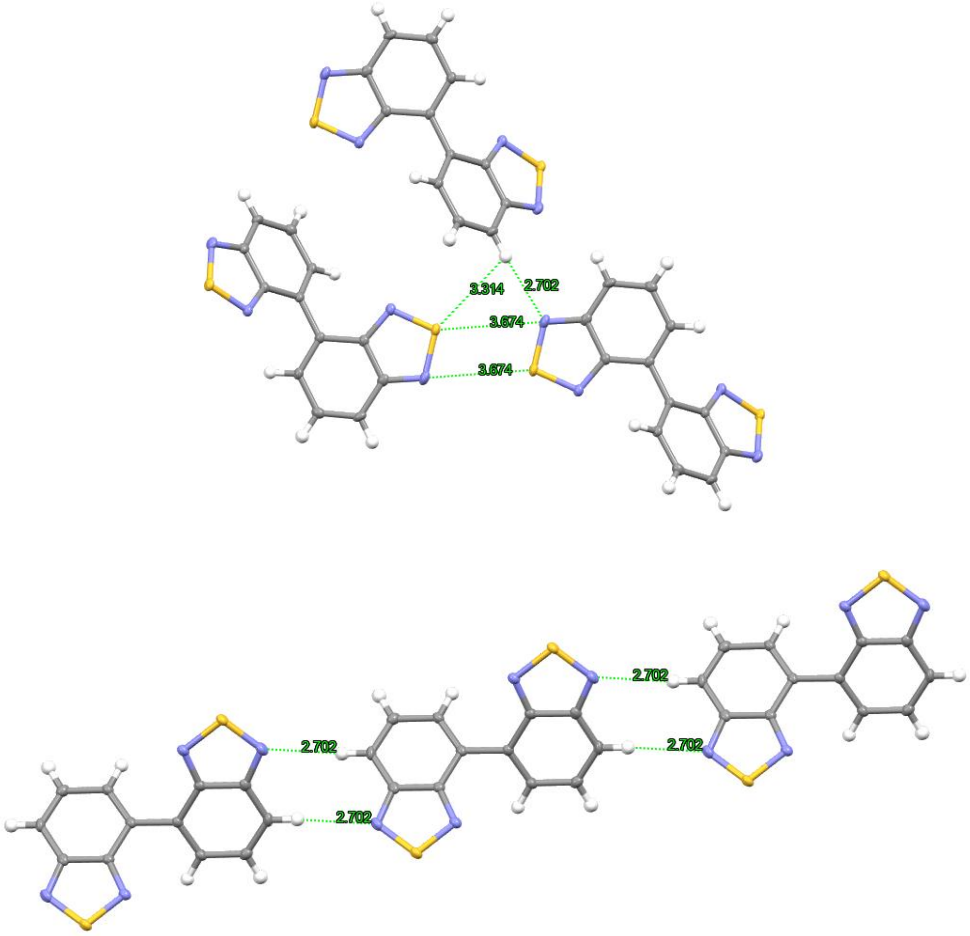

Figure 3.17. Possible intermolecular interactions present in crystal packing.

Table 3.3. Interannular bond angles and distances for respective dimer units analyzed via X-ray spectroscopy.

Dimer unit	Interannular C-C-C-C torsional angle (°)	Interannular C-C bond distance (Å)
EDOT-BTD[a]	162.00	1.469
EDOT-EDOT[b]	180.00	1.442
BTD-BTD	132.63	1.490

[a]Ref. 16 and [b]Ref. 23

From a D-A approach the EDOT-BTD should have the shortest C-C distance of the three due the presence of the resonance structure contributor outlined in Figure 3.1 from the pairing of

a strong donor with a strong acceptor. However, no evidence of the shortening of this bond due to D-A interactions is observed and the deviation from this prediction is therefore likely due to other factors with the most apparent being the steric interactions from the internal hydrogens on the benzo-containing species. These steric interactions likely cause the twisting out of planarity and follow the trend EDOT-EDOT < EDOT-BTD < BTD-BTD with a corresponding reduction in the number of internal hydrogens. Interestingly, once again EDOT-BTD has an interannular torsional angle at the near exact average of the other two. Therefore, although the intramolecular interactions seem to be the dominant factor in the interannular bond distances and angles, the presence of some degree of shortening beyond the averaging of the two homodimer systems should be observed with EDOT-BTD and is notably absent.

Conclusions

In this chapter the model dimer systems provided insight into some of the concepts that are often assumed for D-A systems without having been specifically vetted for variable systems. A significant finding in this study is the limited evidence for the existence of any double bond character between any of the D-A dimeric species. This indicates that the often-stated reduction in bond length alternation as a determining factor for E_g reduction may be overstated. The more important factor in these model systems appears to be the hybridization of frontier MOs and thus the most significant HOMO/LUMO reductions come from the incorporation of ambipolar units with a low-lying LUMOs that also have high-lying HOMOs (Figure 3.18). This being due to the HOMO having contributions from both donor and acceptor units while the LUMO is essentially localized on the acceptor. The information garnered from this study should provide a design motif that can be applied to alternating copolymer systems in which E_g control is a primary focus.

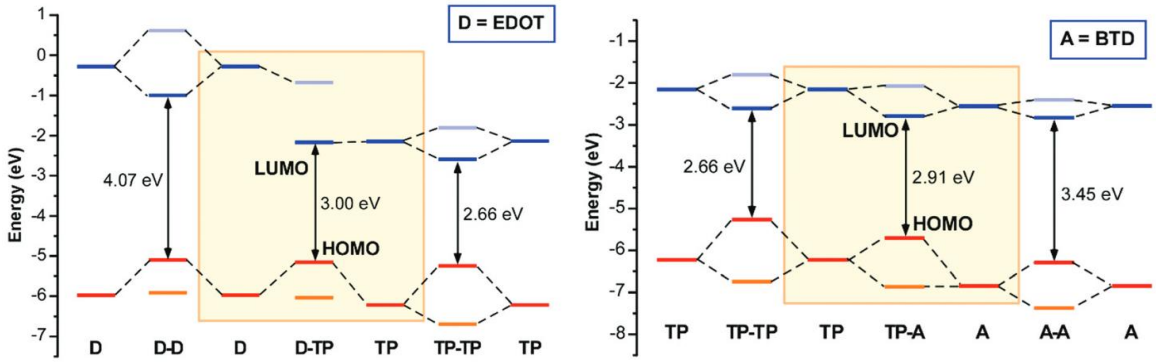

Figure 3.18. Modified D-A frontier orbital diagram showing the reduction in HOMO/LUMO energies with the pairing of TP with donors or acceptors.[16]

Experimental

X-Ray Crystallography

X-Ray quality crystals of EDOT-EDOT were grown via slow evaporation in cyclopently methyl ether for 48 hours. Similarly, X-ray quality crystals of BTD-BTD were grown via slow evaporation in toluene at room temperature for 48 hours followed by cooling to 0 °C for 24 hours. The X-ray intensity data of the crystals were measured at either 273 or 100 K on a CCD-based X-ray diffractometer system equipped with a Cu X-ray tube (l = 1.54178 Å) operated at 2000 W of power. Crystals were then compared to previously reported crystal structure[40] and the structure was confirmed.

Absorption Spectroscopy

A dual beam scanning UV-vis-NIR spectrophotometer was used to perform UV-vis absorption spectroscopy measurements. Extinction coefficients were determined by preparing a 100 mL stock solution of 2.0 x 10^{-4} M dimer sample which was subsequently used to make 25mL diluted solutions containing 1, 2, 3, and 4 mL of the stock solution to generate 8.0 x 10^{-6},

1.6 x 10^{-5}, 2.4 x 10^{-5}, 3.2 x 10^{-5} M solutions respectively. Extinction coefficients were converted to oscillator strengths via spectral fitting and calculated with literature methods.[32]

Electrochemistry

Electrochemical analysis was conducted with a three-electrode cell with platinum disc working and platinum wire reference electrodes. A reference Ag/Ag^+ (0.251 vs. SCE) electrode was built in house and consisted of 0.01 M solution of $AgNO_3$, and 0.1 M solution of tetrabutylammonium hexafluorophosphate ($TBAPF_6$) all in CaH dried MeCN. All electrochemical cells were oven dried and prior to taking measurements, cells were sparged with argon. Measurements were then taken with blanketed argon at a scan rate of 100 mV s^{-1}. Estimated E_{HOMO} and E_{LUMO} were determined by taking the onsets of first oxidation and reduction and compared to ferrocene (50 mV vs. Ag/Ag^+) with a value of 5.1 eV vs. vacuum for ferrocene.[35]

Materials

2,5-Dibromothiophene, 3,4-diamino-2,5-dibromothiophene,[29,43] 2,1,3-benzothiadiazole, and 4-Bromobenzo[*c*][1,2,5]thiadiazole[33] were prepared as previously reported. 4-(3,4-Ethylenedioxythiophen-2-yl)benzo[c][1,2,5]thiadiazole (EDOT-BTD), 2,3-Dihexyl-5-(trimethylstannyl)thieno[3,4-b]pyrazine, 5-(3,4-Ethylenedioxythiophen-2-yl)-2,3-dihexylthieno[3,4-b]pyrazine (EDOT-TP), and 4-(2,3-Dihexylthieno[3,4-b]pyrazin-5-yl)benzo[c][1,2,5]thiadiazole (TP-BTD) were prepared by Trent Anderson.[16] 2,2',3,3'-tetrahexyl-7,7'-bis(trimethylsilyl)-5,5'bis(thieno[3,4-b]pyrazine) (TP-TP) was prepared by Li Wen.[22] Unless specified, all other reagents were purchased and used without further purification. Reactions were carried out under a nitrogen environment with a Schlenk line setup.

Synthesis

4,4'-Bis(benzo[*c*][1,2,5]thiadiazole) (BTD-BTD) The following is a modification of previously reported methods. Zinc powder (0.38 g, 5.7 mmol), Ni(dppp)Cl_2 (0.607 g, 1.12 mmol), and Bu_4NBr (0.122 g, 0.378 mmol) were added to 10 mL of THF and stirred under N_2. 4-Bromobenzo[*c*][1,2,5]thiadiazole (0.830 g, 3.86 mmol) was then added and the mixture was heated at reflux for 6 h. The solvent was removed under reduced pressure and the crude product was purified via silica chromatography with CH_2Cl_2 as the eluent to give a light-yellow solid (85–90% yield). M.p. 240.4– 241.4 1 ˚C (lit. 240–241 1C). ^{1}HNMR: δ 8.27 (dd, J = 1.0, 7.0 Hz, 2H), 8.12 (dd, J = 1.0, 8.8 Hz, 2H), 7.81 (dd, J = 7.0, 8.8 Hz, 2H). ^{13}CNMR: δ 155.5, 153.6, 130.8, 130.0, 129.5, 121.7. NMR data agree well with previously reported values. [16]

2,20-Bis(3,4-ethylenedioxythiophene) (EDOT-EDOT). The following is a modification of previously reported methods.[43] EDOT (1.02 g, 7.18 mmol) was dissolved in 20 mL dry THF. While being stirred, it was then evacuated and backfilled with N_2 three times. The solution was then cooled to -78 ˚C and BuLi (3.0 mL, 2.5 M in hexanes) was added dropwise over a span of 10 min, keeping the temperature below -70 ˚C. Once the BuLi was completely added, the mixture was warmed to 0 ˚C and stirred for 2 h. Anhydrous $CuCl_2$ (1.415 g, 10.5 mmol) was then added, and the mixture stirred for 18 h. The solution was then filtered, and solvent removed under reduced pressure. The crude product was purified via silica chromatography with CH_2Cl_2–hexanes (1:1 v/v) as the eluent to yield 0.44 g of a white solid (43% yield). M.p. 212.1–213.1 ℃ (lit. 183–185 1C). ^{1}H NMR: d 6.29 (s, 2H), 4.35 (ddd, J = 1.9, 5.3, 6.2 Hz, 4H), 4.26 (ddd, J = 1.9, 5.3, 6.2 Hz, 4H). ^{13}C NMR: δ 141.2, 137.0, 109.9, 97.5, 65.0, 64.6. NMR data agree well with previously reported values.[16]

References

1. Roncali, J. *Macromol. Rapid Commun.* **2007**, *28* (17), 1761–1775.
2. Rasmussen, S.C. *Encyclopedia of Polymeric Nanomaterials*; Kobayashi, S., Müllen, K. Eds.; Springer: Berlin Heidelberg, 2013; pp1-13
3. Rasmussen, S. C.; Pomerantz, M. Low Bandgap Conducting Polymers. In *Handbook of Conducting Polymers*; Skotheim, T. A., Reynolds, J. R., Eds.; CRC Press: New York, 2008.
4. Rasmussen, S. C.; Schwiderski, R. L.; Mulholland, M. E. *hem. Commun.* **2011**, *47* (41), 11394–11410.
5. Konkol, K.; Schwiderski, R.; Rasmussen, S. *Materials* **2016**, *9* (404), 1–16.
6. Culver, E. W.; Anderson, T. E.; López Navarrete, J. T.; Ruiz Delgado, M. C.; Rasmussen, S. C. *ACS Macro Lett.* **2018**, *7* (10), 1215–1219.
7. Anderson, T. E.; Culver, E. W.; Almyahi, F.; Dastoor, P. C.; Rasmussen, S. C. *Synlett* **2018**, *29* (19), 2542–2546.
8. Evenson, S. J.; Mulholland, M. E.; Anderson, T. E.; Rasmussen, S. C. *Asian J. Org. Chem.* **2020**, *9* (9), 1333–1339.
9. Van Mullekom, H. A. M.; Vekemans, J. A. J. M.; Havinga, E. E.; Meijer, E. W. *Mater. Sci. Eng.* **2001**, *32*, 1–40.
10. Bundgaard, E.; Krebs, F. C. *Sol. Energy Mater. Sol. Cells* **2007**, *91* (11), 954–985.
11. Beaujuge, P. M.; Amb, C. M.; Reynolds, J. R. *Acc. Chem. Res.* **2010**, *43* (11), 1396–1407.
12. Chochos, C. L.; Choulis, S. A. *Prog. Polym. Sci.* **2011**, *36* (10), 1326–1414.
13. Duan, C.; Huang, F.; Cao, Y. *J. Mater. Chem.* **2012**, *22* (21), 10416–10434.
14. Havinga, E. E.; ten Hoeve, W.; Wynberg, H. *Polym. Bull.* **1992**, *29*, 119–126.

15. Havinga, E. E.; ten Hoeve, W.; Wynberg, H. *Synth. Met.* **1993**, *55* (1), 299–306.
16. Anderson, T. E.; Culver, E. W.; Badı-Dominguez, I.; Wilcox, W. D.; Buysse, C. E.; Ruiz Delgado, M. C.; Rasmussen, S. C. *Phys Chem Chem Phys* **2021**.
17. Kertesz, M.; Choi, C. H.; Yang, S. *Chem. Rev.* **2005**, *105* (10), 3448–3481.
18. Salzner, U.; Karaltı, O.; Durdağı, S. D *J. Mol. Model.* **2006**, *12* (5), 687–701.
19. Kertesz, M.; Yang, S.; Tian, Y. *Handbook of Thiophene- Based Materials*; Perepichka, I. F., Perepichka, D. F., Eds.; John Wiley & Sons: Chichester, West Sussex, UK, 2009; Vol. 1, pp 341–364.
20. Ou, P.; Shen, W.; He, R.; Xie, X.; Zeng, C.; Li, M. *Polym. Int.* **2011**, *60* (9), 1408–1418.
21. Mulholland, M. E.; Konkol, K. L.; Anderson, T. E.; Schwiderski, R. L.; Rasmussen, S. C. *Aust. J. Chem.* **2015**, *68* (11), 1759–1766.
22. Wen, L.; Heth, C. L.; Rasmussen, S. C. *Phys. Chem. Chem. Phys.* **2014**, *16* (16), 7231–7240.
23. Roncali, J.; Blanchard, P.; Frère, P. *J. Mater. Chem.* **2005**, *15* (16), 1589–1610.
24. Wang, Y.; Michinobu, T. *J. Mater. Chem. C* **2016**, *4* (26), 6200–6214.
25. Du, J.; Biewer, M. C.; Stefan, M. C. *J. Mater. Chem. A* **2016**, *4* (41), 15771–15787.
26. Iyoda, M.; Otsuka, H.; Sato, K.; Nisato, N.; Oda, M. *Bull. Chem. Soc. Jpn.* **1990**, *63* (1), 80–87.
27. Velauthamurty, K.; Rajapakse, R. M. G.; Higgins, S. J. *Inorganica Chim. Acta* **2017**, *464*, 59–64.
28. Espinet, P.; Echavarren, A. M. *Angew. Chem. - Int. Ed.* **2004**, *43* (36), 4704–4734.
29. Kenning, D. D.; Mitchell, K. a; Calhoun, T. R.; Funfar, M. R.; Sattler, D. J.; Rasmussen, S. C. *J. Org. Chem.* **2002**, *67* (25), 9073–9076.

30. Rasmussen, S. C.; Sattler, D. J.; Mitchell, K. A.; Maxwell, J. *J. Lumin.* **2004**, *109* (2), 111–119.

31. Burnett, R. W. *J. Res. Natl. Bur. Stand. Sect. Phys. Chem.* **1972**, *76A* (5), 483.

32. Turro, N. J. *Modern Molecular Photochemistry*; University Science Books: Sausalito, CA, 1991; pp 76–152.

33. Tao, Y.-M.; Li, H.-Y.; Xu, Q.-L.; Zhu, Y.-C.; Kang, L.-C.; Zheng, Y.-X.; Zuo, J.-L.; You, X.-Z. *Synth. Met.* **2011**, *161* (9), 718–723.

34. Suppan, P.; Ghoneim, N. *Solvatochromism*; The Royal Society of Chemistry, 1997.

35. Cardona, C. M.; Li, W.; Kaifer, A. E.; Stockdale, D.; Bazan, G. C. *Adv. Mater.* **2011**, *23* (20), 2367–2371.

36. Audebert, P.; Catel, J.-M.; Le Coustumer, G.; Duchenet, V.; Hapiot, P. *J. Phys. Chem. B* **1998**, *102* (44), 8661–8669.

37. Mabbott, G. A. *J. Chem. Educ.* **1983**, *60* (9), 697.

38. Luzzati, V. *Acta Crystallogr.* **1951**, *4* (3), 193–200.

39. *CRC Handbook of Chemistry and Physics*; Lide, D., R., Frederikse, H. P. R., Eds.; CRC Press: Boca Raton, FL, 1995; pp 9–4.

40. Raimundo, J.-M.; Blanchard, P.; Frère, P.; Mercier, N.; Ledoux-Rak, I.; Hierle, R.; Roncali, *Tetrahedron Lett.* **2001**, *42* (8), 1507–1510.

41. Sarma, J. A. R. P.; Desiraju, G. R. *Acc. Chem. Res.* **1986**, *19* (7), 222–228.

42. Janiak, C. *J. Chem. Soc. Dalton Trans.* **2000**, No. 21, 3885–3896.

43. Wen, L.; Nietfeld, J. P.; Amb, C. M.; Rasmussen, S. C. *J. Org. Chem.* **2008**, *73* (21), 8529–8536.

CHAPTER 4. DIRECT ARYLATION POLYMERIZATION OF THIENO[3,4-*b*]PYRAZINE-ACCEPTOR COPOLYMERS

Introduction

The design motif as outlined in chapter 3 showed the pairing of thieno[3,4-*b*]pyrazine (TP) with an electron-deficient acceptor to lower the HOMO/LUMO gap with minimal destabilization of the HOMO.[1] From a polymeric device standpoint this then becomes specifically beneficial by preventing elevated HOMO levels that cause atmospheric instability as well as energetic mismatch between the active layer and the poly(3,4-ethylenedioxythiophene)-modified indium tin oxide (ITO) cathode in photonic devices.[2,3] TP has typically been treated as an electron-accepting unit due to the electron deficiency of the pyrazine ring and has thus been paired with electron-rich donors according to the D-A model.[1] This has led to the underdevelopment of TP-functionalized moieties such as distannyl- and diboroester-substituted analogs which are required for traditional cross-coupling reactions. Therefore, the synthesis of TP-A alternating copolymers by traditional cross-coupling would require the development of new TP analogues in a fashion similar to that of common electron-donating species.[4]

A critical priority for development and implementation of conjugated polymers (CPs) in devices lies in the methods used in their polymerization. While methods vary and have changed over the years, the current primary route to synthesize most CPs is through a small set of cross-coupling reactions (Stille, Suzuki, Negishi, Heck, Kumada). These cross-coupling reactions, while effective in the production of many CPs, have drawbacks such as the need for stoichiometric amounts of main group elements, toxic byproducts, and limited functional group tolerance.[5–9] Therefore, in the pursuit of an ever-expanding toolbox for CP synthesis, a method known as direct arylation polymerizations (DArP) has recently been developed, which reduces

the amount of toxic by-products by avoiding main-group element coupling handles and maintaining a high level of functional group tolerance has found increasing attention.[10–12]

While DArP is currently gaining traction in the literature, it is still somewhat underrepresented as a polymerization method with current a SciFinder search only yielding 523 references while in comparison Stille coupling has over 14,000 reference hits.[13] It then becomes apparent that DArP is still in its infancy and requires further investigation and optimization if it is to replace any of its traditional counterparts. The conditions that will need to be investigated to better understand DArP include temperature, pressure, choice of solvent, additives, and reaction time as a select few parameters that can be altered and investigated for this polymerization method.

Traditional Cross-coupling Methods

In 2010, the Nobel prize was awarded to Richard F. Heck, Ei-ichi Negishi, and Akira Suzuki jointly for their efforts in palladium-catalyzed cross-coupling reactions for organic synthesis.[14] These efforts would lead to a wealth of applications and eventually become the method of choice for most homopolymerizations and copolymerizations of CPs. Additional methods, while not part of the 2010 Nobel prize, have also been developed with the list including Stille (also known as Migita-Stille), Hiyama, and Kumada couplings as other examples that significantly enhanced the utility of palladium cross-couplings for small molecules and polymers[15] (Figure 4.1). Of these additional methods, Stille coupling is a particularly notable example because of John Kenneth Stille's (1930-1989) premature death in a plane crash excluding him from what would have been a share of the 2010 Nobel prize.[16]

These cross-coupling reactions have a few distinct characteristics, with the first and foremost being the presence of a palladium source such as palladium(II) acetate ($Pd(OAc)_2$) or

palladium foil.[5,6,15] Additionally, for each reaction one of the coupling partners is an aryl- or vinyl-halide which has some degree of electrophilicity. While a point of commonality between all but the Heck reaction (has a nucleophilic alkene), the complementary coupling species has a main group functionality which enhances the carbon's nucleophilicity. Thus, an electrophile/nucleophile pair is at the center of these palladium facilitated cross-coupling methods.

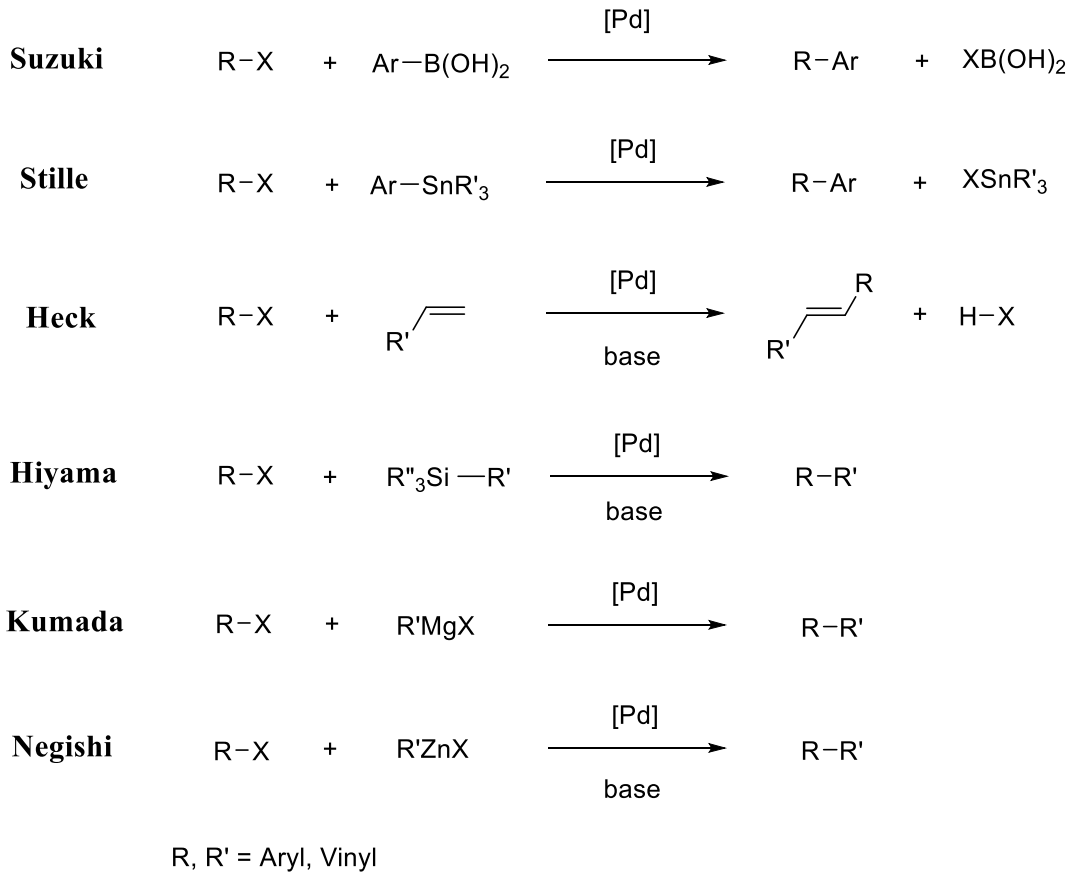

Figure 4.1. Generic schemes of traditional cross-coupling methods.

Of the palladium cross-coupling methods mentioned, the three with specific relevance to CP synthesis are Stille, Suzuki, and Kumada coupling. Stille coupling has been shown to be especially successful in CP synthesis due to high functional group tolerance and the ability to synthesize polymers in good yields.[5] Likewise Suzuki coupling, which incorporates mild

reaction conditions as well as a relatively non-toxic boronic acid handle as a reactive coupling site, is also a frequently used method in CP synthesis.[6] Lastly, Kumada coupling, one of the first palladium based catalytic cross-coupling methods used in CP synthesis[17] has found relatively high usage as a largely in part due to the key benefit to this method coming from the wealth of Grignard precursors that have already been developed albeit at the cost of functional group tolerance.[9]

In general, all palladium cross-coupling reactions mentioned with the exception of the Heck reaction have been proposed to follow the simplified mechanism as outlined in Figure 4.2.[15] This simplified picture is a three step process in which the first step is an oxidative addition of the electrophilic aryl-halide species followed by a transmetallation step for the insertion of the main group functionalized species and finally a reductive elimination to produce the cross coupled species with a newly formed C-C bond.

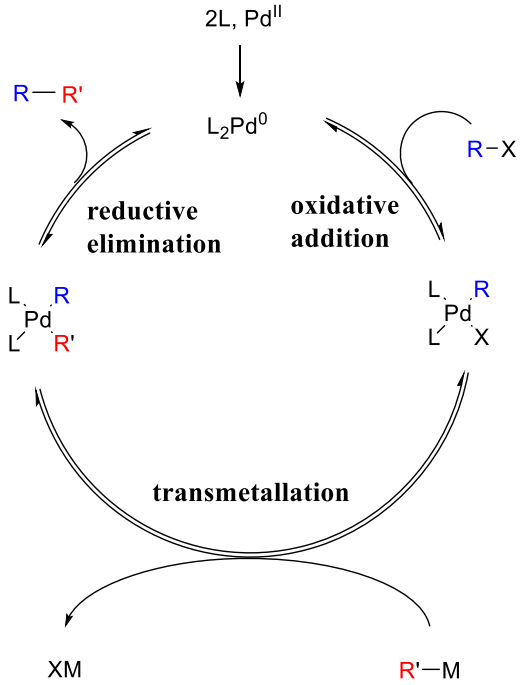

Figure 4.2. Generic proposed mechanism for traditional cross-coupling methods.[15]

Direct Arylation Development

Of the cross-coupling methods previously listed, the Heck coupling reaction is considered the origin of the palladium-based catalysis.[8,15,18] Direct arylation has its origins here as well with couplings being reported as Heck-type reactions even into the 2010s.[19,20] The early direct arylations used a $Pd(OAc)_2$ precatalyst polar amide solvents, and a carbonate or acetate base[10,21,22] which had previously been developed for Heck cross-coupling.[8,18] Likewise the two methods involve the coupling of an aryl-halide species with a non-organometallic species (olefin in Heck and Ar-H in direct arylation). These Heck-type conditions are thus used in many DArP reactions and proposed mechanisms depending on the conditions have been stated as following a Heck-type pathway which is heavily dependent on the electrophilicity of the aryl-halide species.[23,24]

DArP and Conjugated Polymers

The utilization of DArP in the synthesis of conjugated polymers seems to originate in 1999 with one of the first reports coming from Lemaire and coworkers.[25] The initial investigation looked at the synthesis of poly(3-alkylthiophene)s (P3ATs) from 2-iodo-3-alkylthiophene in the presence of a $Pd(OAc)_2$, K_2CO_3, Bu_4NBr, and DMF. This initial report called this coupling "Heck-type" although obviously no olefins are involved in the coupling between the C-H and C-Br on the two different thiophene units leading future investigators to point to this as one of the earliest instances of aryl-aryl coupling via direct arylation for the purposes of polymerization.[23,26,27] The resulting polymers were regioregular, but fairly low molecular weight with M_n= 3000 and a PDI = 2, and it would take until 2010 to be improved by Ozawa et al. where they were able to obtain regioregular polymers with M_n = 30,600.[28] The conditions used here bear a greater resemblance to current conditions in which they used Cs_2CO_3, variable

phosphine ligands, a variety of solvents (THF, DMF, and DMAc) in the presence of either $Pd(OAc)_2$ or Herrmann's catalyst to synthesize poly(3-hexylthiophene) (P3HT) with the conditions shown in Figure 4.3 as their most successful parameters.[28]

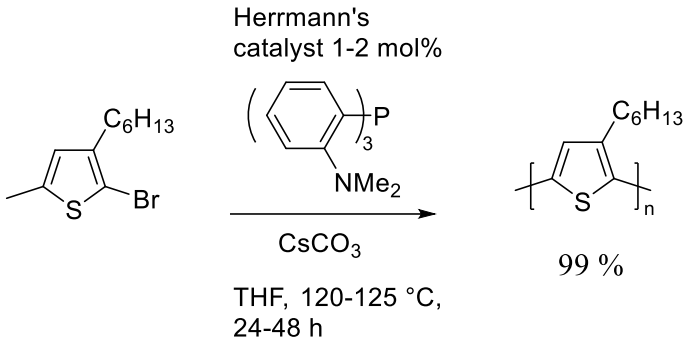

Figure 4.3. Conditions used by Ozawa to synthesize high molecular weight 98% rr P3HT.[28]

The work by Ozawa seems to have been inspired by other work carried out on the synthesis of small molecule species. With a notable previous work coming in 2006 by Fagnou and coworkers[29] where they were able to show that direct arylation need not be limited to the coupling of simple arenes with electron rich species as the previous reactivity had required.[22,30,31] In this work they were able to show successful coupling between simple and electron-deficient arenes with a broad scope of aryl halides, thus expanding the utility of the method.

While the use of Ozawa's conditions and Herrmann's catalyst worked well for the homopolymerization of P3ATs, the initial investigations into donor-acceptor copolymers followed Lemaire's strategy[25] and employed the use of $Pd(OAc)_2$. One of the first donor-acceptor copolymers made in this way came by Kanbara in 2011 where 1,2,4,5-tetrafluorobenzene was coupled with 2,7-dibromo-9,9-dioctylfluorene to make poly[(9,9-dioctylfluorene-2,7-diyl)-*alt*-(2,3,5,6-tetrafluoro-1,4-phenylene)] (PDOF-TFP).[32] Thus with the advances made on both homopolymers and copolymers, DArP has become an increasingly

useful tool in conjugated polymer synthesis with only minor adjustments needed to expand the method to new polymer systems.

Direct Arylation Conditions

Generally, DArP is the catalyzed cross-coupling reaction between two monomers in which one coupling site contains a C-X bond (X = halogen or pseudohalogen) and another contains an aryl sp^2 C-H bond suitably acidic for C-H activation. The coupling results in the formation of a new C-C bond between two aryl units as well as the elimination of H-X. Upon repeated linkage, this forms a polymer as in the reaction shown in Figure 4.4. This method differs from most traditional cross-coupling reactions in that no main-group transition metals are required as a pre-activation step prior to coupling. The transmetallation step which is characteristic of the traditional cross-coupling methods is replaced by a base facilitated concerted metalation deprotonation (CMD) step of the Ar-H species and requires the incorporation of a Brønsted-base such as a carboxylate or carbonate species which can coordinate to the palladium catalyst and remove the Ar'-H proton.

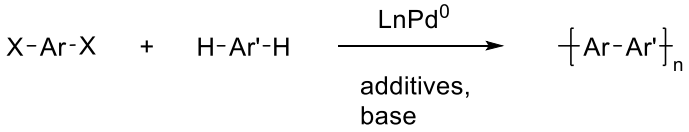

Figure 4.4. General reaction scheme for DArP.

A key parameter that needs to be considered when designing DArP syntheses is the suppression of homocoupling and defect formation. DArP proceeding by the coupling of active C-H bonds is specifically susceptible to this type of unwanted coupling and because defects can significantly impact electronic properties[33], conditions need to be tailored to ensure that coupling only occurs at the desired location. In simple systems such as P3HT the most common defect is the β-coupling, as the proposed mechanism for the CMD step has relatively close activation

energies of 25.6 kcal/mol and 29.9 kcal/mol for the α- and β-positions respectively.[34] The suppression of these coupling defects have been accomplished through low catalyst loadings and precise temperature control.[35] Similarly, in D-A systems the suppression of unwanted homocoupling (D-D and A-A defects) has been accomplished by increasing the steric bulk of phosphine and carboxylate ligand addatives.[36]

The current specifics for DArP reactions include a palladium (others such as copper[37] have also been implemented) catalysts, phosphine ligands, Bronsted bases, carboxylic acids, and depending on the desired products, either a strongly coordinating or polar aprotic solvents.[10–12,38] Reaction specifics will be discussed and analyzed with an emphasis on how these different parameters apply to conjugated polymer synthesis with the specific focus on donor-acceptor systems.

Catalysts

While other metals such as platinum[39] and copper[37] have been used in small molecule direct arylation and DArP reactions, the most common catalysts systems are palladium based.[10–12,33,40] This is due largely in part to the relative stability of Pd(0) with coordinated phosphine ligands that can undergo oxidative addition readily.[41] While multiple Pd-based catalysts have been used, Pd(II) species that can be reduced to Pd(0) in situ are often the starting point due the relative stability of Pd(II) complexes.[15] These include Herrmann-Beller, and $Pd(OAc)_2$ as Pd(II) sources[10] with other Pd(0) precursors such as $Pd_2dba_3{\cdot}CHCl_3$[42] also represented in the DArP literature.

The Herrmann-Beller, or often stated as Herrmann's catalyst (Figure 4.5), has been frequently used in the synthesis of P3ATs. Early success in P3HT synthesis as described by Ozawa were THF superheated to 120-125 ˚C, Hermann-Beller precatalyst (*trans*-di(μ-

acetato)bis[*o*-(di-*o*-tolylphosphino)benzyl]dipalladium(II)) (1-2 mol%), phosphine ligand (tris(2-dimethylaminophenyl)phosphine or tris(o-methoxyphenyl)phosphine)) (2-4 mol%), and Cs_2CO_3 (1 equiv). Under these conditions poly(3-hexylthiophene) was synthesized with M_n up to 30,600 and regioregularity up to 98% head to tail (HT).[28] Later investigations and optimization would show an increase to an M_n of 33,000 and 99.5 HT coupling with Herrmann's catalyst showing superior suppression of β-defects over $Pd(OAc)_2$.[28,43]

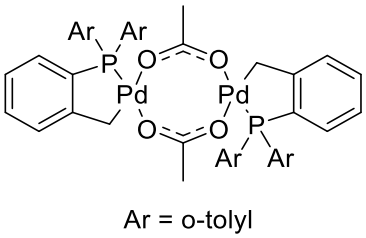

Figure 4.5. Herrmann-Beller Catalyst.

With the origins of DArP coming from the adaption of the Heck reaction, the first palladium source investigated was $Pd(OAc)_2$.[25] This was certainly the case for the initial conditions used by Lemaire, but as previously mentioned, later Herrmann's catalyst was investigated by Ozawa with significant improvements in molecular weights.[28] In the current literature, both catalysts find usage in a variety of cross-coupling reactions.

While Herrmann's catalyst shows superior performance in the synthesis of P3HT, $Pd(OAc)_2$ has continued to find widespread use in DArP procedures.[11,33,42,44] An obvious benefit to using $Pd(OAc)_2$ is that it is simpler than Herrmann's catalyst and as expected, much cheaper. Therefore, its use is preferrable specifically in scenarios where defect formation can be suppressed, or molecular design of the monomers prevents defects altogether.[11]

The activation of $Pd(OAc)_2$ has been shown to proceed by reduction of Pd(II) to Pd(0) by a variety of phosphine ligands.[45–48] This in general requires two additional equivalents of ligand

to be sacrificially oxidized to form phosphine oxide. If the ligand concentration is kept to a minimum, a low ligated Pd(0) is formed which has been shown to be specifically susceptible to oxidative addition with aryl bromides.[47]

Ligands

Depending on the solvent system used, many DArP reactions incorporate phosphine ligands for a variety of reasons including: aggregation disruption of Pd species in solution to generate a higher concentration of active catalyst species[49] and the prevention of homocoupling defects[50] as two studied examples. The ligands that have found the most success in this regard are ortho-substituted triphenyl phosphines such as $P(2\text{-}MeOC_6H_4)_3$ and $P(2\text{-}Me_2NC_6H_4)_3$.[10,11,33] The key features of these ligands being the ability to coordinate to the palladium through the phosphorous as well as through the ortho positioned N or O and potential chelation for enhanced stabilization of the active Pd(0) catalyst.[49,51]

Additional investigations into increasing the steric bulk of tris(o-methoxyphenyl)phosphine at the alkoxy substituent was carried out by Leclerc et al. with the substitution of the methyl group with isopropyl, cyclopentyl, 2-ethylhexyl, methylcyclohexyl, and cycloheptyl groups.[40] Results showed that as the steric bulk of the phosphine ligand increased, the homocoupling and β-defect formations decreased for the coupling between diketopyrrolopyrrole and thiophene. This reactivity was rationalized by a transition state in which the phosphine ligand would be in proximity to a monomer with alkyl sidechains which block the β-site of the coordinated thiophene.

Base Additives

A key difference between DArP and other cross-coupling reactions is the proposed CMD step in the catalytic cycle. Investigations into this step have shown the importance of

incorporating a carbonate base that can coordinate to the catalyst prior to the CMD step and assist in the deprotonation of the incoming Ar-H species.[52,53] Two common reagents in this regard are Cs_2CO_3 and Na_2CO_3. The two carbonate salts have shown similar reactivity with Cs_2CO_3 having a benefit of enhanced solubility in less polar solvents while Na_2CO_3 is significantly more cost effective.[54]

Carboxylic Acids

While carbonate salts alone have been shown to facilitate the CMD step, the addition of carboxylic acids can enhance reactivity through a proposed deprotonation by the carbonate base forming a carboxylate species which can coordinate to the palladium catalyst.[33] In this regard the carboxylic acid species has been deemed a "proton shuttle" in which the coordinated carboxylic acid deprotonates the incoming Ar-H and is sequentially deprotonated by a carbonate base.[11,55] The carboxylate species also brings the added benefit of incorporating variable functionality to fine tune conditions. While a variety of carboxylic acids have been investigated, none have found the success to that of pivalic acid.[11,42] This has been rationalized through the stabilization of the C-H bond breaking transition state over that of carbonates by 1.3 kcal/mol, with sterics seeming to be the crucial factor here, as bulkier carboxylic acids showed inferior polymer products and acetic acid produced no polymer at all.[55]

Solvent

The choice of solvent in direct arylation reactions have typically fallen into one of two categories, polar aprotic solvents for "ligandless" systems with highly coordinating solvents and "non-coordinating" solvents with phosphine ligand additives which can effectively solvate highly rigid CPs.[10] The types of polar aprotic solvents used are typically acetonitrile, *N*-methylpyrrolidone, *N*,*N*-dimethylacetamide, and *N*,*N*-dimethylformamide while the nonpolar

solvents that have found success are toluene, xylenes, tetrahydrofuran, and cyclopentyl methyl ether.[10,12,40] The differences in these two solvent systems for the arylation of 3-(methoxycarbonyl)thiophenes with 1-bromo-3-nitrobenzene has also been shown to alter the selectivity with polar aprotic solvents such as *N*-methylpyrrolidone, arylating at the 2-position of thiophene and non-polar solvents such as toluene selectively arylating at the 5-position of thiophene.[23,56]

Mechanistic Overview of the DArP Catalytic Cycle

Investigations into the catalytic cycle of DArP have shown that the general steps involved are oxidative addition (OA) of the aryl halide followed by CMD[11,29,34] and finally reductive elimination (RE) to form a new C-C bond.[11] Other mechanistic details may vary based on additives such as carbonate salts, carboxylic acids, ligands, solvent, and depending on the coupling species' involved may even proceed through a Heck-like pathway.[23,24]

The reduction of $Pd(OAc)_2$ to $Pd(0)(PR'_3)_2$ in Figure 4.6. has been proposed as the required first step to generate the active Pd(0) catalyst[46–48] and thus proceeds through the proposed mechanism in Figure 4.6. In the catalytic cycle, the first step is the OA of the aryl halide. In the synthetic design of the alternating copolymers the unit judiciously selected for this role is the electron-deficient acceptor species. The acceptor unit is specifically suited for the aryl halide in this regard due to its electrophilic nature toward the electron rich Pd(0). This oxidative addition on the 14 e^- Pd species generates **1,** a 16 e^- species that has the Ar-Br bond cleaved and is added cis preferentially based on a concerted addition pathway.

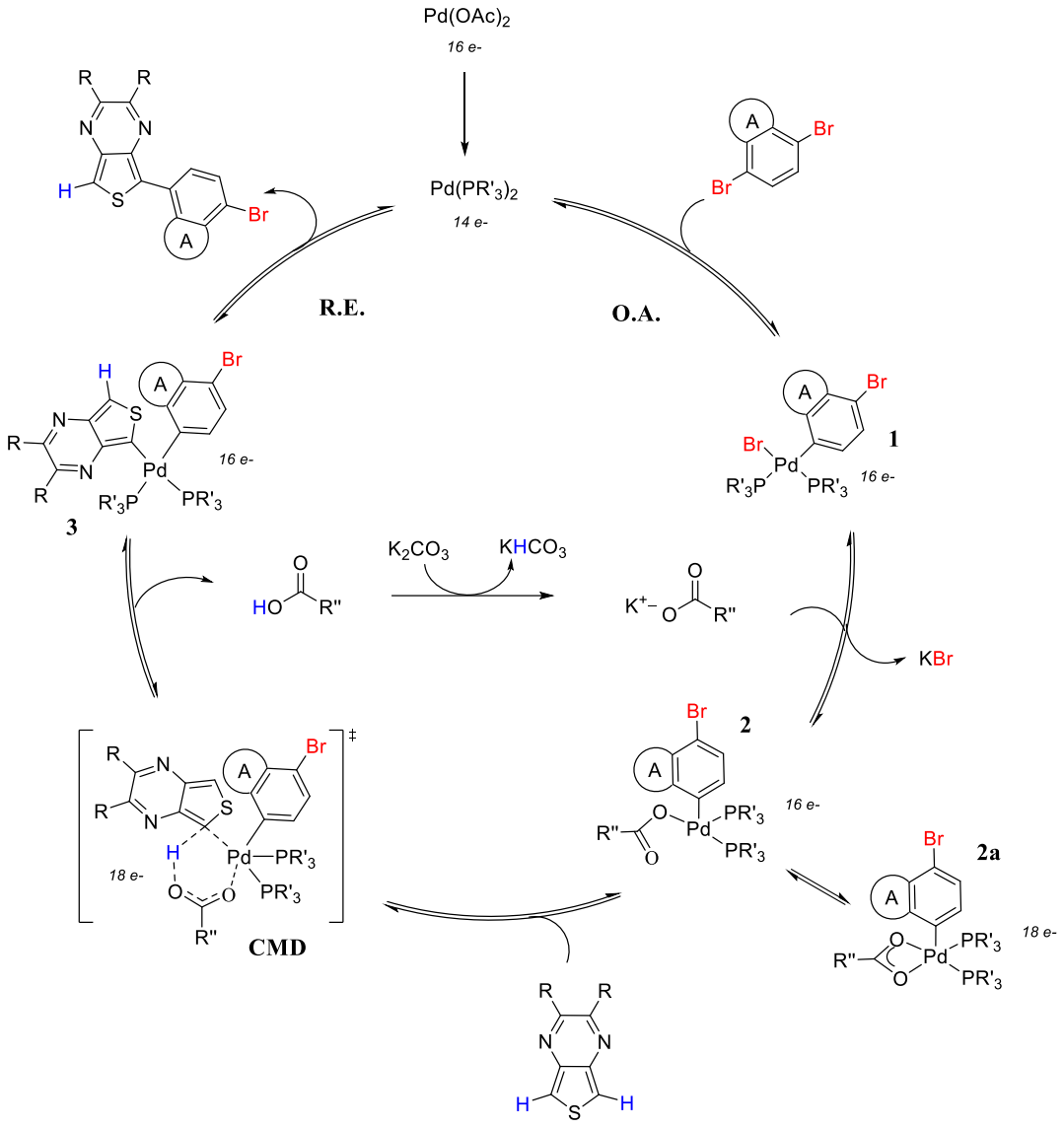

Figure 4.6. Proposed DArP catalytic cycle for TP-A Copolymers.

Upon oxidative addition of the electron deficient unit and the formation of **1**, a proposed pathway for the CMD step is an initial coordination of a carboxylate species with a corresponding removal of bromide on the Pd center. This generates the four coordinate species **2** which has also been proposed to have a chelated analogue **2a.**[57] A base (carboxylate) assisted insertion of the Ar-H via the 18 e^- CMD transition state then generates the 16 e^- species **3** which can undergo reductive elimination and regenerate the active catalyst.

Synthesis of TP-BTD Alternating Copolymers via DArP

With the understanding of the ambipolar nature of TP, 2,1,3-benzothiadiazole (BTD) was selected as a strong acceptor partner for potential low E_g alternating TP-A copolymers. The synthesis of TP-A copolymers was initially considered through a traditional cross coupling route in which a distannyl- or diboroester-species would be paired with a dibromo-species per standard Stille or Suzuki cross-coupling methods.[5,6] While both TP and BTD have known bromination reactions,[58,59] the stannyl and boroester handles have typically been reserved for the electron donating species and therefore to date neither species has a developed synthesis for these functionalized analogues.

The implementation of DArP for this cross-coupling reaction then become an increasingly obvious choice due to the elimination of undeveloped precursor syntheses as well as the elimination of one of the two bromination reactions to make the precursors for cross-coupling. The choice regarding which species would play what role was decided to be TP as the Ar-H species and BTD as the brominated Ar-X species. This decision was based on multiple factors including the limited C-H sites on TP for potential defect formation, relative electron deficiency of benzene over thiophene for increased reactivity in the OA step of the Ar-X species, and the relative electron richness of thiophene over benzene for increased favorability toward coordination to the palladium center in the CMD step.

DArP Condition Considerations

The initial DArP conditions to synthesize poly(2,3-dihexylthieno[3,4-b]pyrazine-alt-2,1,3-benzothiadiazole) (pC_6TP-BTD) and poly(2,3-bis(2-ethylhexyl)thieno[3,4-b]pyrazine-alt-2,1,3-benzothiadiazole) (pEHTP-BTD) were selected based on standard conditions used in other D-A CP syntheses.[10] The general synthetic scheme as shown in Figure 4.7 was applied to both

2,3-dihexylthieno[3,4-*b*]pyrazine (C_6TP) and 2,3-bis(2-ethylhexylthieno[3,4-*b*]pyrazine (EHTP) analogues with variations in pressure and temperature to optimize the polymer properties. The catalyst used was $Pd(OAc)_2$, as used by Lemaire and coworkers with similar catalytic loadings of 10-20%.[25] Likewise the incorporation of the base K_2CO_3 also followed these initial conditions with the base in excess of ~3 molar equivalents.

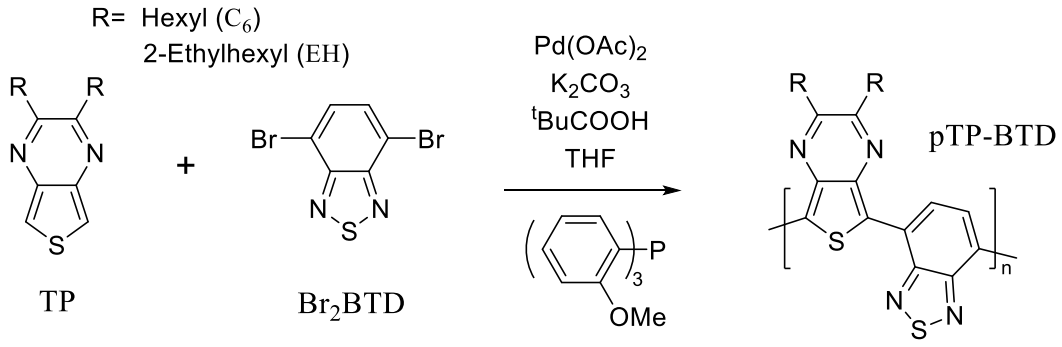

Figure 4.7. Synthesis of pTP-BTD via DArP.

The pivalic acid additive was incorporated due to the evidence supporting the base assisted CMD step as proposed by Fagnou in which the pivalate anion was shown to reduce the transition state energy.[29] The Fagnou conditions have typically used a highly coordinating solvent such as dimethylacetamide (DMAc) which circumvented the need for additional ligands to provide the sufficient coordination saturation and electronic effects required for the DArP catalytic cycle. DMAc however was not used here due to its relative inability to solvate more complex CPs with extended π-systems and the weakly coordinating THF was used instead as it has shown success in other D-A CP systems.[57]

The incorporation of a phosphine ligand has been shown to activate Pd(II) to Pd(0)[47] in addition to stabilize Pd(0) to prevent unwanted Pd black precipitation.[60] While tris(2-methoxyphenyl)phosphine (TMPP) has been shown as an effective ligand in this regard[40] with

the increased bulkiness of other common phosphine ligands not seeming to be necessary due to a lack of β-sites on TP and thus a limited possibility for defect formation.

Superheating of Solvent Under High Pressure Conditions

Initial attempts for DArP synthesis of TP-BTD alternating copolymers was carried out in a Schlenk-tube under nitrogen by Trent Anderson. In THF this only allowed temperatures of <70 ˚C to be achieved due to the low boiling point of THF. Under these conditions, low molecular weight (M_n = 1900 corresponding to a degree of polymerization = 4-5) pC_6TP-BTD materials were generated, indicating limited solubility of the generated polymer product (entry 1 Table 4.1).[61] To overcome this limitation, efforts were then pursued in which higher reaction temperatures could be achieved by super-heating the THF in sealed microwave vials as has been shown to be effective for P3HT homopolymers via DArP.[28] Under these new conditions, temperatures of up to 120 ℃ could be achieved with THF providing both enhanced solubility for the resultant polymer product as well as additional energy to overcome activation barriers for polymerization to occur.

Characterization of Polymer Products

Polymer characterization was done via gel permeation chromatography (GPC), ^{1}HNMR spectroscopy and thermogravimetric analysis (TGA) to determine molecular weights, the presence of defects and thermal stability.

The initial appearance of The ^{1}HNMR data seemed to show that the only observable peaks were in the aliphatic region (Figure 4.8). The observable alkyl band of overlapping peaks indicates a multitude of chemical environments for the various hydrogens in a polydisperse polymer sample. As can be seen from Figure 4.8, The C_6TP-BTD polymer can be differentiated

Table 4.1. Optimization of conditions for the synthesis of TP-BTD copolymers.

Entry	Polymer Name	Monomer 1 Name	Monomer 1 Amount	Monomer 2 Name	Monomer 2 Amount	Solvent (THF) Amount	Yield	Temp	Time
1	pC_6TP-BTD	C_6TP	0.110 g, 0.355 mmol	$BTDBr_2$	0.104 g, 0.355 mmol	10 mL	0.130 g, 83%	70 ˚C*	5 d
2	pC_6TP-BTD	C_6TP	0.108 g, 0.355 mmol	$BTDBr_2$	0.104 g, 0.354 mmol	7 mL	0.110 g, 71%	100 ˚C	24 h
3	pC_6TP-BTD	C_6TP	0.108 g, 0.355 mmol	$BTDBr_2$	0.104 g, 0.354 mmol	7 mL	0.104 g 67%	100 ˚C	24 h
4	pEHTP-BTD	EHTP	0.127 g, 0.354 mmol	$BTDBr_2$	0.1041 g, 0.354 mmol	7 mL	0.130 g, 74%	100 ˚C	24 h
5	pEHTP-BTD	EHTP	0.125 g, 0.347 mmol	$BTDBr_2$	0.105 g, 0.356 mmol	7 mL	0.175 g, 100%	100 ˚C	48 h
6	pEHTP-BTD	EHTP	0.131 g, 0.363 mmol	$BTDBr_2$	0.107 g, 0.365 mmol	7 mL	0.160 g, 73%	100 ˚C	22 h
7	pEHTP-BTD	EHTP	0.173 g, 0.480 mmol	$BTDBr_2$	0.106 g, 0.360 mmol	7 mL	0.210 g, 89%	100 ˚C	21 h
8	pEHTP-BTD	EHTP	0.187 g, 0.519 mmol	$BTDBr_2$	0.108 g, 0.367 mmol	7 mL	0.223 g, 100%	120 ˚C	24 h

Entry 1 was carried out in a Schlenk tube under nitrogen at atmospheric pressure by Trent Anderson*

from the EHTP-BTD polymer by the increase in intensity of proton peaks in the aliphatic region for EHTP-BTD as would be expected for the branched alkyl system having additional solubility in $CDCl_3$ with equal concentration samples.

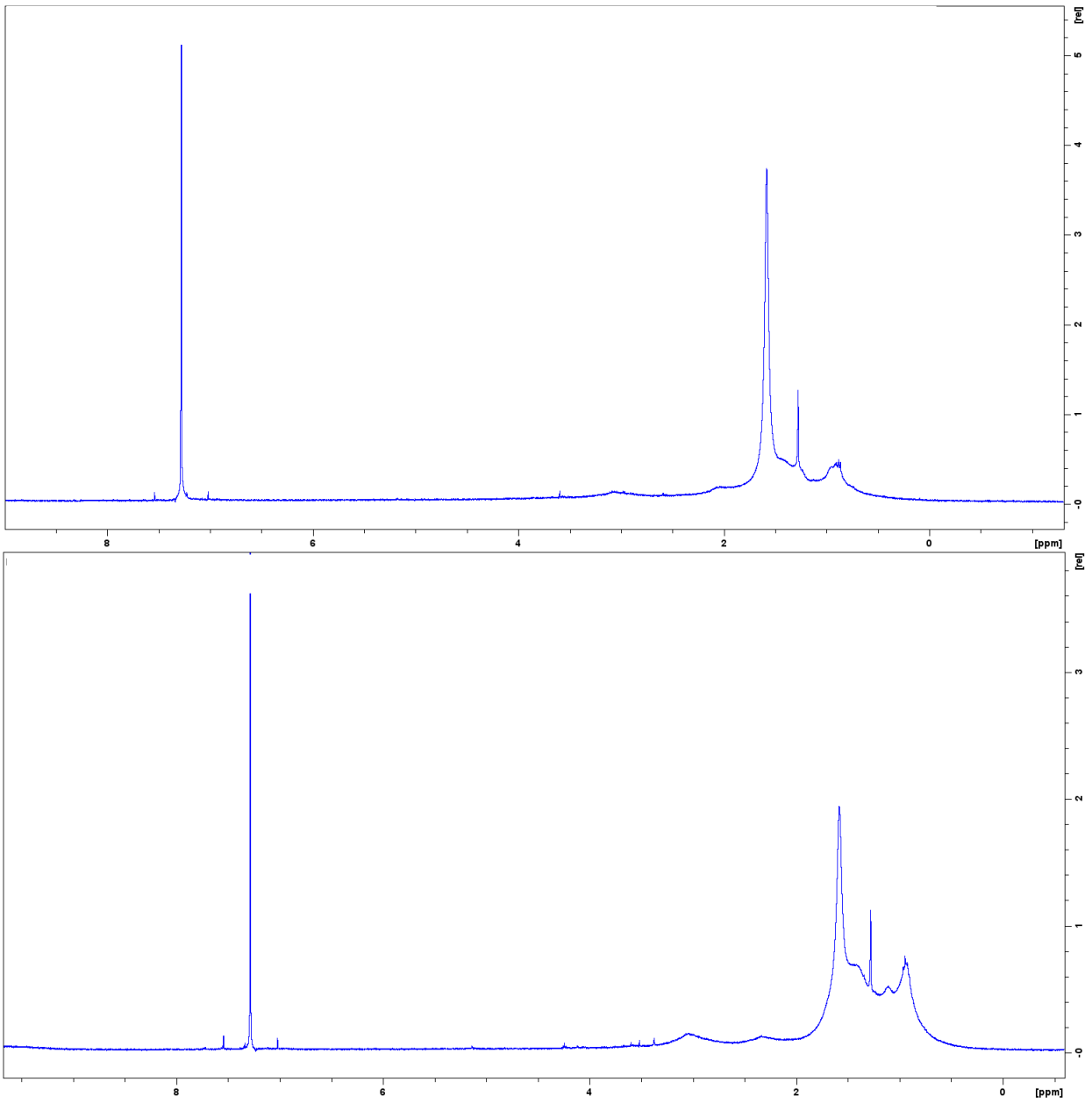

Figure 4.8. (top) ^{1}HNMR data for C_6TP-BTD and (bottom) EHTP-BTD.

Upon further analysis of the spectrum of EHTP-BTD however it became apparent that a band in the aromatic region was indeed visible ca. 9-10 ppm (Figure 4.9). This peak matches well with the previously synthesized TP-BTD dimer which has one of the two BTD peaks shifted significantly downfield at 9.38 ppm.[1] This downfield shifted of the aromatic peak has since been identified as the H on BTD which is capable of hydrogen bonding with the nitrogen on the

pyrazine ring as supported by DFT calculations.[1] Thus, this hydrogen bonding appears to be present in the polymeric material as well, indicating an anti-configuration for the alternating copolymer.

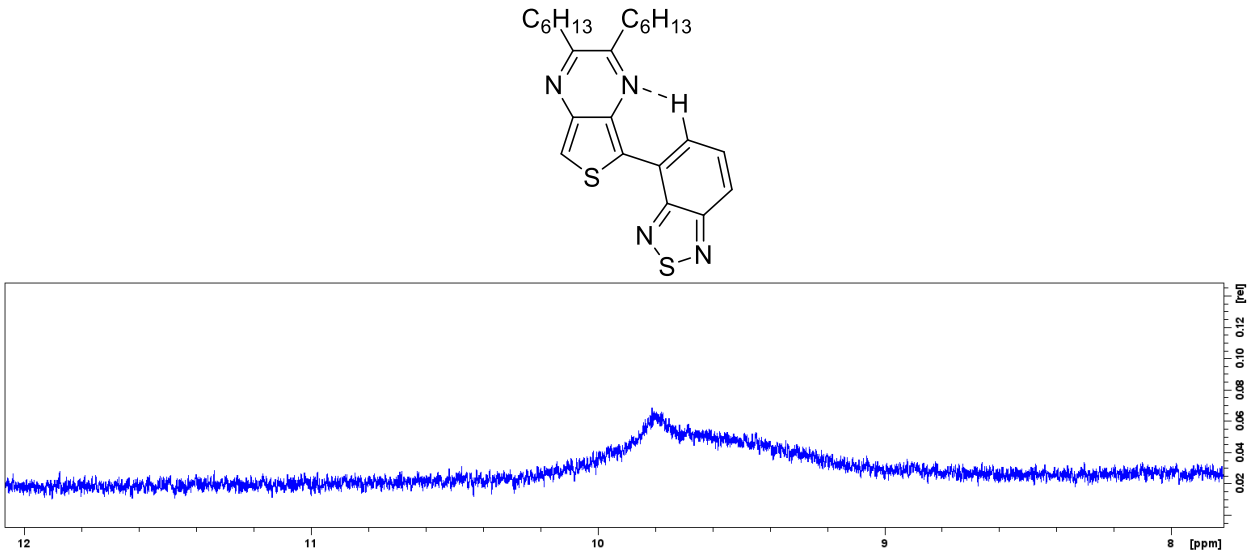

Figure 4.9. (top) Hydrogen bonding between BTD and TP (bottom) aromatic region in the ^{1}HNMR spectra of EHTP-BTD.

The thermal stability of EHTP-BTD was also investigated and showed stability of the polymer up to ~400 ℃ (Figure 4.10). This was carried out with TGA and is well within acceptable parameters for conjugated polymers for devices that have been previously reported.

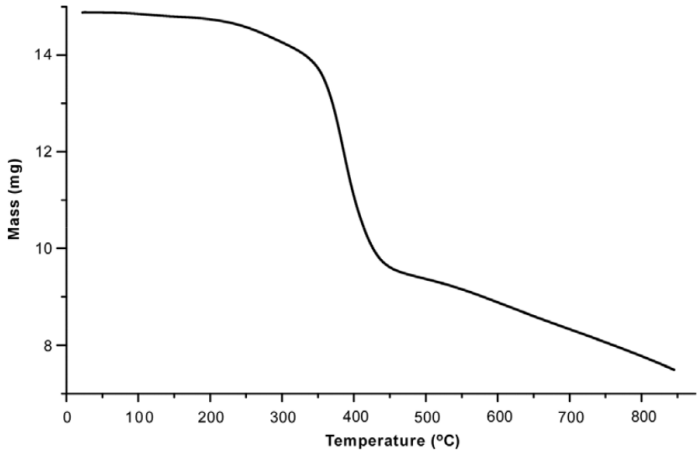

Figure 4.10 TGA of EHTP-BTD.

As mentioned previously, the synthesis of pC_6TP-BTD under atmospheric pressure at 70 °C produced low molecular weight polymers (Table 4.2) that were initially thought to be due to the low temperature polymerization conditions. Once the high-pressure conditions were developed however only slight enhancement of the M_n was observed indicating very little change in polymer molecular weights. Upon further investigation however it was observed that a significant portion of the polymer sample was aggregating in the GPC prefilter and thus the high-end molecular weight products were not soluble enough to be analyzed. Solubility testing was also performed and indicated solubility was poor with solid precipitates observed above concentrations of 10 mg/mL in $CHCl_3$.

A potential solution to this problem was to then make the polymers more soluble through the incorporation of branched sidechains. A potential candidate in this regard that would have limited impact on the electronic properties of the polymers while enhancing the solubility was EHTP-BTD and was the polymer of choice for this study. Once synthesized, EHTP-BTD showed significant increases to both M_n and M_w values in addition to a twofold solubility enhancement (Table 4.2).

Table 4.2. Molecular weight data for TP-BTD copolymers with corresponding solubilities.

Polymer	M_n	M_w	PDI	Solubility in $CHCl_3$ mg/mL
pC_6TP-BTD (low MW)	1900	3000	1.57	10
pC6TP-BTD	2300	3000	1.29	10
pEHTP-BTD	8100	11,700	1.45	20

Synthesis of TP-Qx Alternating Copolymers via DArP

To expand the scope of TP-A alternating copolymers, C_6TP was also paired with a slightly weaker acceptor 2,3-dihexylquinoxaline (Qx) in comparison to the previously studied BTD with the synthesis of poly(2,3-dihexylthieno[3,4-b]pyrazine-alt-2,3-dihexylquinoxaline)

(pC_6TP-Qx).[62] This TP-A would therefore retain the design motif of TP-BTD copolymers while also allowing for the introduction of additional solubilizing side-chains for more soluble polymer products. The conditions used were the same as for the pTP-BTD derivatives with hexyl sidechains on both TP and Qx as outlined in Figure 4.11**.**

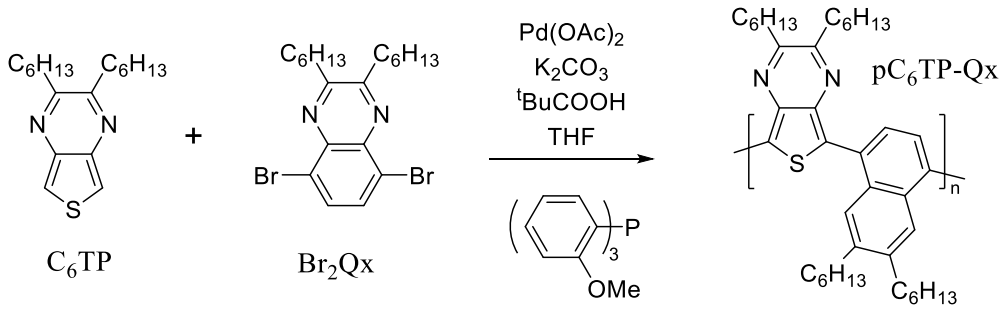

Figure 4.11. Synthesis of pC_6TP-Qx via DArP.[62]

The tailoring of conditions was like TP-BTD in that the initial synthesis was carried out in a Schlenk tube preventing the increase of reaction temperatures above 70 ℃ in THF by Trent Anderson. When high-pressure conditions were implemented, improvements to molecular weights, and yields were observed along with significant reductions in the needed reaction time. The changes in conditions were once again pursued through changes in reaction time and temperature and optimal results were achieved with a 24 h stir time at 100 ℃ (Table 4.3).

Table 4.3. Yield data in the optimization of pC_6TP-C_6Qx.

Entry	Monomer 1		Monomer 2		Solvent (THF)	Yield	Temp.	Time
1	C_6TP	0.108 g, 0.355 mmol	C_6QxBr_2	0.162 g, 0.355 mmol	10 mL	0.093 g, 44%	70 ˚C*	5 d
2	C_6TP	0.089 g, 0.285 mmol	C_6QxBr_2	0.130 g, 0.285 mmol	7 mL	0.11 g 61%	100 ˚C	17 h
3	C_6TP	0.110 g, 0.361 mmol	C_6QxBr_2	0.162 g, 0.355 mmol	7 mL	0.21 g, 99%	100 ˚C	24 h
4	C_6TP	0.110g, 0.361 mmol	C_6QxBr_2	0.167 g, 0.366 mmol	7 mL	0.16 g, 75%	100 ˚C	22 h

Entry 1 was carried out in a Schlenk tube under nitrogen at atmospheric pressure*

Characterization of Polymer Products

In the same capacity as the TP-BTD polymers, the pC_6TP-C_6Qx system was characterized by ^{1}HNMR, and GPC. The aliphatic profile like that of pC_6TP-BTD was due to both the TP and quinoxaline species having hexyl sidechains attached to a pyrazine unit and thus in similar chemical environments (Figure 4.12). Also comparable to the pTP-BTD analogues was the significant increase in molecular weight upon the modification of conditions to allow for high-pressures and elevated temperatures. The pairing of two units with solubilizing sidechains was predicted to be limited by the reaction conditions and not the solubility of the polymer itself. This prediction was supported by the GPC data which showed significant increases in molecular weights ~6x that of the low temp/pressure method (Table 4.4). Solubility was also investigated and like pEHTP-BTD, showed over a twofold increase in solubility in $CHCl_3$.

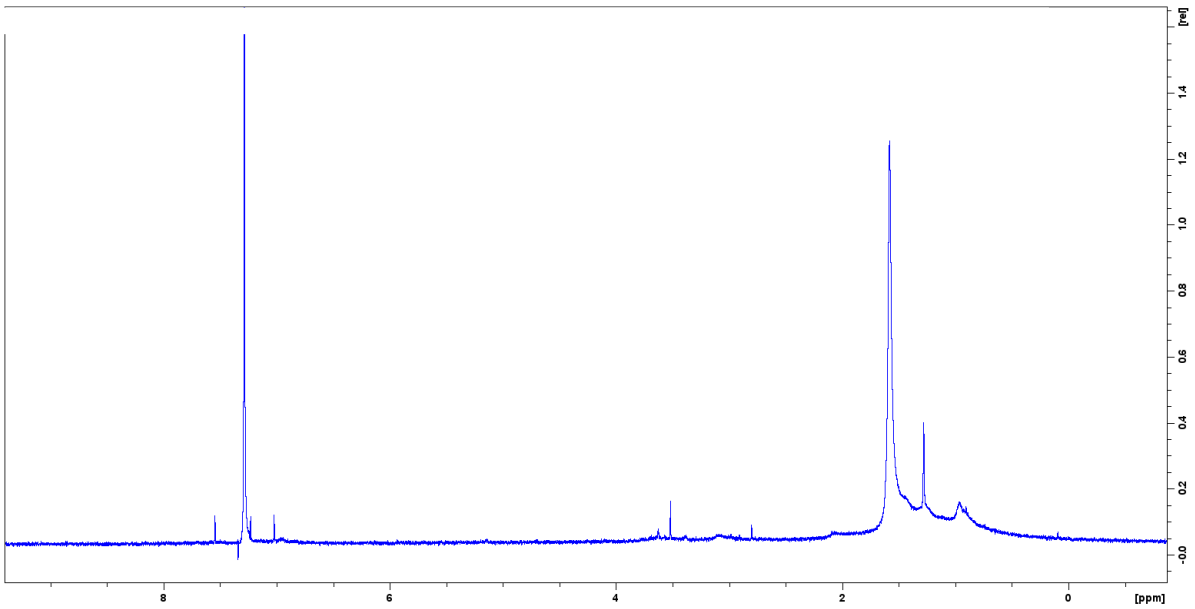

Figure 4.12. ^{1}HNMR spectra for pC_6TP-Qx.

Table 4.4. Molecular weight data for TP-BTD and C_6TP-Qx copolymers.

Polymer	Mn	Mw	PDI
pC_6TP-Qx (low MW)	2700	3400	1.28
pC_6TP-Qx	13,700	18,400	1.34
pC_6TP-BTD	2300	3000	1.29
pEHTP-BTD	8100	11,700	1.45

Similarly, although much less refined in pC_6TP-Qx is the presence of an aromatic band ca. 9-10 ppm (Figure 4.13). In pC_6TP-Qx this band is nearly lost in the baseline but does still appear to be present. This interaction further emphasizes the interaction between TP and phenyl-based acceptors as rigid alternating copolymers that are essentially locked into an anti-planar conformation due to hydrogen bonding. The reduction in intensity however indicates that the hydrogen-bonding here may not be as significant as in EHTP-BTD and thus a higher of diversity of chemical environments for the aromatic protons broadens the aromatic region of the polymer.[63]

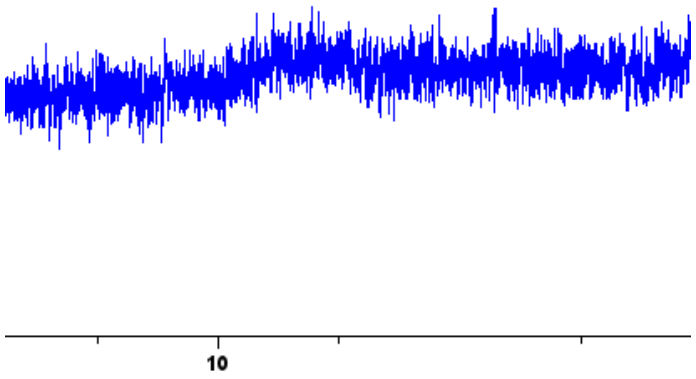

Figure 4.13. Aromatic region in the ^{1}HNMR spectra of C_6TP-Qx.

Optical and Electronic Properties of TP-A Materials

While the two previous sections showed how to optimize DArP conditions in order to be applied to TP-A copolymers, the main aim of the investigation was to investigate these TP-A systems as low E_g materials.[61,62] As with other D-A systems this is typically carried out through UV-vis absorption spectroscopy and electrochemical analysis. Through these techniques the determination of the E_g and estimation of frontier orbitals can be achieved. All the TP-A systems investigated were synthesized by the optimized methods discussed in the previous two sections.

To better understand the impacts of TP-A interactions four A-species were paired with TP. The polymer backbone was kept consistent between the TP-A systems by linking each acceptor moiety through a phenyl ring. The variations to the acceptors therefore would occur through the modification of the pendant fused rings. The acceptors species studied included BTD, Qx, benzene (Bz), and 2,1,3-hexylbenzotriazole (BTA) (synthesized by Wyatt Wilcox) as shown in Figure 4.14.

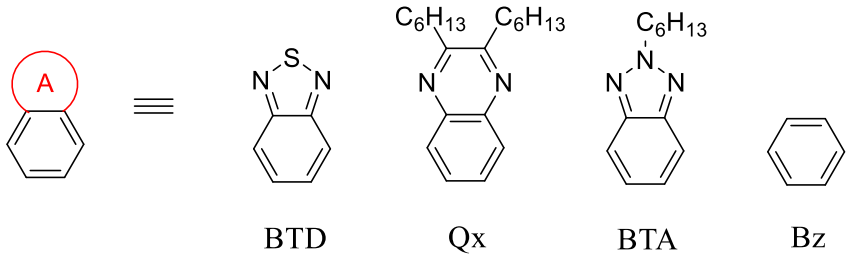

Figure 4.14. Acceptor species paired with TP for TP-A copolymers.

To quantify the electron acceptor strengths each monomer was analyzed by cyclic voltammetry (CV). Figure 4.15 shows the ordering of acceptor strength of each monomer based on reduction potential and proceeds with BTD > TP > Qx > BTA. This trend also corresponds to reductions in Eg and the importance of the pendant accepting ring is clear with the significantly larger E_g of TP-Bz which has no pendant ring to contribute to the LUMO of the polymer.

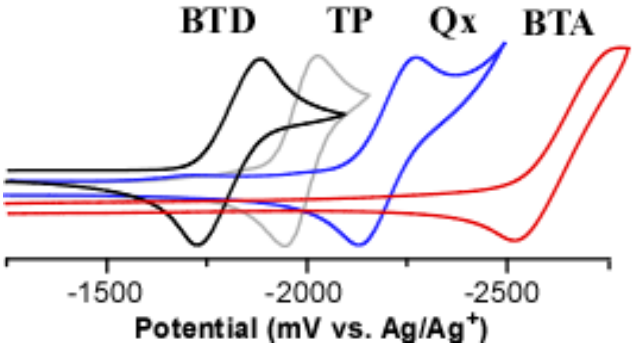

Polymer	E_g (eV)	HOMO (eV)	LUMO (eV)
TP-BTD	0.97	-5.3	-4.0
TP-Qx	1.07	-5.3	-3.9
TP-BTA	1.12	-5.5	-3.8
TP-Bz	1.50	-5.5	-3.5

Figure 4.15. Cyclic voltammograms of acceptor species (left) and electrochemistry data along with estimated HOMO/LUMO energies (right) of TP-A copolymers.

A question that remains somewhat ambiguous is whether the LUMO is delocalized between pendant accepting units (i.e. pyrazine-thiadiazole hybridization, pyrazine-pyrazine, and pyrazine-triazine hybridization). A piece of supporting evidence is the redshift in absorbance for all the TP-A copolymers and a noticeably blue-shifted absorbance for pTP-Bz which has no pendant electron deficient unit for hybridization of the LUMO between units to occur (Figure 4.16).

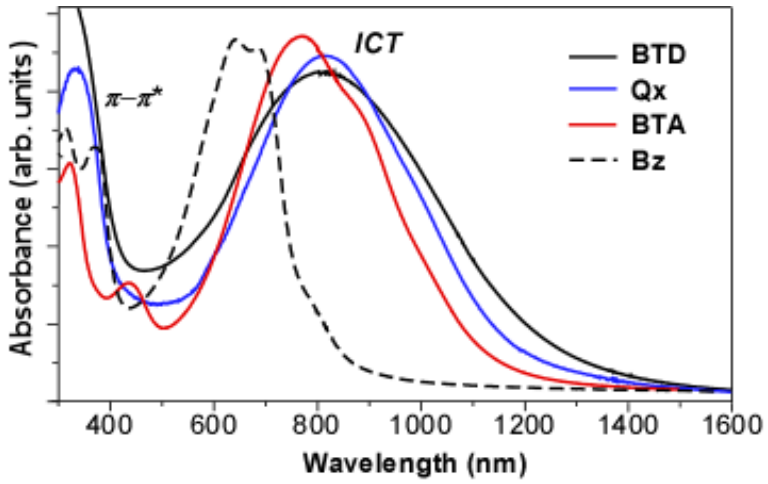

Figure 4.16. UV-vis absorption spectra of TP-A copolymers.

Conversely, the low energy intramolecular charge transfer could exist as overlapping bands with a charge transfer from the polymer backbone HOMO to separate localized acceptor rings. This alternative interpretation would then indicate that the determining factor in the blue-shift of pTP-BZ is solely due to conjugation effects. Of the two potential cases the hybridized LUMO has been supported by DFT calculations.[61] Regardless of which is the case in these examples, Figure 4.16 shows a clear trend in pairing TP with other strong acceptors as a route to low E_g copolymers.

Optimization of TP-BTD Copolymers

In addition to the previous work on the synthesis of TP-BTD copolymers was further investigations into the optimization of EHTP-BTD. This was pursued largely in part due to the lack of any chloroform insoluble fraction post soxhlet extraction. The implication of the lack of an insoluble fraction being that conditions could be altered to increase molecular weights and thus lower the resultant E_g.

The first parameter investigated for further DArP optimization was a variation in solvent. The solvents investigated were THF, xylenes, *N*,*N*-dimethylacetamide (DMAc), and cyclopentyl methyl ether (CPME). These solvents were selected based on previous success in other DArP systems[10,38,42,64], and gave a range of aromatic and non-aromatic, polar and non-polar, and strongly coordinating and weakly coordinating species. In this solvent screening study, all polymer products were then investigated via UV-vis absorption spectroscopy. This preliminary data was then used to determine if conditions were improvements over the previously reported method,[61] with the data presented in Table 4.5.

Table 4.5. Optimization of pEHTP-BTD.

Entry	Solvent	Temp. ˚C	Time	Yield	M_w	PDI	λ_{max}^{CHCl3} (nm)	λ_{max} Film (nm)	λ_{onset} Film (nm)	E_g (eV)
1	THF	100	24	99%	-	-	697	-	-	-
2	THF	100	48	99%	11,700	1.45	813	850	1180	1.05
3	THF	120	24	99%	-	-	815	853	1170	1.06
4	Xylenes	120	24	99%	6,525	1.42	798	842	1140	1.09
5	Xylenes	150	24	trace	-	-	-	-	-	-
6	DMAc	120	24	78%	-	-	625	652	970	1.28
7	DMAc	120	24	61%	-	-	625	-	-	-
8	CPME	120	24	41%	-	-	766	798	1290	0.96
9	CPME	120	48	58%	-	-	716	-	-	-
10	CPME	120	72	24%	-	-	694	-	-	-
11	CPME	130	24	16%	-	-	714	-	-	-

Of the solvents screened THF showed the best overall performance in terms of both yield and optical properties, with the lowest optical E_g value coming from the 48 h stir time at 100 ℃ (entry 2). This was an improvement over the 24 h stir time in THF which showed a blue-shifted lowest energy absorption (entry 1). Interestingly, it was also shown that if reaction temperatures were increased to 120 ℃ the stir time could be cut down to 24 h in THF with limited impact on yield or optical properties (entry 3).

Xylenes provided the opportunity of using a solvent that could be heated to temperatures of up to 150 ˚C without compromising the structural integrity of the microwave vial due to its

relatively high boiling point of ~139 ℃. Initial xylenes conditions were 120 ℃ for 24 hours and based on the previous success of THF (entry 3) and showed high yields with comparable optical properties albeit with a significant decrease in molecular weight of the polymer. An increase of the reaction temperature however only gave trace amounts of polymer product which previous reports have also claimed for DArP reactions carried out above 130 ℃ with $Pd(OAc)_2$ catalysts in other solvents.[11,27,65,66]

DMAc which has found use in what has been deemed "ligandless" DArP systems[22,30,67] provided a strongly coordinating solvent albeit with the TMPP ligand still present. Under these conditions optical absorptions of the resultant polymers (both onsets and λ_{max}) were blue shifted beyond the THF and xylenes samples with a resultant higher calculated E_g values (Entries 6 and 7). EHTP-BTD having the lowest predicted solubility in DMAc is likely limited by this factor, but further investigations and determination of molecular weights is necessary to conclude this definitively.

With the previous success and solubilizing nature of THF, other ether solvents such as 2-methyltetrahydrofuran[68], and CPME[69] have been suggested as "greener" alternatives that can be sourced from biomass and have shown success as solvents for DArP reactions.[70,71] Of the two, CPME was selected to give greater structural diversity when compared to THF in the solvent screening analysis. The results of the CPME investigations were an unexpected red shift in the lowest energy onset of absorption with a corresponding blue shifted λ_{max} (entry 8). This indicated that the CPME conditions produced the lowest E_g of any solvent investigated while also having a much broader absorption profile. Upon the initial findings, further alteration of parameters followed with increases in reaction time up to 72 hours and an increase in reaction temperature of 130 ˚C which all gave inferior results (entries 9-11).

Device Design and Fabrication

The design of TP-A copolymers has interesting implications in that the materials have high enough HOMOs and low enough LUMOs to be able to be applied as either donor or accepting materials in devices. In attempts to investigate the applicability of using pC_6TP-BTD as an accepting material a mixture of pC_6TP-BTD and P3HT was analyzed via solution fluorescence and absorbance spectroscopy (Figure 4.17) by Seth Rasmussen.[61] As the absorption profiles show, the mixing of P3HT and pC_6TP-BTD in solution does not change the respective absorbances for each species. Conversely a reduction in intensity of the assigned emission peak of P3HT is observed upon mixing with pC_6TP-BTD indicating a degree of quenching of the P3HT emission by pC_6TP-BTD.

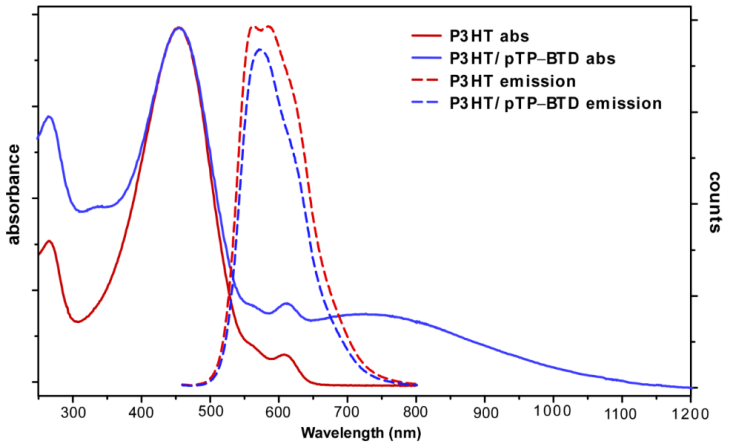

Figure 4.17. Fluorescence quenching of P3HT by pC_6TP-BTD in $CHCl_3$.[61]

In attempts to see how TP-A copolymers perform as donor materials in devices, low M_w pC_6TP-Qx was paired with PCBM as the active layer in OPV devices. The key parameters for device performance were determined, including power conversion efficiency (PCE), open circuit voltage (V_{OC}), fill factor, and short circuit current (J_{SC}) (Table 4.6). The external quantum

efficiency (EQE) measurements were also determined by irradiation of the devices with a confined wavelength range of 400 to 1100 nm to give a resultant EQE of 2.5 % (Figure 4.18).[62]

Table 4.6. Device data from pC_6TP-Qx/PCBM OPV devices.[62]

OPV characteristics			
PCE (%)	V_{OC} (V)	Fill Factor	J_{SC} (mA cm^{-2})
0.05 ± 0.01 (0.06)	0.51 ± 0.01 (0.52)	0.25 ± 0.01 (0.27)	0.39 ± 0.05 (0.43)

The devices fabricated from pC_6TP-Qx showed properties that underperformed in all areas investigated. For example, by comparison in the investigation on the scale-up of P3HT under DArP conditions had corresponding devices made with P3HT/PCBM mixtures that had V_{OC} values in the range of 0.479-0.597 V, J_{SC} values in the range of 8.19-9.04 mA cm^{-2}, fill factors of 0.35-.60, and PCEs of 1.76-2.55%.[72] While these devices were fabricated in a nearly identical fashion it should be noted that a silica column purification step was performed on the P3HT sample prior to device fabrication in order to remove potential salts formed in the DArP synthesis which had been shown to improve device efficiency on other D-A systems.[73] This may be an effective route to improve device efficiency among others to further device efficiency.

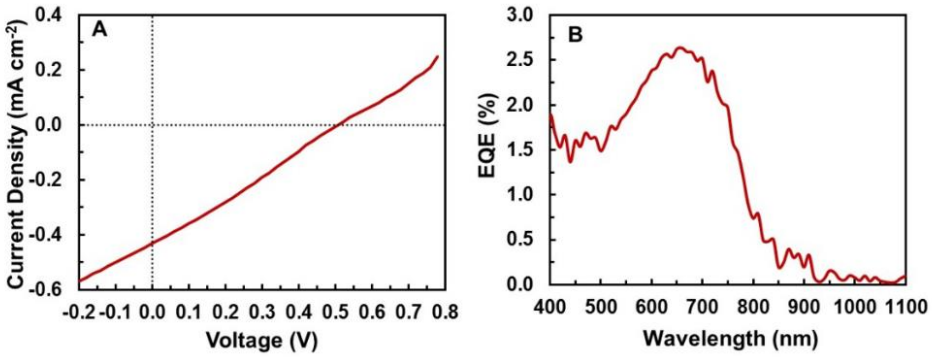

Figure 4.18. (A) I-V curve for pC_6TP-Qx/PCBM OPV devices and (B) EQE determination of pC_6TP-Qx/PCBM OPV devices under 400-1100 nm irradiation.[62]

While not yet published, devices have also been fabricated with a blend of P3HT as the donor material and pEHTP-BTD as a non-fullerene electron accepting material. The preliminary data shows very poor performing devices when compared to P3HT:$PC_{61}BM$ devices (Table 4.7). As can be seen from Table 4.7, the J_{SC} is particularly degraded. The cause of which is likely a morphological issue[74,75] in which domains sizes are not conducive to charge transport. This results in a significantly reduced PCE as shown by the three-fold magnitude reduction for the P3HT:pEHTP-BTD devices. The root cause if this poor performance is believed to be due to the formation of pEHTP-BTD crystallites (Figure 4.19). As can be seen in the Figure 4.19, upon magnification small crystalline domains are visible which are likely the more insoluble pEHTP-BTD. These crystallites prevent effective movement of charge in the bulk heterojunction by trapping electrons in these acceptor "islands". Therefore, further modifications to post processing and the incorporations of additives is a logical next step in this devices design.

Table 4.7. Device data for P3HT:pEHTP-BTD and P3HT:$PC_{61}BM$ blends.

Donor:Acceptor	Bulk_OPV	PCE (%) Average ± STD (Best)	Voc (V) Average ± STD (Best)	FF Average ± STD (Best)	Jsc (mA/cm^2) Average ± STD (Best)
P3HT:pEHTP-BTD	Unannealed	0.002 ± 0.001 (0.003)	0.267 ± 0.131 (0.324)	0.227 ± 0.102 (0.277)	0.024 ± 0.012 (0.037)
	Annealed	0.003 ± 0.001 (0.004)	0.366 ± 0.003 (0.361)	0.266 ± 0.002 (0.268)	0.034 ± 0.004 (0.039)
P3HT:$PC_{61}BM$	Unannealed	2.33 ± 0.18 (2.61)	0.51 ± 0.01 (0.51)	0.53 ± 0.02 (0.55)	8.53 ± 0.51 (9.36)
	Annealed	2.75 ± 0.14 (2.96)	0.58 ± 0.01 (0.58)	0.64 ± 0.02 (0.67)	7.45 ± 0.15 (7.60)

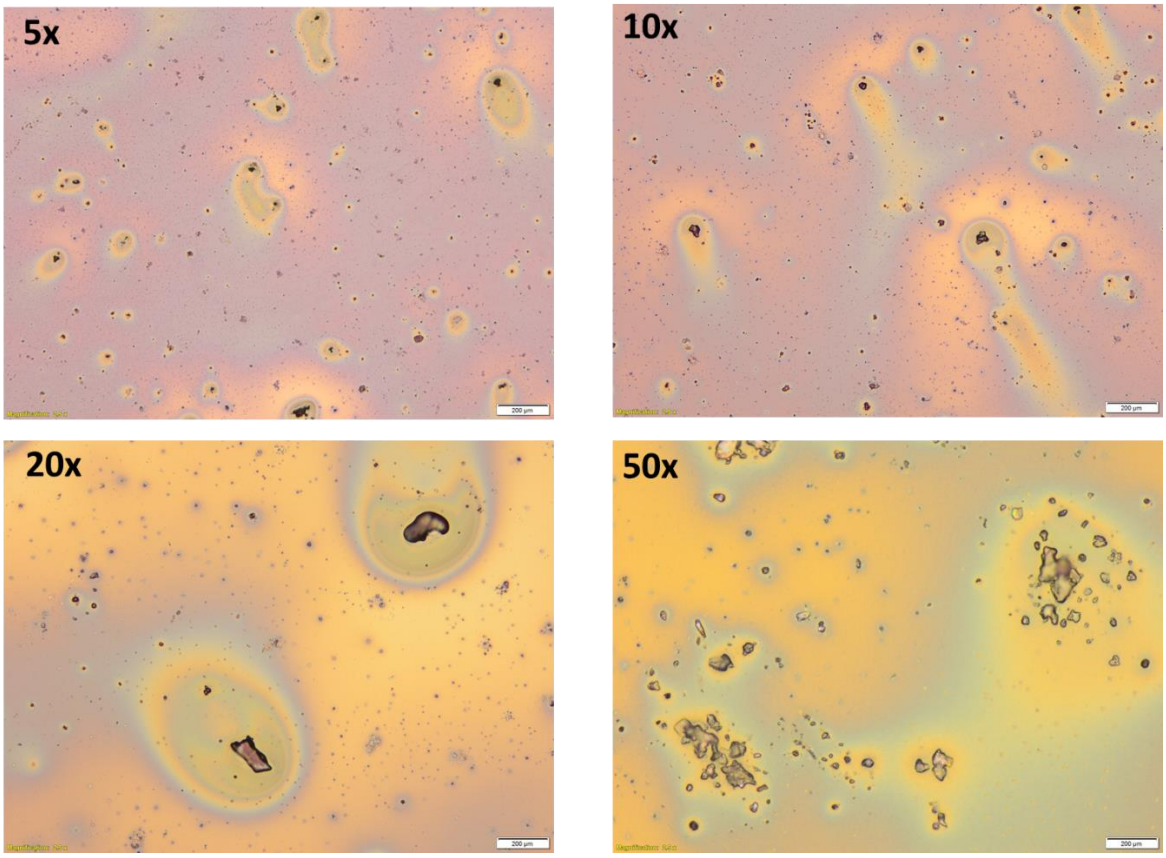

Figure 4.19. Magnification of thin film blends of P3HT:pEHTP-BTD (scale bar is 200 μm).

Conclusions

The synthesis of TP-A copolymers has required the implementation of new methods such as high-pressure DArP to produce high molecular weight, low E_g polymeric materials. As with other DArP systems each reaction typically requires the tailoring of conditions for maximum optimization. In these investigations, solvent, temperature, time, and high pressure were surveyed for a variety of TP-A systems and analyzed according to yield, molecular weight, and optical/electronic properties.

As a system C_6TP-BTD had the lowest E_g, but at the cost of solubility and thus EHTP-BTD may be preferrable in devices due to its enhanced solubility and only slightly larger E_g. While C_6TP-BTD did not show improvements in optical and electronic properties upon increased

pressure, it did provide evidence that the polymer was limited by solubility in terms of molecular weight. EHTP-BTD while not having a resultant reduction in E_g did show a red shifted absorption in solution and thus likely has limitations due to the solid-state packing that may be rectified through additional processing methods.

The investigations into additional TP-A copolymers such as TP-Qx, TP-BTA, and TP-Bz provided some evidence into the hybridization of the LUMOs between TP and the A species. The significant indicator being the LUMO destabilization of TP-Bz which has no pendant acceptor portion to hybridize with TP compared to the other A species. Additionally, these TP-A copolymer systems showed that 0.1 eV LUMO energy tuning could be achieved with no change in HOMO energies for C_6TP-Qx, and C_6TP-BTD.

The further optimization of EHTP-BTD showed that the solvent system plays a significant role in the polymer generated via DArP. The crucial factor seems to be the solubility of the resulting polymer with the solvents THF, xylenes, and CPME showing enhanced molecular weights and optical properties over the more polar/coordinating solvent DMAc. While THF produced the overall highest yield with the best optical properties, CPME produced the lowest E_g EHTP-BTD copolymer to date. The yields with CPME were however poorer than THF and thus further optimization is necessary.

Lastly, the fabricated devices made from the low M_w pC_6TP-Qx showed poor performance in all criteria tested. Therefore, significant optimization will be required to incorporate these materials into OPV devices including additional purification steps, blend ratios, annealing modifications, and even looking at different electron acceptors. Additionally, the devices were fabricated prior to the optimized synthesis to generate higher M_w pC_6TP-Qx and thus the polymer themselves may be a limiting factor in device performance. Even with the poor

device performance the initial TP-A copolymer motif has been shown to be a possible candidate for materials in OPV devices.

Experimental

Absorption Spectroscopy

A dual beam scanning UV-vis-NIR spectrophotometer was used to perform UV-vis absorption spectroscopy measurements. Measurements taken in solution were made in dry $CHCl_3$. Measurements taken in the solid state were spin coated glass slides. All E_g values were estimated from the onset of the lowest energy absorbance.

Electrochemistry

Electrochemical analysis was conducted with a three-electrode cell with platinum disc working and platinum wire reference electrodes. A reference Ag/Ag^+ (0.251 eV vs. SCE) electrode was built in house and consisted of 0.01 M solution of $AgNO_3$, and 0.1 M solution of tetrabutylammonium hexafluorophosphate ($TBAPF_6$) all in CaH dried MeCN. All electrochemical cells were oven dried and prior to taking measurements, cells were sparged with argon. Measurements were then taken with blanketed argon at a scan rate of 100 mV s^{-1}. Estimated E_{HOMO} and E_{LUMO} were determined by taking the onsets of first oxidation and reduction and compared to ferrocene (50 mV vs. Ag/Ag^+) with a value of 5.1 eV vs. vacuum for ferrocene.[76]

OPV Device Fabrication

Bulk heterojunction OPV devices were fabricated by blending a 1:1 mixture of low MW pTP-Qx and phenyl-C61-butyric acid methyl ester (PCBM). The device architecture consisted of ITO/PEDOT:PSS/ pTP-Qx:PCBM/ZnO/Al with a 1:1 (w/w) P3HT:PCBM ratio for the active layer.

OPV Device Characterization

Current density–voltage (J-V) measurements were performed using a Newport Class AAA solar simulator. The light intensity was calibrated to 100 mW cm-2 using a silicon reference solar cell (FHG-ISE). J-V data was recorded in the dark and under illumination using a Keithley 2400 source meter. External quantum efficiency (EQE) measurements were recorded by illuminating the OPV devices with a tungsten halogen lamp passed through an Oriel Cornerstone 130 monochromator. An Ithaco Dynatrac 395 analogue lock-in amplifier an S5 Thorlabs PDA55 silicon diode were employed to collect the reference signal, and a Stanford Research Systems SR830 DSP digitizing lock-in amplifier was employed to measure the device current.[62]

Materials

2,3-dihexylthieno[3,4-*b*]pyrizaine (C_6TP) was made according previously reported methods from 3,4-diaminothiophene.[77,78] 3,4-diamminothiophene was made from 2,5-dibromo-3,4-dinitrothiophene as previously reported.[77,78] 2,5-dibromo-3,4-dinitrothiophene was made from 2,5-dibromothiophene according to previously reported methods modified for 20% fuming sulfuric acid concentrations.[79] 2,5-Dibromothiophene was made according to previously reported methods from thiophene.[80] Thiophene was purchased from Sigma-Aldrich and used without further purification. 3,5-Dibromo-2,1,3-benzothiadiazole was prepared from 2,1,3-benzothiadiazole according to previously reported methods.[59] 2,1,3-benzothiadiazole was made from 1,2-diamminobenze via previously reported methods.[81] 1,2-diamminobenzene was purchased from Alfa Aesar and used without further purification. 5,8-dibromo-2,3-dihexylquinoxaline was prepared from 3,6-Dibromo-1,2-diaminobenzene according to previously reported methods.[62]

Synthesis

2,3-Bis(2-ethylhexyl)thieno[3,4-*b*]pyrazine (**EHTP**). The EHTP monomer was prepared via a modification of the previously reported procedure.[77,78] 5,10-Diethyl-7,8-Tetradecanedione (1.50 g, 5.31 mmol) was dissolved in 50 mL of ethanol and stirred. 3,4-Diaminothiophene (3.81 g, 33.4 mmol) was dissolved in 100 mL of ethanol in a separate flask and sonicated until all solids completely dissolved. The two solutions were then combined along with an additional 250 mL of ethanol and the reaction was stirred for 3 h at room temperature. Solvent was then removed at reduced pressure where a red brown oil was isolated. Water was then added, and the mixture was extracted with dichloromethane and dried with magnesium sulfate. Solvent was once again removed by reduced pressure and the oil was purified by silica gel chromatography (5% ethyl acetate/hexanes) to give a dark yellow oil (0.781 g, 40.9%). ^{1}H NMR ($CDCl_3$): δ 7.80 (s, 2H), 2.83 (d, J = 7.1 Hz, 4H), 2.04 (sept, J = 6.2 Hz, 2H), 1.50-1.25 (m, 16H), 0.94 (t, J = 7.3 Hz, 6H), 0.91 (t, J = 7.3 Hz, 6H).[61] NMR data agree well with previously reported values.[82]

Poly(2,3-dihexylthieno[3,4-b]pyrazine-alt-2,1,3-benzothiadiazole) - High-pressure conditions. 2,3-Dihexylthieno[3,4-*b*]pyrazine (0.108 g, 0.355 mmol), 4,7-dibromo-2,1,3-benzothiadiazole (0.104 g, 0.355 mmol), palladium(II) acetate (0.10 g, 0.041 mmol), tris(o-methoxyphenyl)phosphine (0.022 g, 0.062 mmol), potassium carbonate (0.147 g, 1.07 mmol), and pivalic acid (0.036 g, 0.36 mmol) were all added to a microwave vial and put under nitrogen. The vial was then placed in a dry box where the cap was removed, and tetrahydrofuran was added. A cap was then crimped on the vial and the vial was removed from the glove box where it was then stirred at 100 °C for 24 h to give 0.110 g of dark blue soluble polymer product. GPC: M_n = 2300, M_w = 3000, PDI = 1.29.[61]

Poly(2,3-bis(2-ethyldihexyl)thieno[3,4-b]pyrazine-alt-2,1,3-benzothiadiazole) - High-pressure conditions. 2,3-Bis(2-ethylhexyl)thieno[3,4-b]pyrazine (0.125 g, 0.347 mmol), 4,7-dibromo-2,1,3-benzothiadiazole (0.104 g, 0.354 mmol), palladium(II) acetate (0.011 g, 0.0490 mmol), tris(o-methoxyphenyl)phosphine (0.0237 g, 0.0673mmol), potassium carbonate (0.149 g, 1.08 mmol), and pivalic acid (0.038 g, 0.372 mmol) were all added to a microwave vial and put under nitrogen. The vial was then placed in a dry box where the cap was removed, S4 and 7 mL of tetrahydrofuran was added. A cap was then crimped on the vial and the vial was removed from the glove box where it was then stirred at 100°C for 48 h. Upon completion the polymer solution was added to 200 mL of methanol and stirred for 1 h in an ice bath. A dark blue precipitate formed and was filtered on a coarse frit multiple times until filtrate appeared yellow/clear. The precipitate was then washed with methanol, acetone, and hexanes via Soxhlet prior to chloroform extraction to give near quantitative yield of soluble polymer product. GPC: M_n = 8100, M_w = 11,700, PDI = 1.45.[61]

Poly(2,3-dihexylthieno[3,4-b]pyrazine-alt-2,3-dihexylquinoxaline)) - High-pressure conditions. 2,3-Dihexylthieno[3,4-*b*]pyrazine (0.09 g, 0.285 mmol), 5,8- dibromo-2,3-dihexylquinoxaline (0.130 g, 0.285 mmol), $Pd(OAc)_2$ (0.012 g, 0.053 mmol), tris(o-methoxyphenyl)phosphine (0.022 g, 0.064 mmol), K_2CO_3 (0.147 g, 1.03 mmol), and pivalic acid (0.036 g, 0.36 mmol) were all added to a microwave vial and put under nitrogen. The vial was then placed in a dry box where the cap was removed and 7 mL of anhydrous THF were added. A cap was then crimped onto the vial, and the vial was removed from the glove box where it was then stirred at 100 °C for 48 h. Upon completion, the polymer solution was added to 200 mL of methanol and stirred for 1 h in an ice bath. A dark blue-black precipitate formed and was filtered on a coarse frit multiple times until filtrate appeared yellow/clear. The precipitate was then

washed with methanol and hexanes via Soxhlet extraction, after which the chloroform-soluble fraction was isolated to give 105 mg of blue/black polymer product GPC: M_n = 13,700, M_w = 18,400, PDI = 1.34.[62]

Poly(2,3-bis(2-ethyldihexyl)thieno[3,4-b]pyrazine-alt-*p*-phenylene 2,3-Bis(2-ethylhexyl)thieno[3,4-b]pyrazine (0.133g, 0.369 mmol), 1,4-dibromo-benzene (0.0866 g, 0.366 mmol), palladium(II) acetate (0.012 g, 0.053 mmol), tris(o-methoxyphenyl)phosphine (0.024 g, 0.068 mmol), potassium carbonate (0.148 g, 1.07 mmol), and pivalic acid (0.040 g, 0.39 mmol) were all added to a microwave vial and put under nitrogen. The vial was then placed in a dry box where the cap was removed, and 7 mL of tetrahydrofuran was added. A cap was then crimped on the vial and the vial was removed from the glove box where it was then stirred at 100°C for 46 h. Upon completion the polymer solution was added to 200 mL of methanol and stirred for 1 h in an ice bath. A dark blue precipitate formed and was filtered on a coarse frit multiple times until filtrate appeared yellow/clear. The precipitate was then washed with methanol, acetone, and hexanes via Soxhlet prior to chloroform extraction to give 0.104 g (67% yield) of soluble polymer product.

References

1. Anderson, T. E.; Culver, E. W.; Badı-Dominguez, I.; Wilcox, W. D.; Buysse, C. E.; Ruiz Delgado, M. C.; Rasmussen, S. C. *Phys Chem Chem Phys* **2021**.
2. Konkol, K.; Schwiderski, R.; Rasmussen, S. *Materials* **2016**, *9* (404), 1–16.
3. Evenson, S. J.; Mulholland, M. E.; Anderson, T. E.; Rasmussen, S. C. *Asian J. Org. Chem.* **2020**, *9* (9), 1333–1339.
4. Rasmussen, S. C.; Schwiderski, R. L.; Mulholland, M. E. *Chem. Commun.* **2011**, *47* (41), 11394–11410.

5. Espinet, P.; Echavarren, A. M. *Angew. Chem. Int. Ed.* **2004**, *43* (36), 4704–4734.
6. Hooshmand, S. E.; Heidari, B.; Sedghi, R.; Varma, R. S. *Green Chem.* **2019**, *21* (3), 381–405.
7. Huo, S.; Mroz, R.; Carroll, J. *Org. Chem. Front.* **2015**, *2* (4), 416–445.
8. Heck, R. F.; Nolley, J. P. *J. Org. Chem.* **1972**, *37* (14), 2320–2322.
9. Heravi, M. M.; Zadsirjan, V.; Hajiabbasi, P.; Hamidi, H. *Monatshefte Für Chem. - Chem. Mon.* **2019**, *150* (4), 535–591.
10. Ye, L.; Thompson, B. C. *J. Polym. Sci.* **2022**, *60* (3), 393–428.
11. Bura, T.; Blaskovits, J. T.; Leclerc, M. *J. Am. Chem. Soc.* **2016**, *138* (32), 10056–10071.
12. Leclerc, M.; Brassard, S.; Beaupré, S. *Polym. J.* **2020**, *52* (1), 13–20.
13. SciFinder - Research Topic Candidates. https://scifinder-cas-org.ezproxy.lib.ndsu.nodak.edu/scifinder/view/scifinder/scifinderExplore.jsf (accessed 2022-05-04).
14. The Nobel Prize in Chemistry 2010. NobelPrize.org. https://www.nobelprize.org/prizes/chemistry/2010/summary/ (accessed 2022-05-05).
15. Biffis, A.; Centomo, P.; Del Zotto, A.; Zecca, M. *Chem. Rev.* **2018**, *118* (4), 2249–2295.
16. Cordovilla, C.; Bartolomé, C.; Martínez-Ilarduya, J. M.; Espinet, P. *ACS Catal.* **2015**, *5* (5), 3040–3053.
17. Rasmussen, S. C. *ChemPlusChem* **2020**, *85* (7), 1412–1429.
18. Mizoroki, T.; Mori, K.; Ozaki, A. *Bull. Chem. Soc. Jpn.* **1971**, *44* (2), 581–581.
19. Abdo, N. I.; El-Shehawy, A. A.; El-Barbary, A. A.; Lee, J. S. *Eur. J. Org. Chem.* **2012**, No. 28, 5540–5551.
20. Tang, S.-Y.; Guo, Q.-X.; Fu, Y. *Chem. – Eur. J.* **2011**, *17* (49), 13866–13876.
21. Campeau, L.-C.; Fagnou, K. *Chem. Commun.* **2006**, No. 12, 1253–1264.

22. Lane, B. S.; Brown, M. A.; Sames, D. *J. Am. Chem. Soc.* **2005**, *127* (22), 8050–8057.

23. Alberico, D.; Scott, M. E.; Lautens, M. *Chem. Rev.* **2007**, *107* (1), 174–238.

24. Colletto, C.; Islam, S.; Juliá-Hernández, F.; Larrosa, I. *J. Am. Chem. Soc.* **2016**, *138* (5), 1677–1683.

25. Sévignon, M.; Papillon, J.; Schulz, E.; Lemaire, M. *Tetrahedron Lett.* **1999**, *40* (32), 5873–5876.

26. Satoh, T.; Miura, M. *Chem. Lett.* **2007**, *36* (2), 200–205.

27. Pouliot, J. R.; Grenier, F.; Blaskovits, J. T.; Beaupré, S.; Leclerc, M. *Chem. Rev.* **2016**, *116* (22), 14225–14274.

28. Wang, Q.; Takita, R.; Kikuzaki, Y.; Ozawa, F. *J. Am. Chem. Soc.* **2010**, *132* (33), 11420–11421.

29. Lafrance, M.; Rowley, C. N.; Woo, T. K.; Fagnou, K. *J. Am. Chem. Soc.* **2006**, *128* (27), 8754–8756.

30. Park, C.-H.; Ryabova, V.; Seregi, I. V.; Sromek, A. W.; Gevorgyan, V. *Org. Lett.* **2006**, *6* (7), 1159–1162.

31. Lewis, J. C.; Wiedemann, S. H.; Bergman, R. G.; Ellman, J. A. *Org. Lett.* **2004**, *6* (1), 35–38.

32. Lu, W.; Kuwabara, J.; Kanbara, T. *Macromolecules* **2011**, 1252–1255.

33. Gobalasingham, N. S.; Thompson, B. C. *Prog. Polym. Sci.* **2018**, *83*, 135–201.

34. Gorelsky, S. I.; Lapointe, D.; Fagnou, K. *J. Am. Chem. Soc.* **2008**, *130* (33), 10848–10849.

35. Rudenko, A. E.; Latif, A. A.; Thompson, B. C. *J. Polym. Sci. Part Polym. Chem.* **2015**, *53* (12), 1492–1499.

36. Lombeck, F.; Komber, H.; Gorelsky, S. I.; Sommer, M. *ACS Macro Lett.* **2014**, *3* (8), 819–823.

37. Pankow, R. M.; Ye, L.; Thompson, B. C. Copper Catalyzed Synthesis of Conjugated Copolymers Using Direct Arylation Polymerization. *Polym. Chem.* **2018**, *9* (30), 4120–4124.

38. Rudenko, A. E.; Wiley, C. A.; Tannaci, J. F.; Thompson, B. C. *J. Polym. Sci. Part Polym. Chem.* **2013**, *51* (12), 2660–2668.

39. Wagner, A. M.; Hickman, A. J.; Sanford, M. S. *J. Am. Chem. Soc.* **2013**, *135* (42), 15710–15713.

40. Bura, T.; Beaupré, S.; Légaré, M. A.; Quinn, J.; Rochette, E.; Blaskovits, J. T.; Fontaine, F. G.; Pron, A.; Li, Y.; Leclerc, M. *Chem. Sci.* **2017**, *8* (5), 3913–3925.

41. Cotton, F. A.; Wilkinson, G.; Murillo, C., A.; Bochmann, M. The Elements of the Second and Third Transition Series. In *Advanced Inorganic Chemistry*; Wiley, 1999; pp 877–1107.

42. Wakioka, M.; Kitano, Y.; Ozawa, F. *Macromolecules* **2013**, *46* (2), 370–374.

43. Pouliot, J. R.; Wakioka, M.; Ozawa, F.; Li, Y.; Leclerc, M. *Macromol. Chem. Phys.* **2016**, *217* (13), 1493–1500.

44. Wakioka, M.; Ozawa, F. *Asian J. Org. Chem.* **2018**, *7* (7), 1206–1216.

45. Carole, W. A.; Colacot, T. J. *Chem. - Eur. J.* **2016**, *22* (23), 7686–7695.

46. Ozawa, F.; Kubo, A.; Hayashi, T. *Chem. Lett.* **1992**, *21* (11), 2177–2180.

47. Amatore, C.; Jutand, A.; M'Barki, M. A. *Organometallics* **1992**, *11* (9), 3009–3013.

48. Amatore, C.; Jutand, A.; Thuilliez, A. *Organometallics* **2001**, *20* (15), 3241–3249.

49. Wakioka, M.; Nakamura, Y.; Montgomery, M.; Ozawa, F. *Organometallics* **2015**, *34* (1), 198–205.

50. Iizuka, E.; Wakioka, M.; Ozawa, F. *Macromolecules* **2015**, *48* (9), 2989–2993.

51. Berrouard, P.; Najari, A.; Pron, A.; Gendron, D.; Morin, P.-O.; Pouliot, J.-R.; Veilleux, J.; Leclerc, M. *Angew. Chem.* **2012**, *124* (9), 2110–2113.

52. Lapointe, D.; Fagnou, K. *Chem. Lett.* **2010**, *39* (11), 1118–1126.

53. Boutadla, Y.; Davies, D. L.; Macgregor, S. A.; Poblador-Bahamonde, A. I. *Dalton Trans.* **2009**, No. 30, 5820.

54. Blaskovits, J. T.; Leclerc, M. *Macromol. Rapid Commun.* **2019**, *40* (1), 1–15.

55. Lafrance, M.; Fagnou, K. *J. Am. Chem. Soc.* **2006**, *128* (51), 16496–16497.

56. Glover, B.; Harvey, K. A.; Liu, B.; Sharp, M. J.; Tymoschenko, M. F. *Org. Lett.* **2003**, *5* (3), 301–304.

57. Wakioka, M.; Nakamura, Y.; Hihara, Y.; Ozawa, F.; Sakaki, S. *Organometallics* **2013**, *32* (15), 4423–4430.

58. Wen, L.; Duck, B. C.; Dastoor, P. C.; Rasmussen, S. C. *Macromolecules* **2008**, *41* (13), 4576–4578.

59. Wang, R.; Zhang, C.; Wang, W.; Liu, T. *J. Polym. Sci. Part Polym. Chem.* **2010**, *48* (21), 4867–4874.

60. Kuwabara, J.; Sakai, M.; Zhang, Q.; Kanbara, T. *Org. Chem. Front.* **2015**, *2* (5), 520–525.

61. Culver, E. W.; Anderson, T. E.; López Navarrete, J. T.; Ruiz Delgado, M. C.; Rasmussen, S. C. *ACS Macro Lett.* **2018**, *7* (10), 1215–1219.

62. Anderson, T. E.; Culver, E. W.; Almyahi, F.; Dastoor, P. C.; Rasmussen, S. C. *Synlett* **2018**, *29* (19), 2542–2546.

63. Mascal, M. *Chem. Commun.* **1998**, No. 3, 303–304.

64. Pouliot, J.-R.; Mercier, L. G.; Caron, S.; Leclerc, M. *Macromol. Chem. Phys.* **2013**, *214* (4), 453–457.

65. Mercier, L. G.; Leclerc, M. Direct (Hetero)Arylation: A New Tool for Polymer Chemists. *Acc. Chem. Res.* **2013**, *46* (7), 1597–1605.

66. Wakioka, M.; Ichihara, N.; Kitano, Y.; Ozawa, F. *Macromolecules* **2014**, *47* (2), 626–631.

67. Li, W.; Nelson, D. P.; Jensen, M. S.; Hoerrner, R. S.; Javadi, G. J.; Cai, D.; Larsen, R. D. *Org. Lett.* **2003**, *5* (25), 4835–4837.

68. Gu, Y.; Jérôme, F. *Chem. Soc. Rev.* **2013**, *42* (24), 9550–9570.

69. Azzena, U.; Carraro, M.; Pisano, L.; Monticelli, S.; Bartolotta, R.; Pace, V. *ChemSusChem* **2019**, *12* (1), 40–70.

70. Albano, G.; Punzi, A.; Capozzi, M. A. M.; Farinola, G. *Green Chem.* **2022**.

71. Pankow, R. M.; Ye, L.; Gobalasingham, N. S.; Salami, N.; Samal, S.; Thompson, B. C. *Polym. Chem.* **2018**, *9* (28), 3885–3892.

72. Pappenfus, T. M.; Almyahi, F.; Cooling, N. A.; Culver, E. W.; Rasmussen, S. C.; Dastoor, P. C. *Macromol. Chem. Phys.* **2018**, *219* (21), 1–8.

73. Ma, Z.; Wang, E.; Jarvid, M. E.; Henriksson, P.; Inganäs, O.; Zhang, F.; Andersson, M. R. *Mater Chem* **2012**, *22* (5), 2306–2314.

74. Ray, B.; Nair, P. R.; Alam, M. A. *2010 35th IEEE Photovoltaic Specialists Conference*; 2010; pp 000085–000089.

75. Kline, R. J.; McGehee, M. D. *ym. Rev.* **2006**, *46* (1), 27–45.

76. Cardona, C. M.; Li, W.; Kaifer, A. E.; Stockdale, D.; Bazan, G. C. *Adv. Mater.* **2011**, *23* (20), 2367–2371.

77. Kenning, D. D.; Mitchell, K. A.; Calhoun, T. R.; Funfar, M. R.; Sattler, D. J.; Rasmussen, S. C. *J. Org. Chem.* **2002**, *67* (25), 9073–9076.

78. Wen, L.; Nietfeld, J. P.; Amb, C. M.; Rasmussen, S. C. *J. Org. Chem.* **2008**, *73* (21), 8529–8536.

79. Wen, L.; Rasmussen, S. C. *J. Chem. Crystallogr.* **2007**, *37* (6), 387–398.

80. Kellogg, R. M.; Schaap, A. P.; Harper, E. T.; Wynbert, H. *J. Org. Chem.* **1968**, *33* (7), 2902–2909.

81. Tao, Y.-M.; Li, H.-Y.; Xu, Q.-L.; Zhu, Y.-C.; Kang, L.-C.; Zheng, Y.-X.; Zuo, J.-L.; You, X.-Z. *Synth. Met.* **2011**, *161* (9), 718–723.

82. Chen, C. H.; Hsieh, C. H.; Dubosc, M.; Cheng, Y. J.; Hsu, C. S. *Macromolecules* **2010**, *43* (2), 697–708.

CHAPTER 5. SUMMARY AND FUTURE DIRECTIONS

Summary

As the focus of the previous chapters, thieno[3,4-*b*]pyrazine (TP) has shown significant capability in producing low bandgap (E_g) polymers from a variety of design motifs. The investigations presented here provide a better understanding of conjugated polymers (CPs) from both a theoretical design and practical application standpoint. Much of the utility of TP is derived from its ambipolar nature, allowing for both low E_g homopolymers and copolymers to be synthesized from its analogues.

Extended Ring Thieno[3,4-b]pyrazines

In chapter 2, the extended ring analogues showed that the fusion of additional rings to the TP core could produce polymers with E_g values below 0.5 eV. While this is exceptional electronically, the solubility of these extended ring TPs is extremely poor, limiting their applicability in devices.[1,2] In attempts to produce even lower E_g materials, a synthetic route to poly(2$\lambda^4\delta^2$-dithieno[3,4-*b*:3',4'-*e*]pyrazine) was proposed and attempted with minimal success. In the pursuit of this material, previously unreported TP analogues were synthesized and characterized and thus have added to the family of TP units as potential candidates in low E_g materials.

Model Dimer Systems

Chapter 3 provided a simplified dimer design to investigate donor-acceptor interactions in a set of monomers of consistent conjugation length. The units investigated included the strong donor 3,4-ethylenedioxythiophene, the strong acceptor 2,1,3-benzothiadiazole, and the ambipolar unit TP. The findings of the extensive study provided evidence for the hybridization of the LUMO for the pairing of two units containing pendant electron deficient rings. Conversely, for

strong donor-acceptor pairs, no significant shortening of the bond between units was observed that would result of the resonance structure often invoked for donor-acceptor systems.[3] The study produced a wealth of data including novel synthetic routes to over six compounds and two crystal structures.

Thieno[3,4-b]pyrazine-Acceptor Copolymers

The design motif of pairing TP with strong acceptors was tested in chapter 4. The results of which were materials with E_g values ranging from 1.1 - 0.96 eV. The two acceptors 2,1,3-benzothiadiazole[4] and 2,3-deihexylquinoxaline[5] showed that both electronic properties and solubility could be altered with changes to the acceptor, albeit with improvements of one coinciding with the degradation of the other. The design is particularly enticing in future devices due to the bandgap reduction occurring mainly from LUMO stabilization as opposed to HOMO destabilization and thus the resultant polymers should be more stable to atmospheric oxidation.

Using direct arylation polymerization (DArP) as a method to synthesize these copolymer systems proved to be especially useful by reducing the overall number of synthetic steps by avoiding organometallic functionalization required in many traditional cross-coupling reactions.[6] Additionally, DArP is particularly conducive to the polymers investigated here due to the lack of active C-H bonds available for defect formation. Therefore, the survey of conditions through temperature, reaction time, pressure, and solvent control were investigated as initial modifications to optimize the method for further use. Of the polymers investigated, poly(2,3-bis(2-ethylhexyl)thieno[3,4-*b*]pyrazine-*alt*-2,1,3-benzothiadiazole) produced the lowest E_g polymer with an E_g of 0.96 eV.

Future Directions

Extended Ring Thieno[3,4-b]pyrazines

While unsuccessful in generating CPs with E_g values approaching 0 eV, the extended-ring TP approach may still yet be viable to produce intrinsic conductors. Further work into the protection of the diradical susceptible alpha-positions and polymerization of the previously reported precursors is an option in this regard. The oxidation of 1H,3H-dihydrodithieno[3,4-*b*:3'4'-*e*]pyrazine was specifically problematic and a survey of additional oxidants and conditions may be necessary to acquire yields sufficient for the following Pummerer dehydration step.

Once monomer synthesis has been successful, the next step will be to make any potential homopolymers. The logical choice will be to carry this out electrochemically as with the previously synthesized extended ring TP analogues.[1] With this polymerization method being preferable over other oxidative polymerization methods due to the ability to gather bandgap measurements once the polymer has formed at the electrode surface. Additionally, until solubilizing sidechains are engineered these polymers will likely be insoluble in most solvent systems making any solution-based measurements post polymerization difficult.

Thieno[3,4-b]pyrazine-Acceptor Copolymers

As a design motif, the TP-A copolymer systems investigated show the versatility of the TP building block. Issues with the design however may be due to the arching inherent to pairing a five-membered ring with a six-membered ring in an alternating fashion along the polymer backbone (Figure 5.1). This may be causing reactivity issues in the polymerization due to steric interactions when the chains get long enough to wrap around on themselves and the potential for kinking which hampers delocalization of the π-system.

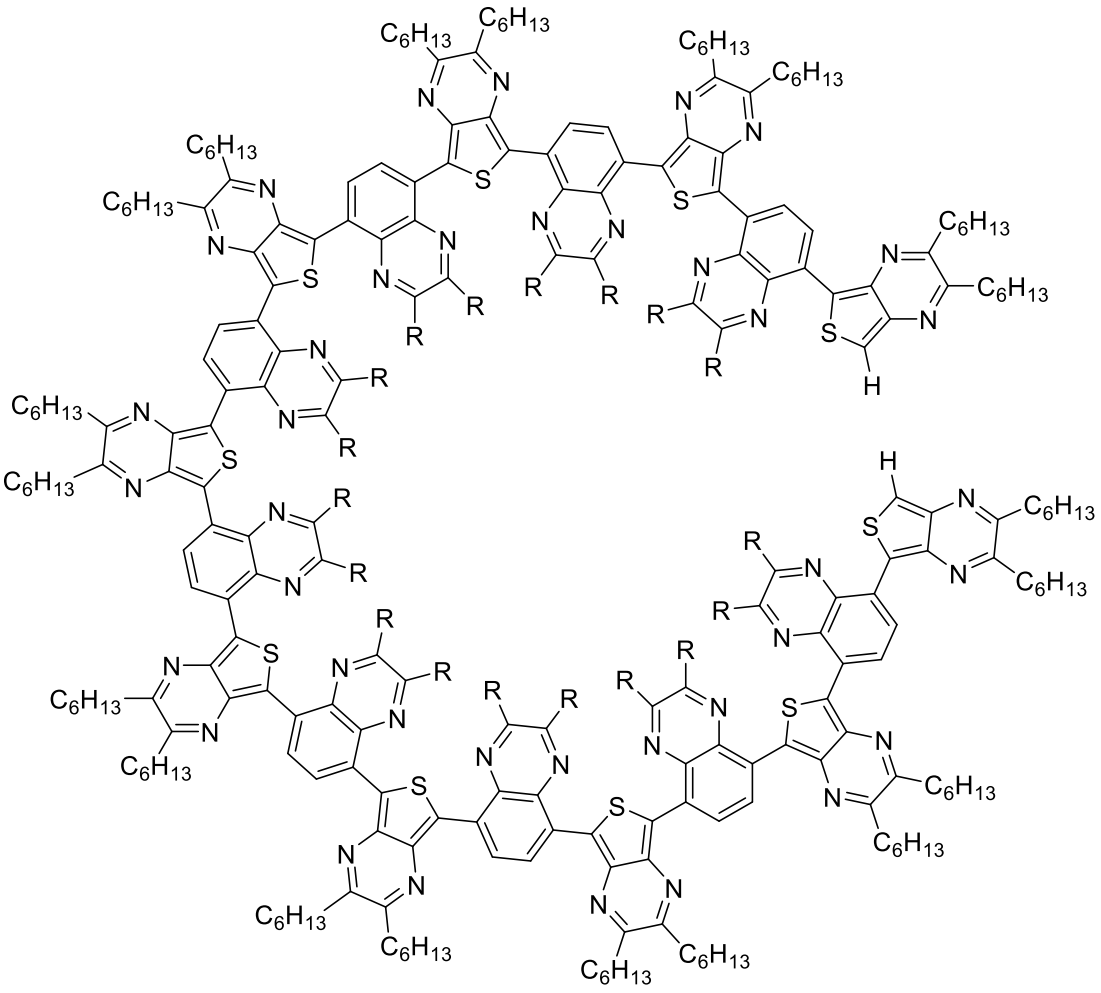

Figure 5.1. Arching in TP-Qx copolymers.

A possible solution to this issue is through the incorporation of fused acceptor units in the CP backbone (Figure 5.2 (top)). This would have the effect of positioning The TP portion anti to one another and allow for the generation of a straight chain. This would however also have the added effect of increasing the total content of BTD in the CP and thus may alter the electronic properties by lowering the HOMO. Additionally, this could also be accomplished through the pairing of TP with an accepter dimer as shown in Figure 5.2 (bottom). This method is particularly interesting because of the already developed chemistry of the 2,1,3-benzothiadiazole dimer chemistry.[3] However, as was pointed out previously in chapter 3, there is significant

twisting between the two BTD units, and in a polymer system may result in reduced delocalization.

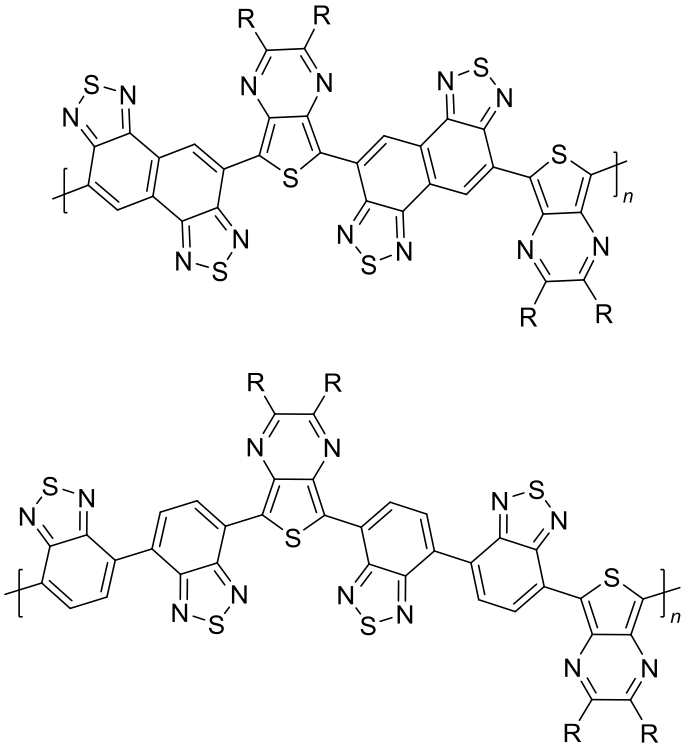

Figure 5.2. (top) Fused acceptor moiety as a solution to addressing arching in TP-A copolymers (bottom) pairing TP with an acceptor dimer to address arching issues.

Extended Ring Thieno[3,4-b]pyrazine-Acceptor Copolymers

Another project with some preliminary data is the pairing of the ERTP acenaphtho[1,2-*b*]thieno[3,4-*b*]pyrazine (ATP) with 2,3-bis(2-ethylhexyl)quinoxaline (EHQx) in an alternating copolymer (Figure 5.3). This copolymer system was initially pursued in the hopes of solubilizing ATP copolymers, but solubility testing in DMF, DMSO, chloroform, and toluene showed little to no solubility of the polymer product. Upon heating in quinoline however it was shown that indeed the polymer could be solubilized, and this was used to cast a thin film for UV-vis analysis and an optical bandgap determination.

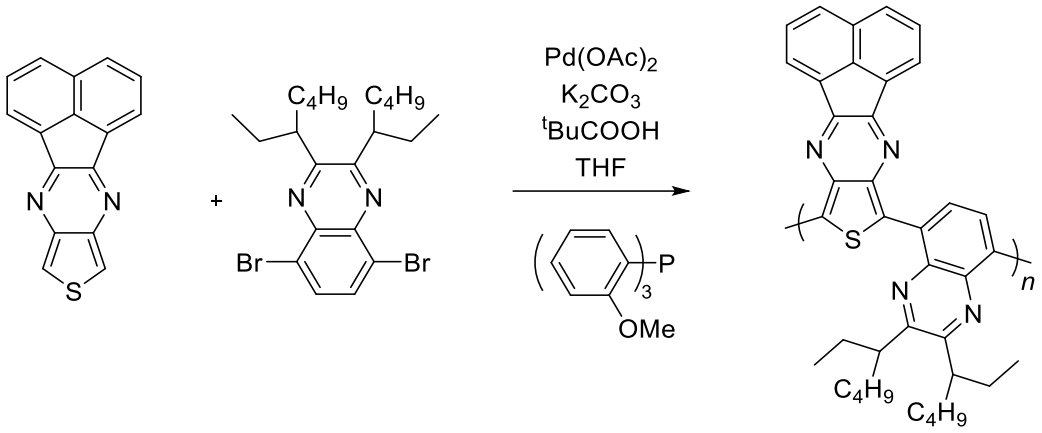

Figure 5.3. Preliminary investigation into ATP-Qx alternating copolymers.

The results of the thin film absorbance analysis showed that the lowest energy absorbance corresponded to an E_g of 1.5 eV (Figure 5.4). This is significantly higher than expected (the homopolymer of ATP has an E_g = 0.45 eV) and with the insolubility, appears to be due to low molecular weight polymers. Further analysis is needed to confirm this, such as gel permeation chromatography to get information about the actual molecular weights of the polymers.

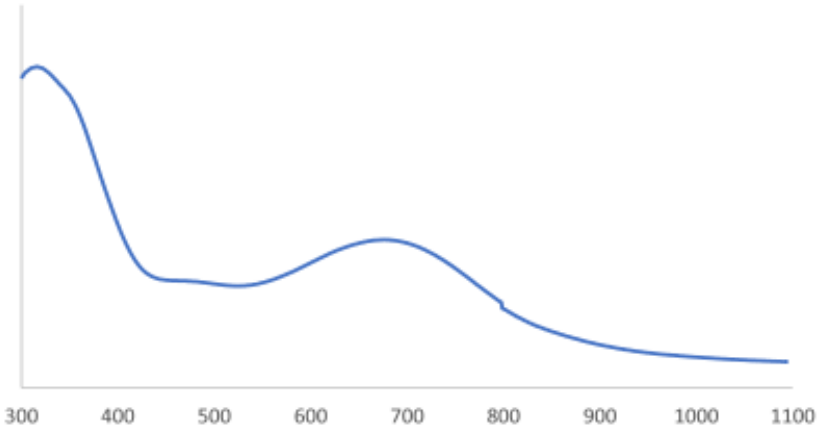

Figure 5.4. UV-vis absorption spectrum of ATP-Qx alternating copolymer thin film.

Conclusions

In conclusion, this study into the nature of TP has provided useful insights into CPs in general, but most importantly into how TP as an ambipolar unit fits within D-A relationships. The dimer investigation has provided evidence for an orbital hybridization rationale in D-A design as a route to lower E_g values while simultaneously casting doubt on the possibility of a new resonance contributor with double bond character between the two units. Additionally, TP as an ambipolar unit paired with other acceptors is a practical strategy for low E_g CPs. While the scope of acceptors that TP has been paired with is still limited, CPs that are soluble and stable under atmospheric conditions have been synthesized largely in part due to the design of limited HOMO destabilization in the TP-acceptor pairing. While current devices have shown poor performance, the use of TP-A polymers as non-fullerene acceptor materials in OPVs is ongoing. The optimization of which could produce devices which absorb nearly the entirety of the solar emission spectrum. Even without practical device applications, the refinement of the D-A model alone shows the utility of this design and further work is sure to improve how we look at D-A copolymer systems in the future.

References

1. Nietfeld, J. P.; Schwiderski, R. L.; Gonnella, T. P.; Rasmussen, S. C. *J. Org. Chem.* **2011**, *76* (15), 6383–6388.
2. Nietfeld, J. P.; Heth, C. L.; Rasmussen, S. C. P *Chem. Commun. Camb. Engl.* **2008**, No. 8, 981–983.
3. Anderson, T. E.; Culver, E. W.; Badı-Dominguez, I.; Wilcox, W. D.; Buysse, C. E.; Ruiz Delgado, M. C.; Rasmussen, S. C. *Phys Chem Chem Phys* **2021**.

4. Culver, E. W.; Anderson, T. E.; López Navarrete, J. T.; Ruiz Delgado, M. C.; Rasmussen, S. C. *ACS Macro Lett.* **2018**, *7* (10), 1215–1219.

5. Anderson, T. E.; Culver, E. W.; Almyahi, F.; Dastoor, P. C.; Rasmussen, S. C. *Synlett* **2018**, *29* (19), 2542–2546.

6. Biffis, A.; Centomo, P.; Del Zotto, A.; Zecca, M. *Chem. Rev.* **2018**, *118* (4), 2249–2295.